Universität Rostock Traditio et Innovatio

Impedimetric Analysis of Biological Cell Monolayers before and after Exposure to Nanosecond Pulsed Electric Fields

Kumulativen Dissertation

zur

Erlangung des akademischen Grades

doktor rerum naturalium (Dr.rer.nat.)

der Mathematisch-Naturwissenschaftlichen Fakultät

der Universität Rostock

vorgelegt von

MSc. Fukun Shi, geb. am 27. September 1988 in Longyan

aus Fujian, China

Rostock, Dezember 2019

https://doi.org/10.18453/rosdok_id00002784

Die vorliegende Arbeit entstand in der Zeit von Oktober 2015 bis Dezember 2019 am Leibniz-Institut für Plasmaforschung und Technologie e.V. und an der Universität Rostock.

The thesis has been performed at Leibniz Institute for Plasma Science and Technology and the University of Rostock in the period from October 2015 to December 2019 and was supervised by Prof. Dr. Juergen F. Kolb.

Gutachter:

1. Gutachter:

   Prof. Dr. Juergen F. Kolb

   Leibniz-Institut für Plasmaforschung und Technologie e.V.

   Institut für Physik, Universität Rostock

2. Gutachter:

   Dr. Martin Sack

   Institut für Hochleistungsimpuls- und Mikrowellentechnik, Karlsruher Institut für Technologie

Datum der Einreichung: 04. Februar 2020

Datum der Verteidigung: 09. Juli 2020

Acknowledgements

First, I would like to thank my supervisor Prof. Dr. Juergen F. Kolb, Greifswald, very much for giving me the opportunity to carry out this work. His commitment and unique insight towards scientific research, also his kind and patient guidance and encouragement inspire me to be a responsible and earnest researcher.

Secondly, I want to thank Prof. Dennis Holfeld and Prof. Rüdiger Köhling, University of Rostock, for being members of my thesis advisory committee (TAC) meeting and giving useful comments and suggestion.

I am truly grateful to all my colleges (former and present) in Leibniz Institute for Plasma Science and Technology (INP Greifswald) for their support and friendship, in particular Dr. Jie Zhuang and Dr. Anna Steuer for their kind introduction in my first year as a PhD candidate.

I appreciate China Scholarship Council for the financial support during my PhD study.

Last but not the least, I would like to thank my parents, my sister and brother, and other family members for their supporting and encouragements, which are essential for me during my PhD study.

Abstract

Models and method for the interpretation of impedance spectra for normal and cancer cells before and after electrical stimulation, focusing on nanosecond pulsed electric fields (nsPEFs), were investigated to describe salient features and their development that were observed in dedicated *in situ* experimental studies. For the first time a non-invasive, real-time and label-free method was established to explore temporal changes and their underlying physical processes of adherent cells for characteristics of cell-cell connections and the extracellular matrix. Therefore, different procedures for a reduction and visualization of impedance data for cell monolayers were developed on the basis of complex nonlinear least squares, multivariate analysis or a deconvolution method. These approaches pave the way for a sensitive distinction and quantification of effects of electrical stimulation on different cell lines. The investigation encourages the further development into a clinical tumor diagnostic, especially for treatments with nsPEFs but in general also other methods of electrical stimulation.

Zusammenfassung

Modelle und Methoden zur Interpretation von Impedanzspektren für normale und Krebszellen vor und nach elektrischer Stimulation, mit dem Fokus auf Nanosekunden-gepulste elektrische Feldern, wurden untersucht, um herausragende Merkmale und deren Entwicklung zu beschreiben, die in speziellen in situ Experimenten beobachtet wurden. Zum ersten Mal wurde eine nicht-invasive, zeitnahe und markierungsfreie Methode entwickelt, um zeitliche Veränderungen und diesen zugrunde liegenden physikalischen Prozessen hinsichtlich der Eigenschaften von Zell-Zell-Verbindungen und der extrazellulären Matrix zu untersuchen. Dazu wurden verschiedene Verfahren zur Reduktion und Visualisierung von Impedanzdaten für Zellmonoschichten auf der Basis komplexer nichtlinearer kleinster Fehlerquadrate, multivariater Analysen oder einer Entfaltungsmethode entwickelt. Diese Ansätze bereiten den Weg für eine sensitive und Quantifizierung von Effekten elektrischen Stimulation auf unterschiedliche Zelllinien. Die Untersuchung ermutigen die Weiterentwicklung hin zu einer klinischen Tumordiagnostik, speziell für Behandlungen mit nsPEFs, aber generell auch anderen Methoden der Elektrostimulation.

Table of Contents

Chapter 1 Summary

1.1 Introduction

Impedance spectroscopy (IS) is widely used for the characterization of the dielectric properties, i.e. conductivity and permittivity, of materials in different fields, including in particular, electrochemistry, but also for biological and medical applications. The strength of the method, in general, is a comprehensive description of the entire system, comprised of the material of interest and the respective interfaces through electrically conductive electrodes [1-4]. IS measurements are usually conducted by interpreting the response to weak electrical signals. Inherent advantages are non-invasiveness, real-time assessment of responses to system changes, and for the application towards biological cells, no need for chemical or other fluorescent labels, along with the description of even sensitive features [5].

IS has therefore benefits especially also for the development of novel cancer therapies that are based on the application of electric fields. In this case, any responses are directly associated and reflected by the electrical properties [6, 7]. A pertinent example are currently emerging tumor treatments with nanosecond pulsed electric fields (nsPEFs), where IS could be used to directly and immediately predict any long-term treatment success [8-13].

The interest in nsPEFs for tumor treatments is based on the discovery of the possibility for intracellular manipulations and especially the induction of apoptosis in early 2000s [14-17]. In the meantime, first clinical trials are being conducted [18-20]. The principle mechanism for the application of nsPEFs is the electroporation of outer cell membrane but more importantly also of intracellular membranes [14]. The concept of electroporation was first proposed in 1972 by Neumann *et al.* to describe the increase of permeability of the outer cell membrane after exposure to intense electric fields [21].

This conventional electroporation is usually observed for pulsed electric fields with durations in the range from microseconds to milliseconds [7, 22]. Typical applications of the method are based on the exploit of the transiently increased permeability of the membrane to introduce drugs, e.g. chemotherapeutics, or genes into the cells [23, 24]. Another application is the induction of an irreversible electroporation and eventual complete loss of cell integrity after more intense exposures to directly kill the cells [22].

Thresholds and exposure conditions for the electroporation of cell membranes strongly depend on the charging time constant of cell membranes, which in turn is determined by the conductivity and permittivity of the membrane [25]. The charging of the cell membranes to transmembrane voltages that are necessary to promote electroporation is in addition also subject to the conductivities of the exposure medium and the cytoplasm (and to some degree also their permittivity). Accordingly, for physiological conditions, the application of rather long electric field pulses with slow rise times, as they are used for conventional electroporation, results only in a charging of the outer cell membrane, whereas due to the simultaneously arising counter-field the cell interior remains essentially field-free. Conversely, short and fast rising pulses, i.e. nsPEFs, can during their application also affect and charge the membranes of organelles. This can be described (in the frequency domain) by the higher frequency components for the applied pulsed electric fields, which are missing for the slower pulses [26, 27]. Yao *et al.* presented in 2009 a consistent model, accordingly, for the frequency-dependent effects of external electric fields on cells [26] confirming biological findings that pulsed electric fields with different durations lead to selective effects on inner and outer membranes due to different charging time constants.

For the strong and direct correlation of underlying physical mechanisms and intended biological responses with dielectric parameters, IS is the method of choice for

their investigation. Accordingly, it could be shown that nsPEFs induce different changes of electrical properties of cells in suspension compared to microsecond PEFs [8, 9, 13]. However, all the studies so far have been conducted to evaluate the characteristics of single cells in suspension. With respect to cells in tumors, there are certain limitations for the relevance of such studies: (i) no cell-to-cell connections and contributions of the extracellular matrix have been taken into consideration, (ii) the interpretation of results highly depends on the prior assumption of electrical models, such as single and double shell models [8, 9, 12].

An alternative model, addressing these shortcomings, is the investigation of cell monolayers. A cell monolayer grown directly on electrodes that are used for electrical exposures and impedance diagnostics, retains the most important features of a complex tissue structures, such as cell-cell interactions and extracellular matrix.

An advanced IS-technique for the analysis of cell monolayers and adherent cells in general is ‘electrical cell-substrate impedance sensing’ (ECIS), which was proposed in the 80s of the last century. Giaever and Keese first developed ECIS to monitor fibroblasts behavior [28-31]. For ECIS, cells are grown on opposing electrodes that are embedded in the bottom of special cell culture dishes. ECIS measurements were proved to be highly sensitive to properties of the cell layer, including cell-cell and cell-substrate adhesions, cellular membrane properties, motility, and thickness of the cellular layer [5, 6, 32].

ECIS offers unique advantages for the study of the electroporation and impedance measurements of adherent cells. Since size and distances between electrodes on an ECIS chip are usually on the order of micrometers, very low voltage can be used to induce electroporation, reducing the requirements of electric field generator and risky

usage of high voltage.

The principle concept of cell growth and associated current flows that are relevant for an impedance analysis by ECIS is illustrated by the diagram presented in Fig. 1. Cell connections are established primarily by tight junctions (TJs). These proteins form an intercellular barrier and intramembrane diffusion fence in epithelial and endothelial cells that govern the permeability for molecules and other cells through the extracellular space [33]. TJs also play an important role in cancer metastasis [34]. Changes of TJs can reveal the transformation of cancer cells from respective normal cells appearing as the loss of the cell-cell association and cell contact inhibition.

Two pathways are shown in Fig. 1 for the possible flow of current either through the paracellular space or intracellular space (represented by the blue and red arrows, respectively). Low frequency currents (blue arrow) are prevented to penetrate through the at low frequencies highly resistive plasma membrane and are therefore prevalent in the paracellular space. In contrast, high frequency currents can capacitively couple across the plasma membrane and pass through the intracellular space.

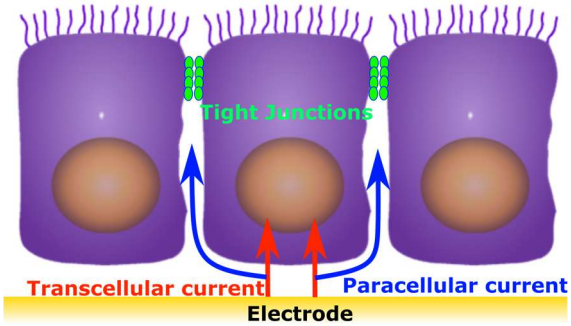

Fig. 1 Pathways of low frequency (blue arrows) and high frequency (red arrows) electrical currents across a cell monolayer grown on an ECIS electrode arrangement.

The availability of ECIS devices prompted an increasing interest for noninvasive and *in situ* impedance monitoring the electroporation of adherent cells [35]. Ghosh *et al.* started using ECIS for measurements at only a single frequency of 4 kHz to monitor electroporation of fibroblasts after exposure to a 200 ms low voltage (1 V) pulse through changes of resistance [31]. The work revealed that the decrease and increase of resistance were related to the electroporation and the subsequent resealing process, respectively.

Stolwijk *et al.* applied AC voltage pulses with frequency of 40 kHz and different pulse amplitudes and durations to induce electroporation of adherent cells and used single-frequency ECIS to monitor any changes of cells [4]. The time-resovled impedance measurements at 4 kHz revealed a transient membrane breakdown immediately after exposure due to electroporation followed by a gradual resealing process within dozens of seconds. Afterwards, the impedance experienced a decrease

again resulting from the changes of the cell shape.

Although ECIS has already successfully applied for the study of conventional electroporation in cell monolayers, so far no studies have been conducted for nsPEF. In addition to this first objective, the presented work aimed concurrently at the development of novel methods for the interpretation of ECIS measurements. The latter so far depends highly on prior assumptions for the underlying electrical models and a priori knowledge of the system.

The extraction of the information from IS spectra is challenging. The multi-frequency impedance data from an IS experiment normally requires dimensionality-reduction for the sake of the investigation. An conventional analysis, i.e. by equivalent circuit models, shows ambiguities, since usually more than one model is capable to fit the experimental data equally well [36, 37]. This poses a problem for the delineation of phenomena, e.g. the effect on TJs. Complex biological systems can include numerous components and phenomena over vast space- and timescales with complex interactions between different components and events at different scales [38]. Therefore, an appropriate interpretation of IS spectra either needs to take this complexity into account or avoid it.

1.2 Objectives and structure of the thesis

Changes of dielectric properties of individual cellular components, e.g. permittivity and conductivity of inner and outer membranes as well as cytoplasm, after exposure to nsPEFs have already successfully been documented for single cells in suspensions. However, so far a similar analysis has not been conducted for the multicellular organization of cells in a monolayer as a model for the complexity of tissues. An investigation of respective responses, with an outlook towards a predictive analysis for

nsPEF tumor therapies, was the main motivation of the presented research project. Therefore, the method of ECIS was adapted and further developed.

The study of nsPEF-effects on cell monolayers in the ECIS-like system required to address several questions: (i) exposure systems and dielectric diagnostics needed to be developed and integrated with each other; (ii) effects of nsPEFs on cells via ECIS have to be confirmed; (iii) effective electrical models to describe the nsPEF-effects on cells have to be developed; (iv) mechanisms and relation with underlying biological responses needed to be confirmed by comparison with standard methods, e.g. fluorescence microscopy; (v) findings needed to be validated for different cell lines and conditions; (vi) novel and practical approaches for the interpretation of impedance data with respect to future clinical applications needed to be developed.

With these questions in mind the following was pursued and is discussed in detail in Chapter 2:

1) Based on standard ECIS electrode arrays, exposure and diagnostic systems as well as methods were devised. Exposures were evaluated by the distribution of electric fields with respect to nsPEF-electroporation requirements. Biological responses, especially for the development of the so far not investigated extracellular space, were compared to results for equivalent exposure conditions by the fluorescent staining of tight junction proteins. A Cole model served as the initial basis for the interpretation of results (c.f. Article no. 1);

2) Method and approach were validated by a comparison of impedance data for different cell lines, i.e. two cancer cell lines and two normal cell lines. As an overreaching goal this suggests the possibility to discriminate normal cells from cancer cells. For a more significant distinction, in addition to the analysis by a

Cole model also a principal component analysis was applied for guiding future clinical applications that do not necessarily require an understanding of physical mechanisms (c.f. article no. 2);

3) A novel and universal strategy of deconvolution of impedance spectra, i.e. distribution of relaxation times (DRT), is developed for cell monolayers before and after exposure to nsPEFs. The approach allows a more sensitive analysis than the Cole model, revealing different and unambiguous dispersions of different components in the cell monolayer (c.f. article no. 3).

1.3 Electrical Models based on Complex Nonlinear Least Squares Fits

Cole *et al.* have proposed the Cole model in 1941 to describe impedance spectra of dielectric materials [39]. The basic model has in the meantime continuously been extended towards different systems, including cells, tissues and implant coatings. Accordingly, nowadays, many electrical models have been applied and documented for biological systems [30, 36]. Cole models are, hence, still the most common strategy and often a first approach for the interpretation of IS spectra.

Therefore, an IS spectrum is fitted into a respective model comprised of resistors, capacitors and constant phase elements that represent the electrical properties of different components of the system. A constant phase element (CPE) is an equivalent circuit component to describe a non-ideal capacitor. Measured impedance spectra are then compared to the response of the model system and parameters of the individual components adjusted (or the model improved by additional components) until a good agreement is achieved between measurements and calculations. This fitting process is

approved by evaluation of complex nonlinear least squares (CNLS), first suggested by Macdonald and Garber in 1977 [40]. The CNLS method can use of all of the data simultaneously, i.e. real and is therefore a practical approach [41].

A standard way to derive CNLS is to look at an object function (S) for a given model with $Z_{fit}(\omega; \boldsymbol{P})$, describing the impedance of the system as a function of both angular frequency (ω), and a set of model parameters (**P**), waiting to be determined by minimizing the object function:

$$S = \sum_{i=1}^{k} \left\{ \left[\frac{Z'_{exp} - Z'_{fit}(\omega_i; \boldsymbol{P})}{Z'_{exp}} \right]^2 + \left[\frac{Z''_{exp} - Z''_{fit}(\omega_i; \boldsymbol{P})}{Z''_{exp}} \right]^2 \right\} \quad (1)$$

The underlying electrical models can be classified either as 'explanatory' or 'descriptive' [42]. An explanatory model aims to reflect the electrical properties of the various microanatomical structures and components, requiring comprehensive knowledge about the physical mechanisms behind phenomena in biological materials. This level of understanding is difficult or even impossible to obtain for an in reality only deficient to describe system. In contrast, a descriptive model does not consider the anatomy of the biological system and only needs to find one electric circuit matching system admittance and measured frequency response. Therefore, this approach is simpler and more practicable than the setting up of an explanatory model. Nevertheless, considerable efforts are required to correlate descriptive model parameters with phenomena of the biological system.

The development of specific models is further challenged by a necessary and truthful representation of the electrodes and electrode processes that are interacting with the biological system and which cannot a priori be avoided or neglected. This is in

particular the case for cells actually growing and adhering on the electrodes of a standard ECIS electrode array. In comparison, for impedance measurements on cells in suspension, basically only processes of the electrolyte with the electrodes need to be taken into account.

Giaever and Keese regarded adherent cells as circular disks (with radius r_c) hovering in a distance, d_{cleft}, above the electrode surface and developed an explanatory model for a confluent cell layer as shown in Fig. 2 [30]. The impedance of the system included contributions from the electrode-electrolyte interface (Z_n) and cell layer (Z_m) as well as the resistance of the paracellular space (R_p). The model is based on several assumptions. The resistance of the cytoplasm (R_{cyt}) and the membrane (R_m) was neglected, considering to very small values for R_{cyt} and very large values for R_m for most cell types [43]. Accordingly, Z_m is dominated by the membrane capacitance (C_m), of cells, described by $Z_m = 2/(i\omega C_m)$. Eventually, the impedance for a cell-covered electrode can be expressed:

$$\mathrm{Z} = (Z_n + Z_m)\left(1 + \frac{\frac{Z_m}{Z_n}}{\frac{i\gamma r_c}{2}\frac{I_0(\gamma r_c)}{I_1(\gamma r_c)} + R_p(\frac{1}{Z_n} + \frac{1}{Z_m})}\right)^{-1} \quad (2)$$

with

$$\gamma = \frac{\alpha}{r_c}\sqrt{\frac{1}{Z_n} + \frac{1}{Z_m}} \quad (3)$$

$$\alpha = r_c \cdot \sqrt{\frac{\rho}{d}} \quad (4)$$

where I_0 and I_1 are modified Bessel functions of the first kind of order 0 and 1, respectively.

This initial model was completed by introducing a constant phase element (CPE) to approximate the impedance of the electrode/electrolyte interface and an additional resistance of the bulk electrolyte (R_{med}). This changes the equation as follows:

$$\mathrm{Z} = (Z_{CPE} + Z_m)\left(1 + \frac{\frac{Z_m}{Z_{CPE}}}{\frac{i\gamma r_c}{2}\frac{I_0(\gamma r_c)}{I_1(\gamma r_c)} + R_p(\frac{1}{Z_{CPE}} + \frac{1}{Z_m})}\right)^{-1} + R_{med} \quad (5)$$

with

$$\gamma = \frac{\alpha}{r_c}\sqrt{\frac{1}{Z_{CPE}} + \frac{1}{Z_m}} \quad (6)$$

and the impedance of the electrode/electrolyte interface described by

$$Z_{CPE} = \frac{1}{K(i\omega)^{\eta}} \quad (7)$$

where K is a constant related to the capacitance and $0<\eta<1$, it is purely capacitive when $\eta = 1$.

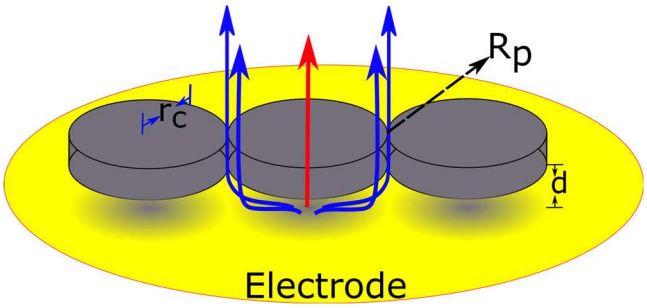

Fig 2 A disk-shaped cell model with radius r_c and thickness d for original ECIS measurement. Low frequency currents (blue arrows) flow the paracellular space, high frequency currents (red arrows) can pass through cells.

In 1995, Lo *et al.* extended the model to be more applicable to confluent epithelial cell monolayers with high junctional resistance by additionally including a pathway for the currents flowing through the lateral membrane (in contact with the electrode) and out through the apical membrane [44].

Later on, Lo *et al.* modified the model further, assuming a rectangular cell shape, tapering into a half disk shape attached at each end, to appropriately describe normal fibroblasts [45]. The impedance of the cell-covered electrode was calculated according to $Z_c = (cell\ area)*V/I$. The total current (I) was derived by individually calculating the currents for the flow through the rectangular shape (I_{rec}) and through the disk (I_{disk}) by $I = I_{rec}+I_{disk}$. The evaluated cell-substrate distance for this extended model had a better agreement with the results obtained from interference reflection microscopy than the previously assumed disk shape (shown in Fig. 2).

With an increasing number of studies for ECIS, also some simplified models were suggested. Wegener et al. presented a rudimentary descriptive model to investigate

bovine aortic endothelial cells, where the cell layer was related just to a resistor and a capacitor in parallel and the electrode polarization was represented by a CPE [46]. The resistance was determined by the paracellular resistance and the capacitance represented the capacitance of the plasma membrane.

Goda *et al.* proposed a mathematical model considering the impedance of the medium between cells (Z_{med}), of the cells (Z_{cell}) and for the electrode polarization (Z_{EP}) without restrictions on cell shape and size [47]. Both Z_{med} and Z_{cell} comprised a circuit element of a resistor and a capacitor connected in parallel. The RC circuit for Z_{med} resembled the cell-cell separation and Z_{EP} depended on the cell-substrate distance. The model is shown in Fig. 3.

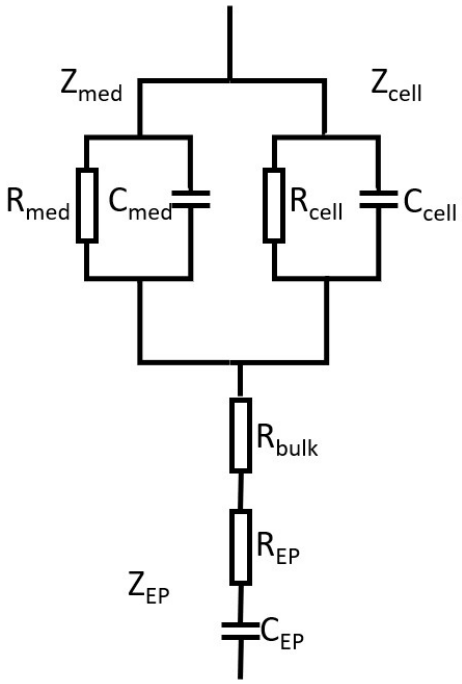

Fig. 3 The equivalent circuit model proposed by Goda et al..

Rahman *et al.* reported a model utilizing a CPE and a resistor in parallel to represent the cell layer [48]. The electrode was coated with a polymer layer and its impedance together with the electrode polarization were represented by two CPEs connected in parallel. The model approximated the experimental data over a broad frequency range from 100 Hz to 10 MHz.

More recently, Szulcek *et al.* presented a general equivalent circuit model for cell-covered electrodes in the article to summarize a protocol for ECIS experiments [5]. This model specifically included resistors to separately characterize junction resistance and cell-substrate resistance as shown in Fig. 4.

Abovementioned models have been used successfully for the description of

dielectric characteristics of cell monolayers. However, none of them have been applied towards the study of pulsed electric field exposures and electroporation, respectively. The pathways that are introduced by an increased permeability of cell membranes conceivable require the modification by additional circuit elements for this phenomenon.

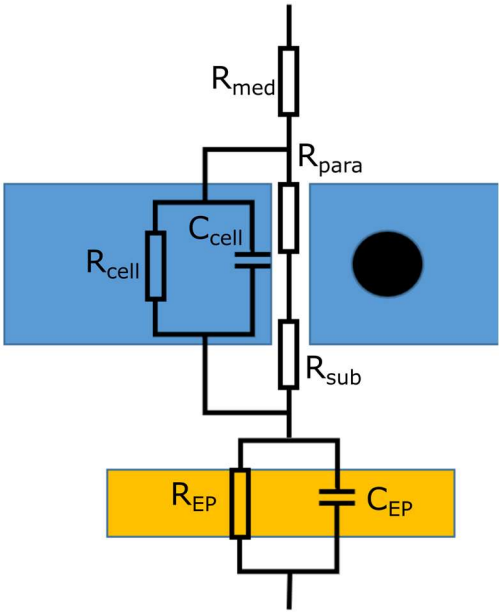

Fig. 4 A simplified and general equivalent circuit model for an adherent cell layer on ECIS electrodes.

García-Sánchez *et al.* used a Cole model to investigate impedance spectra of adherent cells during electroporation [49]. The recording of the impedance of cells and trigger of electroporation was performed *in situ* by a spiral microelectrode assembly above the cell monolayer. The temporal evolution of a Cole parameter (R_0) representing resistance at very low frequencies showed two different developments after the

exposure of cells to PEFs of microsecond duration. One is a short-term impedance drop, followed by recovery, consistent with transient membrane electroporation and subsequently resealing between two pulses. The other one is a long-term impedance drop resulting from the accumulation of more stable pores that were generated.

Since this Cole model explicitly incudes also electroporation phenomena for a real-time exposure and diagnostic system, it was also chosen for the work presented here (article no. 1 and article no. 2).

1.4 Statistical Analysis

Multi-frequency impedance measurements result in large amounts of correlated and possibly redundant data. A data reduction can be achieved by the aforementioned model-based approaches. Fitting experimental spectra to a mathematical equation of an assumed model, e.g. equivalent circuit representations, which provide the uncorrelated model parameters of interest. However, the method requires a priori assumption for the system and is therefore inevitably ambiguous. Conversely, data reduction can be accomplished by a multivariate analysis directly from the raw data without model assumptions. An instructive straightforward procedure is available through a principal component analysis (PCA), invented by Pearson in 1901 [50]. The number of possibly correlated dimensions of the measurements is reduced by removing in particular linearly dependent information.

Suppose experimental data for m samples with n features for each sample, e.g. n phase values for respective frequencies. This data set can be described by a $m \times n$ matrix $\vec{X}$ with m dimension determined by the number of samples and n dimensions according to the results obtained for each frequency of an individual sample. The aim of a PCA is to reduce the corresponding large number of original features by defining new and

fewer common characteristics, which are well distinguished from each other.

First, the matrix $\vec{X}$ is scaled to normalize values for individual frequencies. This step is in particular necessary for impedance measurement since a typical impedance measurement spans several orders of magnitude for measurements at different frequencies and the associated amplitudes of respective impedance values. The largest amplitudes will determine the performance of the PCA. A matrix $\vec{B}$ can then be calculated according to $\vec{B} = \frac{\vec{X} - \bar{X}}{var(\vec{X})}$ resulting in a vanishing mean (zero) and normalized variance (one) for each column.

In the next step, the covariance matrix for $\vec{B}$ is calculated, i.e. $\vec{C} = \frac{\vec{B}^T \vec{B}}{n-1}$. Afterwards, eigenvector $\vec{V}$ and eigenvalues $\vec{D}$ are derived through $\vec{V}^{-1}\vec{B}\vec{V} = \vec{D}$. Eventually, the dimensionality by choosing only the eigenvectors with the highest eigenvalues for a matrix representation, i.e. the principal components of the data set.

PCA has become a popular method for the classification and evaluation of bioimpedance measurements. Lindholm-Sethson *et al.* utilized PCA to identify the differences of diabetes-related changes between males and females as well as for the discrimination of diabetic patients and control groups [51]. Cannizzaro *et al.* used various methods, including PCA, to develop an on-line biomass monitoring system for CHO perfusion cultures. Especially the frequency range for the largest differences between capacitances of different biomass could be determined by PCA [52]. Nejadgholi *et al.* compared the classification accuracy for various sets of bioimpedance of a cylindrical body organ simulated by an electrical circuit through PCA, soft independent modeling of class analogy (SIMCA) and Cole model, PCA was found more discriminant than an evaluation of Cole parameters [53].

The performance of PCA for differentiation and classification by impedance spectroscopy in these different applications suggests the method also for the discrimination of cancer and normal cells and their response to nsPEF (article no. 2).

1.5 Deconvolution of Impedance Spectra

Two common strategies for the interpretation of impedance measurements have been described in the preceding chapters. Both approaches have been successfully applied towards the investigation of nsPEF-effects on cell monolayers (c.f. articles no. 1 and 2). Despite their success, the respective evaluations encourage the pursuit of alternatives that would allow to overcome individual shortcomings of both approaches. The interpretation of impedance measurements by an equivalent circuit model is prone to ambiguities since the data can usually be fitted to more than one model equally well. Conversely, no physical meaning can be associated to a distinction of results by an in essence purely statistical treatment, such as PCA. A descriptive method that in part relies on a statistical analysis but delivers parameter that are inherently associated with fundamental physical mechanisms, is the distribution of relaxation times (DRT).

The polarization processes in an electrochemical system are directly characterized by the respective relaxation times and relaxation amplitudes (loss factors) [2]. Therefore, the distribution of relaxation times (DRT) becomes the basic quantity of interest in an impedance analysis. The DRT is directly related to polarization processes and therefore a method without the need of prior assumptions for electrical models or any a priori knowledge of the system. However, the necessary complicated and computation cumbersome deconvolution of impedance spectra has limited the wider spread use of the DRT method until recently.

The impedance ($Z_{DRT}(f)$) at a specific frequency (f) was described by Fuoss and

Kirkwood by an integral function, i.e. convolution function, for the probability density function ($\gamma(\tau)$) describing the distribution of relaxation times (τ) [54].

$$Z_{DRT}(f) = R_{ohmic} + R_{pol}\int_0^{\infty} \frac{\gamma(\tau)}{1 + i2\pi f\tau} d\tau \tag{8}$$

with

$$\int_0^{\infty} \gamma(\tau) d\tau = 1 \tag{9}$$

where R_{ohmic} is the ohmic part of the impedance (frequency-independent) and, R_{pol} is the polarization resistance of the impedance.

A succinct derivation of equation 8 can be obtained with the assumption that all physical processes are relaxations and consequently an electrical response (e.g. voltage) will decay exponentially after a step perturbation input, e.g. a current impulse, according to Ciucci et al. [55] and Kobayashi *et al.* [56].

The voltage response ($v(t)$) is a result of the input current ($i(t)$) which can be related by a transfer function ($z(t)$) as follows

$$v(t) = (z * i)(t) \tag{10}$$

with the right-side term defining the convolution function

$$(z * i)(t) = \int_{-\infty}^{\infty} z(t')i(t-t')dt' \tag{10}$$

Since $z(t)$ describes a relaxation response (as mentioned above), the function can be expressed as the sum of a series of relaxations processes with characteristic time constants $\tau_1 < \tau_2 < \cdots < \tau_N$

$$z(t) = r_0\delta(t) + \sum_{n=1}^{N} \frac{r_n}{\tau_n} H(t)e^{-t/\tau_n} \tag{11}$$

with $r_n \geq 0$ related to the relaxation amplitude and $H(t)$ indicating the Heaviside step function (which can be defined as the integral of the Dirac delta function $H(t) := \int_{-\infty}^{t} \delta(s)ds$). On the right side of equation 11, the first term ($r_0\delta(t)$) is a purely resistive quantity, corresponding to a characteristic time $\tau_0 \to 0$. The sum collects the contributions of all respective polarization portions.

An example for the illustration of the method and equation 11 is shown in Fig. 5. Assuming that r_n has a normal distribution with a mean of 10 and a standard deviation of 100 (arbitrary units), i.e. $r_n = \mathcal{N}(10, 100^2)$. The transfer function $z(t)$ according to equation 11 has then values as presented in Fig. 5.

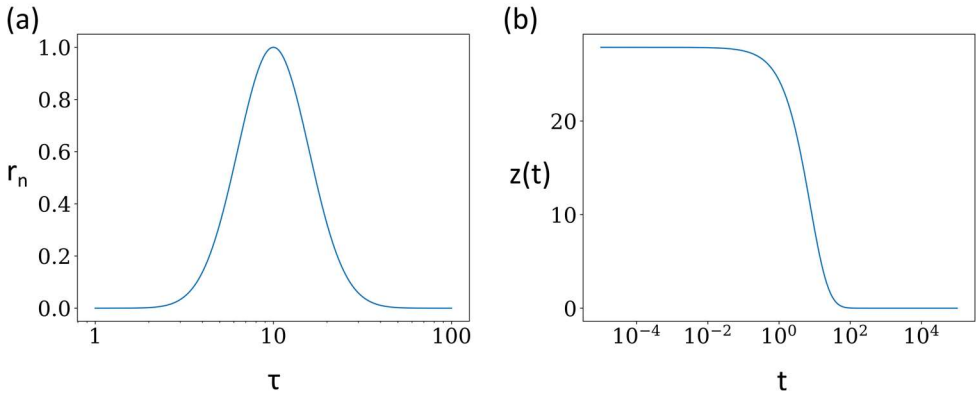

Fig. 5. A normal distribution function (a) and the respective transfer function $z(t)$ (b). The unit for relaxation time and time for $z(t)$ is second.

The impedance of the system in frequency domain can be obtained by Fourier transformation of equation 11, taking $\int_{-\infty}^{\infty} \delta(s)ds = 1$ into consideration:

$$Z_{DRT}(f) = \int_{-\infty}^{\infty} z(t)e^{-i2\pi f}\, dt = \int_{-\infty}^{\infty} r_0\delta(t)e^{-i2\pi ft}dt$$
$$+\sum_{n=1}^{N}\frac{r_n}{\tau_n}\int_{-\infty}^{\infty} H(t)e^{-\frac{t}{\tau_n}}e^{-i2\pi f}\, dt = r_0 + \sum_{n=1}^{N}\frac{r_n}{1+i2\pi f\tau_n} \quad (12)$$

The respective impedance in the frequency domain for Fig. 5 can be reconstructed

according to equation 12 and as shown in Fig. 6.

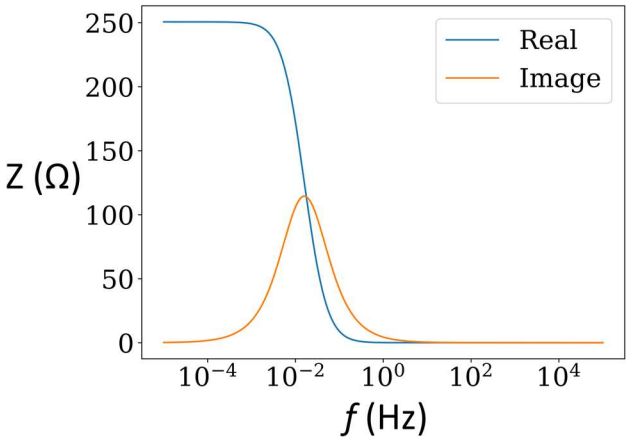

Fig. 6. The impedance calculated from equation 12 based on r_n in the Fig. 5.

Equation 12 is a discrete form that can be approximated with some transformations to be consistent with equation 8: (1) set $r_n = g_n \Delta\tau$ to be an infinitesimal quantity, where g_n is the distribution function of relaxation times, (2) extend *N* to be infinite, (3) allow τ_n to span the entire real line, (4) make $r_0 = R_{ohm}$, then:

$$Z_{DRT}(f) = R_{ohmic} + \sum_{n=1}^{N} \frac{g_n \Delta\tau}{1 + i2\pi f\tau_n} \approx R_{ohmic} + \int_0^{\infty} \frac{g(\tau)}{1 + i2\pi f\tau} d\tau \qquad (13)$$

Polarization portions of equation 12 and 13, i.e. the summation and integration, can also be graphically interpreted by a serial connection of RC-elements [2, 57], for each RC-element with a characteristic time $\tau_n = R_n C_n$.

Since the frequencies of impedance measurements are conventionally sampled

logarithmically, equation 13 is rewritten as follows:

$$Z_{DRT}(f) = R_{\infty} + \int_{0}^{\infty} \frac{G(\tau)}{1 + i2\pi f\tau} dln\tau \tag{15}$$

substituting the original variables:

$$\tau = e^{ln\tau}, d\tau = e^{ln\tau} dln\tau = \tau dln\tau \tag{16}$$

and accordingly, $G(\tau) = \tau g(\tau)$.

The deconvolution of $G(\tau)$ from equation 15 is a well-known ill-posed problem, meaning there are more than one solution for the equation. In this regard, various methods have been developed to solve the equation, including maximum entropy [57], Monte Carlo technique [58], Fourier transform [2], genetic programming [59], and Tikhonov Regularization, i.e. Ridge regression [60].

Ciucci pointed out that Tikhonov Regularization is particular appealing since it can be recast as a constrained quadratic programming problem, which has a unique solution. The method can further be extended for a multidimensional and Bayesian impedance data analysis [61]. The core of the Tikhonov Regularization method is to express r_n in equation 12 as a weighted radial basis function (RBF), i.e. $r_n = \kappa_n \Psi_n(\tau)$, with κ_n the weight and $\Psi_n(\tau)$ the correlated RBF. RBFs can have very different shapes or descriptions, respectively, e.g. they could be piece-wise linear (PWL) approximations, Gaussian functions or a step function [62, 63].

With the assistance of this deconvolution methods, the DRT approach has been applied for different electrochemical systems and biological tissues. Schichlein *et al.* in

the group of Prof. Ivers-Tiffée developed the Fourier transform-based DRT method and used the DRT for the identification of the reaction mechanisms of solid oxide fuel cells (SOFEs) [2]. Later on, an attempt to correlate peaks of distribution functions with physicochemical processes was also performed by a comparison of a physical model. Afterwards, other members in her group, Sonn and Leonide presented a strategy to combine the DRT method and CNLS fit to improve the interpretation of the electrochemical processes in Ni/8YSZ (yttria-stabilized zirconia) cermet anodes [64]. Different electrochemical processes were distinguished by the DRT and then the results were used to aid establishing an equivalent circuit model. Schmidt *et al.* extended the application of the DRT to investigate lithium iron phosphate ($LiFePO_4$) batteries [65-67]. The approach particularly included an elimination of the capacitive diffusion branch at low frequency before conducting the DRT. The branch results from the solid-state diffusion in the intercalation electrode and intercalation capacity, which cannot be modeled into The DRT since the DRT does not include a pure capacitive behavior. More recently, Seo *et al.* included the DRT to enhance the quantitative evaluation of the impact of $(Pr,Ce)O_{2-\delta}$ (PCO) overcoats on the activity and stability of Pt thin-film O_2-electrodes of SOFCs with different temperatures [68].

Recently, Ramírez-Chavarría *et al.* measured the impedance spectra of different *ex vivo* rat organ tissues and individual tissues were discriminated by the deconvoluted DRTs from the respective impedance spectra [69]. However, no discussion on the correlation between distribution functions and physical or biological counterparts of tissues have been given.

The application of the DRT on biological cells requires a careful processing of electrode polarization, which is an inevitable phenomenon in two-electrode measurements and has a significant influence on the evaluation of the DRT. However,

in comparison with Cole models and PCA, a finer resolution of polarization processes can be derived from the DRT especially for tissues or cell monolayers, with complex tissue structure and several components contributing to polarization processes and, hence, being superimposed in the distribution of relaxation times (c.f. article on. 3).

1.6 General Conclusion

In the present thesis, the response of cell monolayers to nsPEFs was investigated by interpreting impedance spectra, obtained for cell monolayers, by different methods, including equivalent circuit models, multivariate analysis and the distribution of relaxation times. Besides the discrimination of untreated cells, did the individual approaches clearly reveal pulse number dependent responses for the application of nsPEFs. The respective analyses show different advantages and sensitivities with respect to cell characteristics and related dispersion mechanisms.

In Paper 1 *in situ* impedance spectra of a rat liver epithelial cell line, i.e. WB-F344, before and after 8, 20 and 60 exposures, applied at 1 Hz, to nsPEFs of 100 ns duration and an average field strength of 20 kV/cm were measured and analyzed by a Cole model. Three pathways for the flow of low frequency electrical currents through a cell monolayer could be discriminated that are reflected by significant changes of a Cole parameter (R_0) i.e. the resistance at very low frequency:

1. Changes to current flow, after exposure to nsPEFs, along the paracellular pathway mainly resulted from the disruption of cell-cell cohesion, in particular tight junctions, resulting in a decrease of R_0;

2. Changes to current flow, after exposure to nsPEFs, along the transcellular pathway were due to electroporation that was observed immediately after

exposure and was also associated with a decrease of R_0;

3. Changes to current flow, after exposure to intense nsPEFs (60 pulses), along the trans-monolayer pathway arises from dead cells corresponding to a fast decrease of R_0 and a relative long recovery from small resistance values.

In addition to the changes of the monolayer integrity reflected by R_0, also other Cole-parameters, i.e. dispersion width α and time constant τ, respectively, could be related to changes of the morphology of the extracellular space and cell membrane permeabilization in general.

In Paper 2, impedance spectra of four cell lines, i.e. WB-F344, WB-ras, HaCat and Sk-Mel-28, were investigated before and after exposure to 8, 16 and 24 pulses of nsPEFs by means of the Cole model and PCA. PCA is a non-parametric representation evading disadvantages of the Cole model, e.g. inevitable fitting errors and the requirement of the prior knowledge of the system.

1. Both Cole parameters and PCA showed significant differences between different cell lines either before exposures or in the temporal evolution after exposures;

2. PCA loading plots of phase spectra indicated that nsPEF-effects for normal cell monolayers were rather reflected by the response at lower frequencies in comparison to cancer cell monolayers;

3. The study suggested that the discrimination of cell monolayers is determined by the extracellular resistance. This emphasizes the vital roles of cell-cell connections and extracellular matrix and the respective difference between normal and cancer cells for the response to nsPEFs.

In Paper 3, a universal and sensitive deconvolution of impedance spectra was developed for identifying relaxation processes without the need for a priori assumptions as it is required for example for the description by equivalent electrical circuit models. Moreover, a multi-peak analysis using a series of Gaussian functions was utilized to quantify individual polarization processes. The approach revealed three polarization processes and provided a high resolution of the differentiation of polarization process and straightforward biophysical meaning comparing to the Cole model and PCA.

1. Low frequency relaxation processes at about 10 kHz was distinguished and may be associated with a response of the extracellular matrix;

2. Moderate frequency relaxation processes at about 100 kHz dominated changes of the distribution function for each cell monolayer after exposures and were associated with the interfacial polarization of the cell membrane;

3. A small high frequency relaxation processes at around 3 MHz presumably could be associated with the interfacial polarization of organelle membranes.

1.7 Prospective research directions

In this thesis, the analysis of impedance spectra has increased knowledge and understanding of nsPEF-effects on cells, in particular exposing the crucial roles of cell-cell connections and of extracellular matrix for cell assemblies, i.e. cell monolayers and tissues. Expanded studies and continued improvements of methods and systems can be expected to further enhance the understanding:

(i) Time scales for different dynamics of nsPEF-effects span several orders of magnitude. A high temporal resolution of impedance measurements up to millisecond-scale is important to distinguish dynamics, e.g. pathways of

electrical currents. To achieve this goal, a fast scanning impedance analyzer and a fast switch for the exchange between the electrical exposure and impedance measurements are required;

(ii) Impedance datasets for nsPEF treatments on a specific tumor cell line or tissue type can be examined by machine learning to improve the discrimination and eventually develop a clinical diagnosis;

(iii) The DRT method can guide to establish a robust explanatory model that is taking into account physical processes. The model can, hence, be improved and validated by uncertainty quantification. Eventually this approach in particular also holds the potential for a sensitive analysis of other methods of electrical stimulation as well;

(iv) To understand nsPEF-effects and develop IS and nsPEFs as a diagnosis and therapeutic system, more cell lines or tissue types as well as more exposure parameters and eventually *in vivo* experiments are necessary for the establishment of quantitative relationship between IS measurements and nsPEF-effects.

1.8 References

[1] J.W.S. Rocha, M.A. Vicente, B.N. Melo, M.d.L.S.P. Marques, R.C.L. Guimarães, C.M.S. Sad, E.V.R. Castro, M.F.P. Santos 2019 Investigation of electrical properties with medium and heavy Brazilian crude oils by electrochemical impedance spectroscopy *Fuel* **241** 42-52

[2] H. Schichlein, A.C. Müller, M. Voigts, A. Krügel, E. Ivers-Tiffée 2002 Deconvolution of electrochemical impedance spectra for the identification of electrode reaction mechanisms in solid oxide fuel cells *Journal of Applied Electrochemistry* **32** 875-882

[3] M. Genescà, A. Ivorra, A. Sola, L. Palacios, J.-M. Goujon, T. Hauet, R. Villa, J. Aguiló, G. Hotter 2005 Electrical bioimpedance measurement during hypothermic rat kidney preservation for assessing ischemic injury *Biosensors and Bioelectronics* **20** 1866-1871

[4] J.A. Stolwijk, C. Hartmann, P. Balani, S. Albermann, C.R. Keese, I. Giaever, J. Wegener 2011 Impedance analysis of adherent cells after in situ electroporation: Non-invasive monitoring during intracellular manipulations *Biosensors and Bioelectronics* **26** 4720-4727

[5] R. Szulcek, H.J. Bogaard, G.P. van Nieuw Amerongen 2014 Electric cell-substrate impedance sensing for the quantification of endothelial proliferation, barrier function, and motility *J Vis Exp* 51300

[6] T. García-Sánchez, R. Bragós, L.M. Mir 2018 In vitro analysis of various cell lines responses to electroporative electric pulses by means of electrical impedance spectroscopy *Biosensors and Bioelectronics* **117** 207-216

[7] A. Ivorra, B. Rubinsky 2007 In vivo electrical impedance measurements during and after electroporation of rat liver *Bioelectrochemistry* **70** 287-295

[8] A.L. Garner, C. Nianyong, Y. Jing, J. Kolb, R.J. Swanson, K.C. Loftin, S.J. Beebe, R.P. Joshi, K.H. Schoenbach 2004 Time domain dielectric spectroscopy measurements of HL-60 cell suspensions after microsecond and nanosecond electrical pulses *IEEE Transactions on Plasma Science* **32** 2073-2084

[9] A.L. Garner, G. Chen, N. Chen, V. Sridhara, J.F. Kolb, R.J. Swanson, S.J. Beebe, R.P. Joshi, K.H. Schoenbach 2007 Ultrashort electric pulse induced changes in cellular dielectric properties *Biochem. Biophys. Res. Commun.* **362** 139-144

[10] U. Pliquett, R.P. Joshi, V. Sridhara, K.H. Schoenbach 2007 High electrical field effects on cell membranes *Bioelectrochemistry* **70** 275-282

[11] U.F. Pliquett, K.H. Schoenbach 2009 Changes in electrical impedance of biological matter due to the application of ultrashort high voltage pulses *IEEE Transactions on Dielectrics and Electrical Insulation* **16** 1273-1279

[12] J. Zhuang, J.F. Kolb 2015 Time domain dielectric spectroscopy of nanosecond pulsed electric field induced changes in dielectric properties of pig whole blood *Bioelectrochemistry* **103** 28-33

[13] J. Zhuang, W. Ren, Y. Jing, J.F. Kolb 2012 Dielectric evolution of mammalian cell

membranes after exposure to pulsed electric fields *IEEE Transactions on Dielectrics and Electrical Insulation* **19** 609-622

[14] K.H. Schoenbach, S.J. Beebe, E.S. Buescher 2001 Intracellular effect of ultrashort electrical pulses *Bioelectromagnetics* **22** 440-448

[15] S.J. Beebe, J. White, P.F. Blackmore, Y. Deng, K. Somers, K.H. Schoenbach 2003 Diverse effects of nanosecond pulsed electric fields on cells and tissues *DNA and Cell Biology* **22** 785-796

[16] K.H. Schoenbach, S.J. Hargrave, R.P. Joshi, J.F. Kolb, R. Nuccitelli, C. Osgood, A. Pakhomov, M. Stacey, R.J. Swanson, J.A. White, S. Xiao, J. Zhang, S.J. Beebe, P.F. Blackmore, E.S. Buescher 2007 Bioelectric Effects of Intense Nanosecond Pulses *IEEE Transactions on Dielectrics and Electrical Insulation* **14** 1088-1109

[17] J. Guo, J. Dang, K. Wang, J. Zhang, J. Fang 2018 Effects of nanosecond pulsed electric fields (nsPEFs) on the human fungal pathogen Candida albicans: an in vitro study *Journal of Physics D: Applied Physics* **51** 185402

[18] G.S. Munavalli, B.D. Zelickson, M.M. Selim, S.L. Kilmer, T.E. Rohrer, J. Newman, L. Jauregui, W.A. Knape, E. Ebbers, D. Uecker 2019 Safety and Efficacy of Nanosecond Pulsed Electric Field Treatment of Sebaceous Gland Hyperplasia *Dermatologic surgery: official publication for American Society for Dermatologic Surgery*

[19] D. Kaufman, M. Martinez, L. Jauregui, E. Ebbers, R. Nuccitelli, W.A. Knape, D. Uecker, D. Mehregan 2019 A dose-response study of a novel method of selective tissue modification of cellular structures in the skin with nanosecond pulsed electric fields *Lasers in surgery*

medicine

[20] R. Nuccitelli 2019 Application of pulsed electric fields to cancer therapy *Bioelectricity* **1** 30-34

[21] E. Neumann, K.J.T.J.o.M.B. Rosenheck 1972 Permeability changes induced by electric impulses in vesicular membranes **10** 279-290

[22] E. Ben-David, M. Ahmed, M. Faroja, M. Moussa, A. Wandel, J. Sosna, L. Appelbaum, I. Nissenbaum, S.N. Goldberg 2013 Irreversible electroporation: treatment effect is susceptible to local environment and tissue properties *Radiology* **269** 738-747

[23] R.M. Atkins, T.J. Fawcett, R. Gilbert, A.M. Hoff, R. Connolly, D.W. Brown, A.J. Llewellyn, M.J. Jaroszeski 2017 Impedance spectroscopy as an indicator for successful in vivo electric field mediated gene delivery in a murine model *Bioelectrochemistry* **115** 33-40

[24] U. Probst, I. Fuhrmann, L. Beyer, P. Wiggermann 2018 Electrochemotherapy as a New Modality in Interventional Oncology: A Review *Technol. Cancer Res. Treat.* **17** 1533033818785329-1533033818785329

[25] P. omas Vernier, Nanoscale Restructuring of Lipid Bilayers in Nanosecond Electric Fields, Advanced Electroporation Techniques in Biology and Medicine, CRC Press2010, pp. 181-196.

[26] C. Yao, X. Hu, Y. Mi, C. Li, C. Sun 2009 Window effect of pulsed electric field on biological cells *IEEE Transactions on Dielectrics and Electrical Insulation* **16** 1259-1266

[27] T. Kotnik, D. Miklavčič 2000 Theoretical evaluation of the distributed power dissipation in biological cells exposed to electric fields *Bioelectromagnetics* **21** 385-394

[28] I. Giaever, C.R. Keese 1984 Monitoring fibroblast behavior in tissue culture with an applied electric field *Proceedings of the National Academy of Sciences* **81** 3761

[29] I. Giaever, C.R. Keese 1986 Use of Electric Fields to Monitor the Dynamical Aspect of Cell Behavior in Tissue Culture *IEEE Trans. Biomed. Eng.* **BME-33** 242-247

[30] I. Giaever, C.R. Keese 1991 Micromotion of mammalian cells measured electrically *Proceedings of the National Academy of Sciences* **88** 7896

[31] I. Giaever, C.R. Keese 1993 A morphological biosensor for mammalian cells *Nature* **366** 591-592

[32] W.G. Jiang, 2012, Electric cell-substrate impedance sensing and cancer metastasis, Springer Science & Business Media.

[33] K. Matter, M.S. Balda 2003 Functional analysis of tight junctions *Methods* **30** 228-234

[34] T.A. Martin, W.G. Jiang 2009 Loss of tight junction barrier function and its role in cancer metastasis *Biochimica et Biophysica Acta (BBA) - Biomembranes* **1788** 872-891

[35] J. Wegener, C.R. Keese, I.J.B. Giaever 2002 Recovery of adherent cells after in situ electroporation monitored electrically **33** 348-357

[36] E.T. McAdams, J. Jossinet 1996 Problems in equivalent circuit modelling of the electrical properties of biological tissues *Bioelectrochemistry and Bioenergetics* **40** 147-152

[37] M.B. Effat, F. Ciucci 2017 Bayesian and Hierarchical Bayesian Based Regularization for Deconvolving the Distribution of Relaxation Times from Electrochemical Impedance Spectroscopy Data *Electrochimica Acta* **247** 1117-1129

[38] R.C. Smith, 2013, Uncertainty quantification: theory, implementation, and applications, Siam.

[39] K.S. Cole, R.H. Cole 1941 Dispersion and Absorption in Dielectrics I. Alternating Current Characteristics *The Journal of Chemical Physics* **9** 341-351

[40] J.R. Macdonald, J.A. Garber 1977 Analysis of Impedance and Admittance Data for Solids and Liquids *Journal of The Electrochemical Society* **124** 1022-1030

[41] E. Barsoukov, J.R. Macdonald, 2018, Impedance spectroscopy: theory, experiment, and applications, John Wiley & Sons.

[42] S. Grimnes, Ø.G. Martinsen, Chapter 9 - Data and Models, in: S. Grimnes, Ø.G. Martinsen (Eds.), Bioimpedance and Bioelectricity Basics (Third Edition), Academic Press, Oxford, 2015, pp. 329-404.

[43] B. Reiss, J. Wegener, Impedance analysis of different cell monolayers grown on gold-film electrodes, 2015 37th Annual International Conference of the IEEE Engineering in Medicine and Biology Society (EMBC), 2015, pp. 7079-7082.

[44] C.M. Lo, C.R. Keese, I. Giaever 1995 Impedance analysis of MDCK cells measured by electric cell-substrate impedance sensing *Biophys. J.* **69** 2800-2807

[45] C.-M. Lo, J. Ferrier 1998 Impedance analysis of fibroblastic cell layers measured by electric cell-substrate impedance sensing *Physical Review E* **57** 6982-6987

[46] J. Wegener, S. Zink, P. Rösen, H.J. Galla 1999 Use of electrochemical impedance measurements to monitor β-adrenergic stimulation of bovine aortic endothelial cells *Pflügers Archiv* **437** 925-934

[47] N. Goda, Y. Yamamoto, N. Kataoka, T. Nakamura, T. Kusuhara, S. Mohri, K.

Naruse, F. Kajiya, Quantitative evaluation of nano-order micromotion of cultured cells using electric cell-substrate impedance sensing method, in: H. Scharfetter, R. Merwa (Eds.) 13th International Conference on Electrical Bioimpedance and the 8th Conference on Electrical Impedance Tomography, Springer Berlin Heidelberg, Berlin, Heidelberg, 2007, pp. 122-125.

[48] A.R.A. Rahman, C. Lo, S. Bhansali 2009 A Detailed Model for High-Frequency Impedance Characterization of Ovarian Cancer Epithelial Cell Layer Using ECIS Electrodes *IEEE Trans. Biomed. Eng.* **56** 485-492

[49] T. García-Sánchez, A. Azan, I. Leray, J. Rosell-Ferrer, R. Bragós, L.M. Mir 2015 Interpulse multifrequency electrical impedance measurements during electroporation of adherent differentiated myotubes *Bioelectrochemistry* **105** 123-135

[50] K. Pearson 1901 LIII. On lines and planes of closest fit to systems of points in space *The London, Edinburgh, and Dublin Philosophical Magazine and Journal of Science* **2** 559-572

[51] B. Lindholm-Sethson, S. Han, S. Ollmar, I. Nicander, G. Jonsson, F. Lithner, U. Bertheim, P. Geladi 1998 Multivariate analysis of skin impedance data in long-term type 1 diabetic patients *Chemometrics Intellig. Lab. Syst.* **44** 381-394

[52] M. Dabros, D. Dennewald, D.J. Currie, M.H. Lee, R.W. Todd, I.W. Marison, U. von Stockar 2008 Cole–Cole, linear and multivariate modeling of capacitance data for on-line monitoring of biomass *Bioprocess Biosystems Eng.* **32** 161

[53] I. Nejadgholi, M. Bolic 2015 A comparative study of PCA, SIMCA and Cole model for classification of bioimpedance spectroscopy measurements *Computers in Biology and Medicine* **63** 42-51

[54] R.M. Fuoss, J.G. Kirkwood 1941 Electrical Properties of Solids. VIII. Dipole Moments in Polyvinyl Chloride-Diphenyl Systems* *J. Am. Chem. Soc.* **63** 385-394

[55] F. Ciucci, C. Chen 2015 Analysis of Electrochemical Impedance Spectroscopy Data Using the Distribution of Relaxation Times: A Bayesian and Hierarchical Bayesian Approach *Electrochimica Acta* **167** 439-454

[56] K. Kobayashi, T.S.J.J.o.t.P.S.o.J. Suzuki 2018 Distribution of Relaxation Time Analysis for Non-ideal Immittance Spectrum: Discussion and Progress **87** 094002

[57] T. Hörlin 1998 Deconvolution and maximum entropy in impedance spectroscopy of noninductive systems *Solid State Ionics* **107** 241-253

[58] E. Tuncer, S.M. Gubanski 2001 On dielectric data analysis. Using the Monte Carlo method to obtain relaxation time distribution and comparing non-linear spectral function fits *IEEE Transactions on Dielectrics and Electrical Insulation* **8** 310-320

[59] A.B. Tesler, D.R. Lewin, S. Baltianski, Y. Tsur 2010 Analyzing results of impedance spectroscopy using novel evolutionary programming techniques *J. Electroceram.* **24** 245-260

[60] M. Saccoccio, T.H. Wan, C. Chen, F. Ciucci 2014 Optimal Regularization in Distribution of Relaxation Times applied to Electrochemical Impedance Spectroscopy: Ridge and Lasso Regression Methods - A Theoretical and Experimental Study *Electrochimica Acta* **147** 470-482

[61] F. Ciucci 2019 Modeling electrochemical impedance spectroscopy *Current Opinion in Electrochemistry* **13** 132-139

[62] T.H. Wan, M. Saccoccio, C. Chen, F. Ciucci 2015 Influence of the discretization methods on the distribution of relaxation times deconvolution: implementing radial basis functions with DRTtools *Electrochimica Acta* **184** 483-499

[63] X. Li, M. Ahmadi, L. Collins, S.V. Kalinin 2019 Deconvolving distribution of relaxation times, resistances and inductance from electrochemical impedance spectroscopy via statistical model selection: Exploiting structural-sparsity regularization and data-driven parameter tuning *Electrochimica Acta* **313** 570-583

[64] V. Sonn, A. Leonide, E. Ivers-Tiffée 2008 Combined Deconvolution and CNLS Fitting Approach Applied on the Impedance Response of Technical Ni/8YSZ Cermet Electrodes *Journal of The Electrochemical Society* **155** B675-B679

[65] J.P. Schmidt, T. Chrobak, M. Ender, J. Illig, D. Klotz, E. Ivers-Tiffée 2011 Studies on LiFePO4 as cathode material using impedance spectroscopy *J. Power Sources* **196** 5342-5348

[66] J. Illig, M. Ender, T. Chrobak, J.P. Schmidt, D. Klotz, E. Ivers-Tiffée 2012 Separation of charge transfer and contact resistance in LiFePO4-cathodes by impedance modeling *Journal of The Electrochemical Society* **159** A952-A960

[67] J.P. Schmidt, P. Berg, M. Schönleber, A. Weber, E. Ivers-Tiffée 2013 The distribution of relaxation times as basis for generalized time-domain models for Li-ion batteries *J. Power Sources* **221** 70-77

[68] H.G. Seo, Y. Choi, W.J.A.E.M. Jung 2018 Exceptionally Enhanced Electrode

Activity of (Pr, Ce) O2− δ-Based Cathodes for Thin-Film Solid Oxide Fuel Cells *Advanced Energy Materials* **8** 1703647

[69] R.G. Ramírez-Chavarría, C. Sanchez-Perez, D. Matatagui, N. Qureshi, A. Pérez-García, J. Hernandez-Ruiz 2018 Ex-vivo biological tissue differentiation by the Distribution of Relaxation Times method applied to Electrical Impedance Spectroscopy *Electrochimica Acta* **276** 214-222

Chapter 2 Publications

2.1 Bioimpedance Analysis of Epithelial Monolayers After Exposure to Nanosecond Pulsed Electric Fields

IEEE Transactions on Biomedical Engineering, 2019, 66(7): 2010-2021

DOI: http://dx.doi.org/10.1109/TBME.2018.2882299

Author contributions

Term	Definition	Author name
Conceptualization	Ideas; formulation or evolution of overarching research goals and aims	F. Shi, J. Zhuang, J. Kolb
Methodology	Development or design of methodology; creation of models	F. Shi
Software	Programming, software development; designing computer programs; implementation of the computer code and supporting algorithms; testing of existing code components	F. Shi, J. Zhuang
Validation	Verification, whether as a part of the activity or separate, of the overall replication/ reproducibility of results/experiments and other research outputs	F. Shi
Formal Analysis	Application of statistical, mathematical, computational, or other formal techniques to analyze or synthesize study data	F. Shi
Investigation	Conducting a research and investigation process, specifically performing the experiments, or data/evidence collection	F. Shi

Resources	Provision of study materials, reagents, materials, patients, laboratory samples, animals, instrumentation, computing resources, or other analysis tools	F. Shi
Data Curation	Management activities to annotate (produce metadata), scrub data and maintain research data (including software code, where it is necessary for interpreting the data itself) for initial use and later reuse	F. Shi
Writing – Original Draft	Preparation, creation and/or presentation of the published work, specifically writing the initial draft (including substantive translation)	F. Shi
Writing – Review & Editing	Preparation, creation and/or presentation of the published work by those from the original research group, specifically critical review, commentary or revision – including pre-or postpublication stages	F. Shi, A. Steuer, J. Kolb
Visualization	Preparation, creation and/or presentation of the published work, specifically visualization/ data presentation	F. Shi
Supervision	Oversight and leadership responsibility for the research activity planning and execution, including mentorship external to the core team	J. Zhuang, J. Kolb
Project Administration	Management and coordination responsibility for the research activity planning and execution	J. Kolb
Funding Acquisition	Acquisition of the financial support for the project leading to this publication	J. Kolb

Bioimpedance Analysis of Epithelial Monolayers After Exposure to Nanosecond Pulsed Electric Fields

Fukun Shi, *Student Member, IEEE*, Anna Steuer, Jie Zhuang, and Juergen F. Kolb, *Senior Member, IEEE*

***Abstract*—Exposures to pulsed electric fields (PEFs) are known to affect cell membranes and consequently also cell–cell interactions as well as associated characteristics. Bioimpedance analysis offers direct and non-invasive insights into structural and functional changes of cell membranes and extracellular matrices through a rigorous evaluation of electrical parameters. Accordingly, the multi-frequency impedance of confluent monolayers of rat liver epithelial WB-F344 cells was monitored *in situ* before and after exposure to nanosecond PEFs. The results were fitted by two Cole models in series to obtain the Cole parameters for the monolayer. For an interpretation of the results, dielectric parameters were correlated with changes of the TJ-protein zonula occludens (ZO-1) and the paracellular permeability of the monolayer. Cole parameters, in general, change as a function of pulse number and time. The findings demonstrate that impedance analysis is an effective method to monitor changes in cell–cell contacts and paracellular permeability and relate them to exposure parameters.**

***Index Terms*—Nanosecond pulsed electric fields, electroporation, bioimpedance, Cole model, tight junctions, paracellular permeability.**

I. Introduction

THE last decades have witnessed growing interest in using intense pulsed electric fields (PEFs) for biological and medical applications. PEF-exposures are considered intense when exposure parameters are sufficient to result in instant and nonlinear changes, in particular for cell membranes. Classical membrane permeabilization results from pulsed electric fields with durations of milliseconds to microseconds [1]–[3]. Accordingly, reversible electroporation is used in electrochemotherapy [4]–[9] and irreversible electroporation for straightforward tumor ablation [10]–[13]. More recently, PEFs of extreme field strength and ultrashort, nanosecond duration have been shown to manipulate intracellular functions [14], [15]. In particular, nanosecond pulsed electric field (nsPEF) exposures can induce apoptosis and are therefore being investigated as a novel tumor treatment method [16], [17].

In order to understand nsPEFs as a valid clinical therapy, interactions between nsPEFs and cells or tissues in general and with specific cell components in particular are crucial. The investigations of effects of nsPEFs on cell structures, such as cytoskeleton, membranes, and cell functions have so far mainly focused on studies for single cells [18]–[22], which were immersed in an electrolyte. However, cells in most *in vivo* conditions are surrounded by other cells that interact with each other and with a complex extracellular matrix. This situation is very different from cells suspended in the medium. Consequently, PEF-effects on connected cells, and in particular on associated membrane structures and components, can be expected to differ and involve mechanisms that cannot be observed for single cells. An overall tissue response might be significantly determined by these processes. Recent results from simulations furthermore suggest that the frequency dependence of the electric field (EF) penetration and cell responses were not the same for adherent cells in comparison with suspended cells [23].

The therapeutic potential of nsPEFs was demonstrated repeatedly on solid tumors *in vivo* [24], [25]. In this case, however, does the complex structure and nature of the tissue not readily permit to differentiate and investigate specific effects on cell membranes and cellular components. This appears to be a question for the study of an intermediate system, i.e., for exposures of cells that are grown in a monolayer. Since not all cell types form connections in confluent monolayers, model and cell lines have to be chosen carefully. Steuer *et al.* have reported an appropriate model of rat liver epithelial cell monolayers with WB-F344 cells, which was used to evaluate the transient inhibition of gap junctional intercellular communication (GIJC) after exposure to sub-lethal nsPEF-exposures [26]. GIJC is important for the regulation of cell proliferation and the formation of tissues. Another important connection between cells is provided by tight junctions (TJs) with vital roles in multicellular integrity, cell surface polarity, and separation of different compartments in tissues. TJs in epithelial and endothelial cells are mainly responsible for the formation and maintenance of a semipermeable diffusion

Manuscript received March 28, 2018; revised August 14, 2018; accepted November 8, 2018. Date of publication November 19, 2018; date of current version June 21, 2019. This work was supported by the Collaborative Research Center CRC 1270 funded by the German Research Foundation (DFG). The work of Fukun Shi was supported by the China Scholarship Council under contract 201506750010. *(Corresponding author: Juergen F. Kolb.)*

F. Shi and A. Steuer are with the Leibniz Institute for Plasma Science and Technology.

J. Zhuang is with the Suzhou Institute of Biomedical Engineering and Technology, Chinese Academy of Sciences.

J. F. Kolb is with the Leibniz Institute for Plasma Science and Technology, Greifswald 17489, Germany (e-mail: juergen.kolb@inp-greifswald.de).

Digital Object Identifier 10.1109/TBME.2018.2882299

barrier between cells [27]. Moreover, TJs were also proposed to be a frontline that cancer needs to overcome in metastasis [28]–[30]. Accordingly, the study of PEF-effects on cell-cell interactions is crucial for a better understanding of exposures and therapies.

The integrity of an epithelial monolayer can be determined by several approaches, including immunocytochemistry of tight junction proteins, microscopy of cell morphology and paracellular flux of fluorescent tracers [31]. These methods are generally time-consuming, label-based and irreversible. Alternative methods for the evaluation of the integrity of monolayers without these constraints are electrical measurements [32], [33]. Measurements of the trans-epithelial electrical resistance (TEER) evaluate the ohmic resistance of the cell layer that is measured by direct current (DC) or alternating current (AC) at a very low frequency [34]. However, the method has the drawbacks that results strongly depend on electrode configurations. Furthermore, cell-substrate interactions cannot be monitored and the methods in general have rather poor sensitivities with respect to changes of cell and monolayer morphologies. Limited to a resistance-analysis at very low frequencies only, information on cell constituents, which is contained in particular in higher frequency responses, is not available [35].

Electrical cell-substrate impedance sensing (ECIS) is another non-invasive, label-free, real-time electrical method for monitoring barrier functions, which was first reported by Tiruppathi *et al.* [36]. They have investigated the barrier function change of bovine pulmonary endothelial cells when exposed to α-thrombin. This and other methods that are exploiting impedance changes are based on evaluating different current pathways through the monolayer for different frequencies. High frequency AC stimuli are passing through the capacitive cell membranes and the associated measured impedance mainly reflects intracellular events. In contrast are low frequency currents bypassing cells and spreading through paracellular pathways which are dominated by tight junctions. Few studies so far have used impedance analysis for the investigation of PEF-effects on tissues. A study of PEF-effects on potatoes based on a Cole model confirmed that both the resistive part and the capacitive part of the model need to be taken into account to characterize permeabilization of tissue [37].

In this work, we explored changes of cell-to-cell interactions caused by nsPEFs by *in situ* bioimpedance measurements. The impedance was recorded before and after exposures to 8, 20 and 60 rectangular voltage pulses of 100 ns duration and about 20 kV/cm. Exposures to 8 and 20 pulses were considered mild and moderate, respectively. In contrast, the application of 60 pulses was regarded as intense exposure, which induced a considerable reduction in cell viability.

The results of impedance measurements were fitted into two Cole models in series, which allowed separation of electrode polarization and tissue response [38]. A Cole model is generally described by four independent parameters which can be related to different cell-cell interconnections and components [37], [39], [40]. In short: the resistance at very high frequency, R_∞, represents medium and intracellular resistance, the resistance at very low frequency, R_0, is correlated with the paracellular resistance, the characteristic relaxation time constant, τ, is related to membrane capacitance, and the 'dispersion width', α, describes the morphology of the extracellular spaces.

The bioimpedance analysis hence provides real-time monitoring of ongoing changes of the monolayer and cell membrane morphologies. Accordingly, development of the bioimpedance method and analysis might eventually afford a detailed diagnostic tool for the direct evaluation of PEF-treatments that is capable of predicting biological responses and therapeutic success.

II. Methodology

A. Cell Culture

The WB-F344 cell line was derived from a normal adult male Fischer 344 rat liver by J.W. Grisham and colleagues [41]. The WB-F344 culture was obtained from Prof. J. E. Trosko, Michigan State University, East Lansing, MI, USA. Cells were cultured in DMEM with 4.5 g/L glucose supplemented with 2 mM L-glutamine, 5% fetal calf serum (FCS) and 1% penicillin/streptomycin (all purchased from PAN-Biotech GmbH, Aidenbach, Germany). The osmolality of the medium was 325 mOsmol/kg (OSMOMAT 3000, Gonotec GmbH, Berlin, Germany). For the experiments, cells were seeded in ECIS-8W20idf plates (Applied Biophysics, Inc., Troy, NY, USA), which were pretreated with 10 mM L-cysteine 15 min before seeding to improve cell attachment [35]. Each well was filled with 300 µl cell culture medium and a cell seeding density of 5×10^4 cells, resulting in a confluent monolayer after 48 h of incubation. This was confirmed by a stable impedance observed at 20 kHz after 2 days of incubation, according to established procedures [42]. PEF-exposure was conducted after an additional 24 h of incubation when a stable tight junction performance was confirmed by impedance measurement. Each well of the 8W20idf plate included an interdigitated electrode array with a total electrode area of 3.985 mm^2. A relatively high number of cells (4,000-8,000) was found to smooth impedance fluctuations due to the possible micromotion of cells.

B. Pulsed Electric Field Exposures

ECIS-8W20idf electrode arrays were connected to an in-house built Blumlein transmission line square-wave pulse generator, delivering 100-ns rectangular voltage pulses across electrodes next to each other, as depicted in Fig. 1. A detailed description of the nsPEF-generator can be found elsewhere [26]. To monitor the applied electric pulses, a high voltage probe (P5100A, Tektronix, Beaverton, OR, USA) was connected to a fast oscilloscope (TDS3054, Tektronix, Beaverton, OR, USA). A number of 8, 20, and 60 consecutive 100-ns pulses, with a voltage of 330 V and a repetition rate of 1 Hz, was applied to the monolayer in full medium. For other experiments, 32 pulses with 165 V and 2 pulses with 660 V were applied, hence with the same energy as 8 pulses of 330 V. The energy was derived from the electrical energy density, $\Delta \mathrm{E} = \mathrm{N}\sigma E^2 \mathrm{T}$, where N is the pulse number, σ is the conductivity of the electrolyte, T the pulse duration and E is the electric field strength [43]. All experiments were conducted 15 min after taking the plates out of the incubator and allowing the samples to cool down to room temperature.

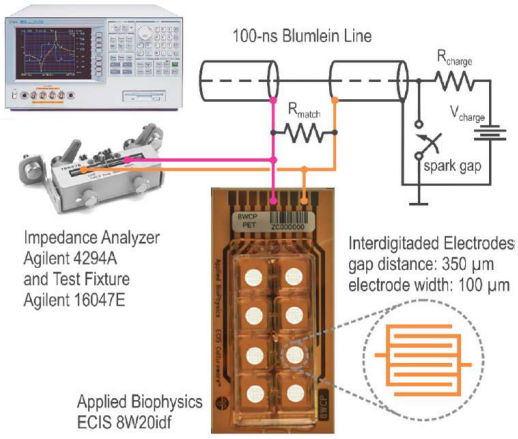

Fig. 1. Setup for nsPEF-application and impedance measurement. ECIS 8W20idf arrays were connected with a Blumlein line pulse generator for nsPEFs-exposure and subsequently with the impedance analyzer.

C. Impedance Measurements

Impedance measurements were performed with an Agilent 4294A impedance analyzer (Agilent Technologies Japan Ltd., Murotani, Kobeshinishiku, Japan) and with the same ECIS-chip used for stimulation before and after nsPEFs-exposure. The measurement started 1 min after exposure. Compared to conventional ECIS, the interdigitated electrode (IDE) offers the advantage that a large number of cells can be investigated and impedance fluctuations due to random cell movements are reduced [44]–[46]. The individual components of the experimental setup are shown in Fig. 1. The impedance analyzer, Agilent 4294A, was calibrated together with the test fixtures, Agilent 16047E, for open and short compensation according to operating instructions. As described by Rahman *et al.*, the amplitude of the AC voltage signal was 10 mV peak-to-peak to fulfill the linearity criteria of impedance spectroscopy [47]. The scanning frequency for the impedance measurement runs from 100 Hz to 10 MHz. However, to avoid the possible impact of parasitic capacities and inductivities in the high frequency range, data were only evaluated for a frequency range of 100 Hz to 500 kHz. Due to its resistive characteristic, the paracellular pathway dominates the ion transport that is underlying low frequency currents, while cell membranes exhibit a capacitance which allows high frequency currents to pass. Accordingly, ECIS offers the possibility to monitor barrier function and cell attachment.

D. Two-Cole System for Dielectric Characterization

The impedance data were fitted into a two-Cole system. The Cole equation is a common model to describe the dispersion of biological systems [48]. Two Cole elements in series, as shown in equation 1 and Fig. 2(a), were chosen to separate dispersions derived from electrode polarization (EP) and from adherent cells. The overall impedance of the system (monolayer and electrode effects) can be described according to [49]:

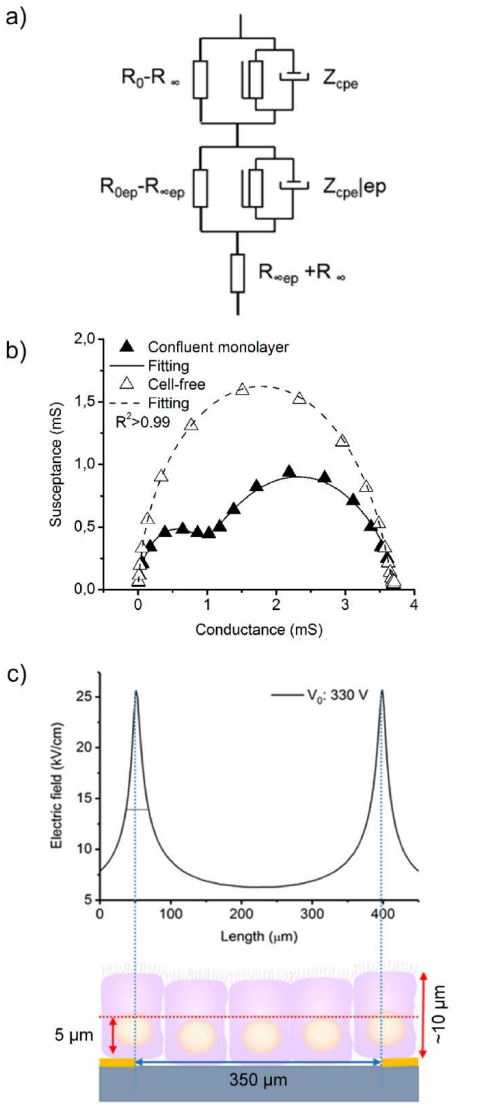

Fig. 2. Equivalent circuit model for the dielectric characterization of monolayers. Two Cole systems in series represent the two dispersions corresponding to electrode polarization (EP) and contributions from cells (a). Complex plane of admittance of cell-free and cell-covered electrodes before exposure (b). Simulation of the electric field strength 5 µm above the electrode surface (i.e., through the plane of the indicated cells in the monolayer) for an applied voltage of 330 V (c).

$$Z = Z_{ep} + Z_{cells} = \left[R_{\infty ep} + \frac{R_{0ep} - R_{\infty ep}}{1 + (i\omega\tau_{ep})^{\alpha_{ep}}}\right] + \left[R_{\infty} + \frac{R_0 - R_{\infty}}{1 + (i\omega\tau)^{\alpha}}\right] \quad (1)$$

where Z is the total impedance at frequency ω. Terms including a subscript 'ep' describe contributions from electrode polarization. Electrode polarization was characterized and validated from impedance measurements with medium only, i.e., without cells. The stability of parameters that are associated with electrode polarization, including R_{0ep}, $\alpha_{ep,}$ and τ_{ep}, was confirmed by measurements conducted for up to two days. The second bracket describes contributions from adherent cells. R_0 is the resistance at very low frequency, R_∞ is the resistance at infinite frequency, τ is the characteristic time constant and α is a dimensionless dispersion factor with values between 0 and 1. The term $(i\omega\tau)^\alpha$ is known as a constant phase element, Z_{cpe}. Since $R_{\infty ep}$ is rather small in comparison to R_∞, it can actually be neglected [38], [50] and the impedance, including electrode polarization and contribution from cells, can be expressed by:

$$Z = R_\infty + \frac{R_{0ep}}{1 + (i\omega\tau_{ep})^{\alpha_{ep}}} + \frac{R_0 - R_\infty}{1 + (i\omega\tau)^\alpha} \qquad (2)$$

The fitting of all parameters, by comparing measured and calculated impedance values, was conducted by non-linear least-squares regression analysis in MATLAB (MathWorks, Natick, MA, USA). Cole parameters were estimated with MATLAB's function *lsqnonlin* using the trust-region-reflective algorithm. Parameters were determined with the narrowest 95% confidence interval. A stochastic approach, e.g., as suggested by Merla and co-workers, would offer the advantage to evaluate potential correlations between parameters [51], [52]. This would be in particular interesting for different exposure parameters, e.g., pulse number and amplitudes. Conversely, the Cole parameters R_0, α, and τ are considered independent from each other [49], [53], [54]. Measurements and respective derivations of Cole parameters were repeated at least three times and are presented as mean values with standard deviations (error bars). Since electrode polarization is reflected by capacitive characteristics, the resistance at very low frequency should be rather large and the relaxation time for EP is several orders of magnitude higher than that for cells. This fact served as a guideline to separate contributions from EP and cells. The resistance of the monolayer at infinite frequency, R_∞, includes contributions from extra-cellular and intra-cellular medium, which do not change significantly under electrical stimulations. On the other hand, the resistance at very low frequency, R_0, represents in particular changes of the resistance of the extracellular matrix in the monolayer.

The admittance of the confluent monolayer is described in a Wessel diagram (Fig. 2(b)). Two semi-arcs are typical for a confluent monolayer, indicating two relaxation processes within the frequency range of the measurements. The left arc derives from electrode polarization while the other arc represents the cell-covered surface. Without cells, the admittance is determined by the medium and electrode polarization. The goodness of the fit between measurements and the numerical model was calculated by the function *goodnessOfFit* with the cost function of normalized root mean square error in MATLAB, showing coefficients of determination (R^2) larger than 0.98 for all estimations, some were even higher than 0.99 as indicated in Fig. 2(b). The fitting curve agrees well with the experimental data confirming that this is a suitable method to derive Cole parameters and compare respective effects for different external stimuli.

The electric field between conductive strips of the ECIS-chip is not homogeneous and the field strength in the gaps is rather low. The electric field distribution for electrodes covered with medium only, i.e., without cells, was evaluated based on a finite element method (Comsol Multiphysics® 5.3, Burlington, MA, USA) confirming that the electric field approaches its peak value along the edge of the electrode. The simulation was conducted in the electric current (ec) module of the AC/DC physics package. The electrical conductivity of the gold electrode was set to be 4.4×10^7 S/m, for the medium to be 1.7 S/m [55] and for polyethylene terephthalate (PET, the material of the ECIS substrate) to be 1×10^{-12} S/m [56]. With 9-15 µm are individual cells much smaller than the gap distance of 350 µm [57]. However, cells close to the edge of the electrodes are exposed to high electric fields, exceeding 10 kV/cm up to a distance of 100 µm, i.e., 6–11 µm cell diameters, and cells on the edge experience more than 20 kV/cm for an applied voltage of 330 V. Intense exposure along the edges of the electrodes was also verified by observed cell death. The field distribution for the voltage of 10 mV that is applied during the impedance analysis, is qualitatively similar. The comparison of impedance measurements for cell-free electrodes and for monolayers exposed to fatal nsPEFs, which only killed cells along the edges of the electrodes, confirms for both cases similar areas of interest (data not shown). A detailed spatially resolved and frequency dependent modeling of field distributions in the presence of an actual monolayer would require prior knowledge on dielectric parameters and their development, which to obtain is one of the goals of the study. From the simulation, the area of interest was determined to be about 15 µm wide along each side of the electrode. Fig. 2(c) depicts the electric field strength 5 µm above the electrode surface (along the dashed red line) for a voltage of 330 V applied between two electrodes. The height of the monolayer was assumed to be about 10 µm. The field strength along the edge of the electrodes peaks at about 25 kV/cm (blue dashed lines) and the field strength at the boundary of the area of interest is about 14 kV/cm. Accordingly, the average field strength in the area of interest was assumed to be on the order of 20 kV/cm which is also in agreement with observations for propidium iodide uptake and viability that were compared with experiments with more homogenous wire electrode exposure systems [26].

E. Immunofluorescence Staining

Localization of TJs was assessed by immunofluorescence staining of the tight junction protein zonula occludens, ZO-1, which connects transmembrane proteins and cytoskeleton [58]. WB-F344 cells were cultured on glass cover slips (#630-1597, 13 mm diameter, VWR, Darmstadt, Germany) until a confluent monolayer was obtained. In this case, rectangular voltage pulses of 100 ns were applied between two parallel stainless steel wire electrodes with a diameter of 1 mm and a gap distance of 0.5 cm that were pressed onto the monolayer. With an applied voltage of 10 kV from the Blumlein line, the electric field between the

wires is about 20 kV/cm except for higher values close to the wires [26]. Cells were fixed in 4% paraformaldehyde 30 min, 1 h and 3 h after exposure, and then permeabilized with 0.25% Triton X-100 in PBS. Subsequently, cells were blocked for 1 h with 3% BSA/PBS and afterward incubated overnight at 4°C with the primary antibody ZO-1 (QA213066, Life Technologies, Darmstadt Germany; 1:200 in 1% BSA/PBS). Next day, cells were incubated for 1 h with a secondary antibody conjugated with Alexa Fluor 546 (A-11035, Life Technologies; 1:1000). Finally, nuclei were stained with Hoechst 33342 and fluorescence was observed under a fluorescence microscope (AxioObserverD1, Carl Zeiss, Jena, Germany).

F. Permeability Assay

The integrity of the confluent monolayers before and after exposure to nsPEFs was assessed by a paracellular permeability assay according to Ghartey-Tagoe [59]. FITC (Fluorescein Isothiocyanate Labeled) conjugated with dextran of 70 kDa (Sigma-Aldrich, Merck, Germany) was chosen as a transporting marker since it is a membrane-impermeable fluorescence dye. WB-F344 cells were seeded with a density of 10^4 cells/cm^2 onto 12-mm transwell inserts with a 0.4-µm pore polyester membrane (Sigma-Aldrich, Merck, Germany). After two days, the apical cell culture medium in each insert was replaced by 500 µl medium supplemented with FITC-dextran (100 µg/ml) while the cell culture medium in the wells was not exchanged. Afterward, monolayers at the center of the insert were exposed between two parallel stainless-steel wire electrodes with a gap distance of 0.6 cm, and a length of 0.5 cm that were pressed onto the monolayer. The exposure area is thus 0.3 cm^2. Rectangular voltage pulses of 100 ns and 12 kV applied with the Blumlein line resulted in a fairly homogeneous electric field in the exposed area of about 20 kV/cm. The permeability of each monolayer was monitored 1.5 h prior to exposure until 5 h after exposure by transferring each insert every 30 min to a well with 700 µl fresh cell culture medium to maintain sink conditions. 100 µl basal solution from each well was analyzed for FITC-dextran concentration by means of a plate reader (Tecan F200, Männedorf, Switzerland; emission: 485 nm, excitation: 535 nm).

The apparent permeability, P_{app} (cm/s), was calculated by equation (3) based on Fick's first law [60].

$$P_{\mathrm{app}} = \frac{dC}{dt} \cdot \frac{1}{AC_0} \tag{3}$$

where dC/dt is the rate at which the marker appears in the receiver solution (mol/s), C_0 is the initial concentration of the apical solution (mol/ml), and A is the exposure area, which equals 0.3 cm^2. The derivative dC/dt is determined from the slope of the cumulative number of moles of FITC-dextran in the samples collected versus time. The paracellular permeability assay was conducted in triplicate for every set of exposure parameters and results are presented as mean values with standard deviations.

All impedance measurements for each exposure condition were replicated three times. The statistical significance (p-value) was evaluated by the paired-sample *t*-test in MATLAB (MathWorks, Natick, MA, USA).

III. Results

A. Bioimpedance Analysis

The temporal development of the Cole parameters for the investigated confluent monolayers exhibited different responses for a different number of pulses that were applied for otherwise similar exposure parameters. Fig. 3(a), 3(b) and 3(c) display the changes of R_0, α, and τ after exposures to electrical pulses of 330 V, respectively. Results were normalized to initial values before exposures. The values for the controls were not changing for the time of observation, except for a small decrease of R_0 after 30 min. R_0, α, and τ were especially dependent on the number of applied pulses.

Results for the resistance R_0 suggested a short-lived slight increase within about 1 min after exposure to 8 and 20 pulses (inset Fig. 3(a)). This short-lived increase was confirmed in every replication of the experiment although with no statistical significance ($p > 0.05$) for the averages. For later observation times, a fast drop of R_0 was recorded for all treatment conditions. The resistance was half that of the initial value within 1 h for cells treated with 60 pulses. For cells exposed to 20 pulses, R_0 decreased only by about 40%. For 20 and 60 pulses, the resistance of the monolayer started to recover 1 h after exposure and it took about 3 h for treatments with 20 pulses and about 7 h for cells treated with 60 pulses to approach values similar to unexposed monolayers again. The resistance R_0 of cells that were exposed to 8 pulses only dropped by about 20% before cells started to recover already within 30 min after exposure.

The dependency on pulse number was even more pronounced for the dispersion width α (Fig. 3(b)). Cells treated with 60 pulses reached a minimum value of about 70% of the initial value and started to recover 3 h after exposure. The minimum value of α for cells exposed to 20 pulses fell to about 76%; for cells treated with 8 pulses values dropped to about 89%. Recovery processes started within 1 h and 30 min, respectively. In contrast, the characteristic time constant τ increased after pulse exposure and maximum values for all pulse conditions were reached within 1 h for mild and moderate exposures, and within 3 h for intense exposures (Fig. 3(c)). The by far most pronounced effect was evident after the application of 60 pulses. In this case, τ increased about 11-fold before it dropped again to its initial value within 7 h. In comparison, after exposures to 20 pulses, the characteristic time constant increased only about 6-fold and had nearly completely recovered within 3 h after exposure. The application of 8 pulses had only a slight effect on τ with an about 2-fold increase at most.

B. Immunofluorescence of Tight Junction Protein ZO-1

For comparison with impedance measurements, WB-F344 monolayers were fixed and ZO-1 proteins were stained 30 min, 1 h and 3 h after exposure to 60 pulses with 330 V, according to the most pronounced impedance changes (Fig. 4). In

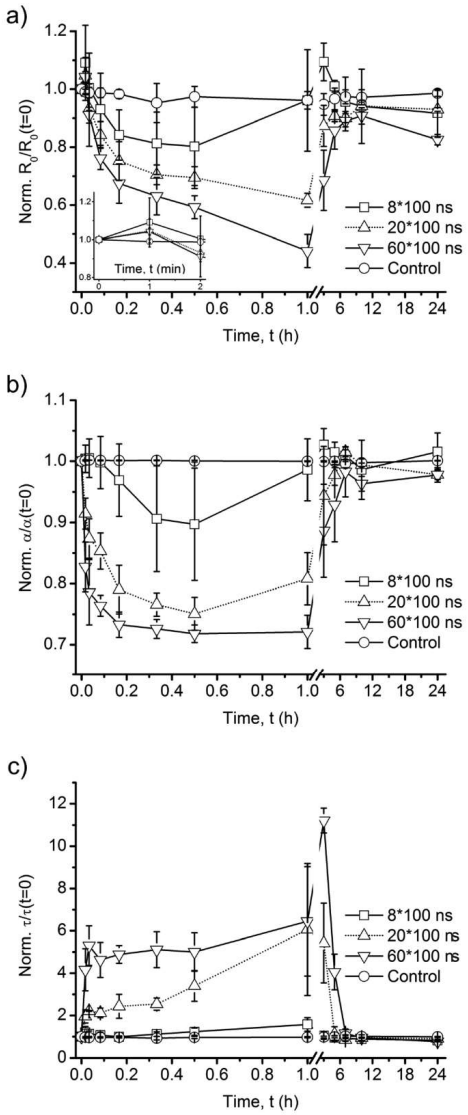

Fig. 3. Temporal development of the resistance at very low frequency, R_0 (a), the dimensionless dispersion parameter, α (b), and the characteristic time constant, τ (c) for monolayers exposed to 8, 20, and 60 rectangular voltage pulses of 100 ns duration and an amplitude of 330 V in comparison to controls. The inset in panel (a) shows the development of R_0 for the first two minutes.

control cells, ZO-1 formed a continuous border around cells with diffuse background fluorescence from the cytosol but no spot-like localized fluorescence indicating the protein (Fig. 4(d)). Within 30 min after application of 60 pulses, cells outlined by

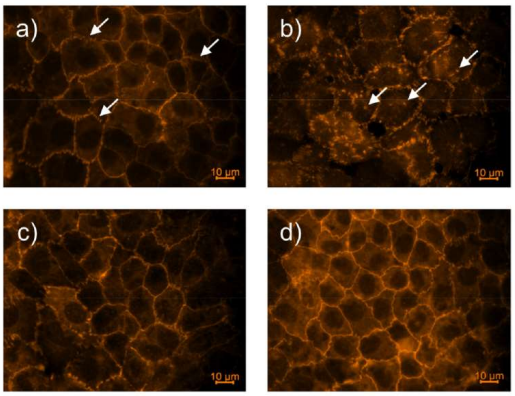

Fig. 4. Staining of tight junction protein ZO-1 in confluent WB-F344 monolayers 30 min (a), 1 h (b), and 3 h (c) after exposure to 60 rectangular voltage pulses of 100 ns duration and an amplitude of 330 V in comparison to control (d).

ZO-1 staining appeared ruffled and in some places interrupted by spots apparently without ZO-1 (Fig. 4(a), white arrows pointing out gaps). Still, no cytosolic ZO-1 was observed. Within 1 h after pulse application, TJs in the plasma membrane seemed almost completely disintegrated. Outlines of the cells were difficult to distinguish and ZO-1 proteins could be found in the cytosol (Fig. 4(b), white arrows pointing out protein in the cytosol). After an incubation time of 3 h, following exposure, TJs had partly recovered and images looked similar to results obtained 30 min after exposure. Marginal fluorescence indicates ZO-1 was still present in the cytosol (Fig. 4(c)).

C. Monolayer Permeability Assay

The assay of trans-epithelial transport of molecules through confluent WB-F344 monolayers, which is associated with disruption of TJs, was measured before and after application of 8, 20 and 60 rectangular voltage pulses of 100 ns for an applied voltage of 330 V (Fig. 5). The cumulative transport of FITC-dextran through the monolayer was measured every 30 min for 5 h after exposure (Fig. 5(a)). Control monolayers showed only a very slight increase of trans-epithelial molecular transport over time. While almost no marker transport through monolayers before exposure could be detected, the amount of trans-epithelial transported molecules of exposed monolayers increased after pulse application in a pulse number-dependent manner. Monolayers that were exposed to 8 pulses reached a saturation regarding the cumulative transport within 3.5 h after pulse application with a final value of barely 0.2 nmol. Much more dye molecules were transported through the monolayers within 5 h after the application of 20 and 60 pulses, with 0.4 and 0.95 nmol, respectively. The increase of the amount of trans-epithelial transported molecules over time was not linear. Furthermore, no linear correlation could be found between the cumulative transport and

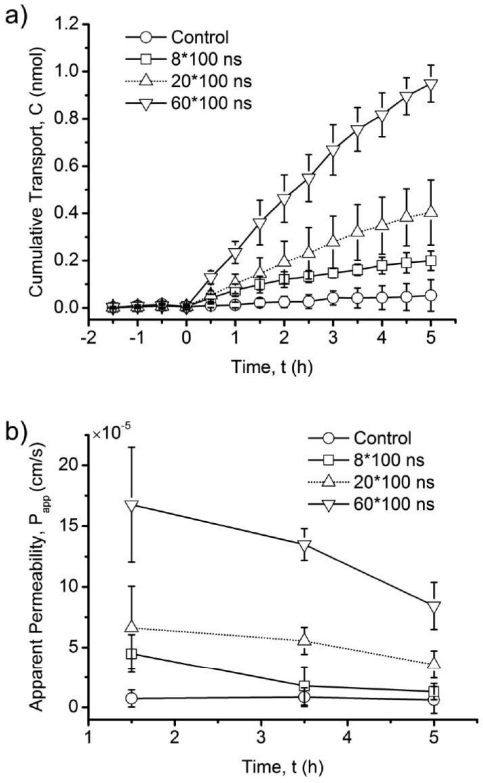

Fig. 5. Cumulative transport of dextran across monolayers before and after exposure to 8, 20, and 60 rectangular voltage pulses of 100 ns duration and an amplitude of 330 V (a), and the respective apparent permeabilities (b) compared to controls.

the number of applied pulses. The apparent permeability, P_{app}, which is based on the accumulation of FITC-dextran in the receiver solution, is shown in Fig. 5(b). Values for P_{app} were calculated for 1.5 h, 3.5 h and 5 h from the respective slopes as shown in Fig. 5(a), i.e., the increase up to 1.5 h, between 1.5 h and 3.5 h and from 3.5 h to 5 h, respectively. For control monolayers, P_{app} was quite stable at a value below 10^{-5} cm/s. In contrast, the marker appearance rate, P_{app}, increased to about $4.5{\cdot}10^{-5}$ cm/s, $6.6{\cdot}10^{-5}$ cm/s and $16.8{\cdot}10^{-5}$ cm/s for monolayers exposed to 8, 20 and 60 pulses, respectively, within 1.5 h after exposures. When compared to controls, FITC-dextran transport across monolayers hence increased 6-fold, 9-fold, and 23-fold for the application of 8, 20 and 60 pulses. Notable, monolayers exposed to 8 pulses recovered within 3.5 h and transport afterward was only about 2-fold higher than for controls. Conversely, the apparent permeability, P_{app}, decreased to just 83% and 80% of the initial values of monolayers exposed to 20 and 60 pulses after 3.5 h, respectively, and to about half of the initial value within 5 h.

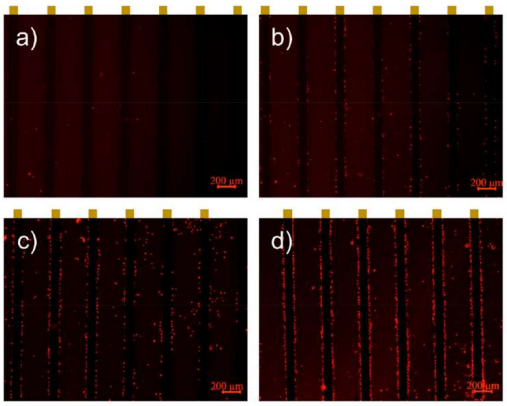

Fig. 6. PI uptake of control (a), and after exposure to 8 pulses (b), 20 pulses (c), and 60 pulses (d) of 100-ns duration and an amplitude of 330 V. The gold rectangles above each image and dark bands within the images indicate the position of the electrodes incorporated in the ECIS-chips.

D. Cell Membrane Permeability

Uptake of propidium iodide (PI) by cells exposed to electric fields is a common method to demonstrate cell membrane permeability. To conduct the assay, 3-μM PI in culture medium was incubated with cells 15 min before exposures. Afterward, the fluorescence of PI was observed 15 min after pulse application by a fluorescence microscope. PI uptake of a confluent monolayer without stimulation (control) is shown in Fig. 6(a). (All images were increased in brightness by 60% for better presentation.) PI uptakes of monolayers after exposure to 8, 20 and 60 pulses of 330 V are shown in Fig. 6(b), 6(c), and 6(d). The gold-colored rectangles above each figure indicate the positions of electrodes for the ECIS-chips and red fluorescent signals indicate cells with PI uptake. It can be seen that there is only a very limited number of cells positive for PI for controls, which indicates cells that are apparently already dead. After exposure to nsPEFs, the number of cells showing PI uptake and the respective intensity of fluorescence increased with increasing pulse number. PI-positive cells are mainly aligned along the edges of electrodes (dark bands in figures) corresponding to sufficiently high electric fields according to Fig. 2(c). In comparison to controls, there are only a few more cells showing PI uptake along edges of the electrodes after exposures to 8 pulses (Fig. 6(b)). The number of cells taking up PI increased considerably for exposures to 20 pules as shown in Fig. 6(c). After the application of 60 pulses, almost all cells along the edges of the electrodes exhibited PI uptake (Fig. 6(d)).

We also studied PI uptake by adding PI at 5, 10 and 15 min after application of 8, 20 and 60 pulses, respectively. For 8 and 20 pulses, PI-uptake was reduced in agreement with the possibility of reversible membrane poration during the first 15 minutes. Likewise, also for exposures to 60 pulses, a decrease in PI

uptake was observed but still a considerable number of cells exhibited PI (data not shown).

E. Comparison of Cole Parameters for Different Pulse Amplitudes but Same Delivered Energy

In order to expand the investigation of the effects of pulsed electric field exposures, 32 pulses of 165 V and 2 pulses of 660 V were applied in addition to exposures with 8 pulses of 330 V. Accordingly, the same energy was provided for all treatment options. The evolution of the Cole parameters over a time of 7 h after exposure is depicted in Fig. 7. In general, all three treatments resulted in similar changes of the Cole parameters with distinct differences especially observed within the first 5 min after pulse application. Resistance R_0 (Fig. 7(a)) appeared to transiently increase within 1 min. For 8 pulses of 330 V an increase of ∼9% was observed 1 min after exposure that is followed by dropping resistance values. In contrast, 32 pulses of 165 V and 2 pulses of 660 V both resulted in a similar lasting increase of R_0 of ∼12% and ∼5%, respectively. A significant decrease of resistance values below initial values started at about 5 min after exposures. For all exposure conditions, R_0 continued to decrease for up to 20–30 min altogether until resistance started to recover. After 2 h the resistance eventually even exceeded initial values. The largest increase was observed 2 h after exposures with 10%, 14% and 10% after the application of 32 pulses of 165 V, 8 pulses of 330 V and 2 pulses of 660 V, respectively. Afterward, R_0 moderately dropped again within the next 2-3 h.

The dimensionless dispersion width parameter α showed a development similar to the resistance R_0 (Fig. 7(b)). However, an initial increase of the parameter was not observed and α started to fall off instantly after exposure. The most significant decrease of 14%, for 32 pulses of 165 V, was observed 30 min after exposure. Values of α dropped by about 11% from the initial measurement 30 min after exposure to either 8 pulses of 330 V or 2 pulses of 660 V. Then α gradually recovered and regained values comparable to pre-exposure conditions 3 h after pulse application with little change of these values thereafter.

A different development is observed for the time constant τ (Fig. 7(c)). Immediately after exposure, time constants were increasing. Peak values that were obtained 1 h after exposure to 32 pulses of 165 V were on average ∼2.7 times larger than pre-exposure values. For 2 pulses of 660 V and 8 pulses of 330 V were values for τ ∼1.5 times larger 1 h after exposure. From the peak values, time constants gradually decreased towards their initial values within 5 h after exposure. Altogether, average values for different time points for the comparison of these exposure protocols are afflicted by considerable errors. However, individual repetition of experiments unambiguously always showed the same general trend.

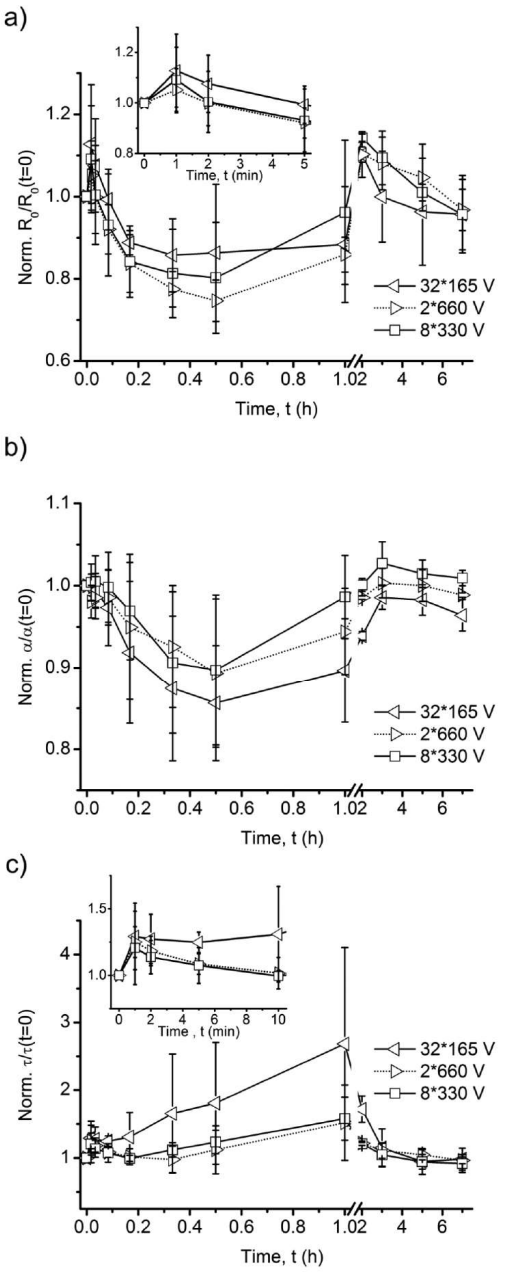

Fig. 7. Development of Cole parameters after exposure to different numbers of rectangular voltage pulses of 100-ns duration and with the same energy but different amplitudes (32 pulses of 165 V, 8 pulses of 330 V, 2 pulses of 660 V). Resistance at very low frequency, R_0 (a), Cole parameter, α, (b), and time constant, τ (c). The insets in panels (a) and (c) show the development of R_0 for the first five minutes and of τ for the first ten minutes, respectively.

IV. Discussion

Bioimpedance analysis is a powerful tool to obtain information about structural and functional changes of cell membranes

uptake was observed but still a considerable number of cells exhibited PI (data not shown).

E. Comparison of Cole Parameters for Different Pulse Amplitudes but Same Delivered Energy

In order to expand the investigation of the effects of pulsed electric field exposures, 32 pulses of 165 V and 2 pulses of 660 V were applied in addition to exposures with 8 pulses of 330 V. Accordingly, the same energy was provided for all treatment options. The evolution of the Cole parameters over a time of 7 h after exposure is depicted in Fig. 7. In general, all three treatments resulted in similar changes of the Cole parameters with distinct differences especially observed within the first 5 min after pulse application. Resistance R_0 (Fig. 7(a)) appeared to transiently increase within 1 min. For 8 pulses of 330 V an increase of ∼9% was observed 1 min after exposure that is followed by dropping resistance values. In contrast, 32 pulses of 165 V and 2 pulses of 660 V both resulted in a similar lasting increase of R_0 of ∼12% and ∼5%, respectively. A significant decrease of resistance values below initial values started at about 5 min after exposures. For all exposure conditions, R_0 continued to decrease for up to 20–30 min altogether until resistance started to recover. After 2 h the resistance eventually even exceeded initial values. The largest increase was observed 2 h after exposures with 10%, 14% and 10% after the application of 32 pulses of 165 V, 8 pulses of 330 V and 2 pulses of 660 V, respectively. Afterward, R_0 moderately dropped again within the next 2-3 h.

The dimensionless dispersion width parameter α showed a development similar to the resistance R_0 (Fig. 7(b)). However, an initial increase of the parameter was not observed and α started to fall off instantly after exposure. The most significant decrease of 14%, for 32 pulses of 165 V, was observed 30 min after exposure. Values of α dropped by about 11% from the initial measurement 30 min after exposure to either 8 pulses of 330 V or 2 pulses of 660 V. Then α gradually recovered and regained values comparable to pre-exposure conditions 3 h after pulse application with little change of these values thereafter.

A different development is observed for the time constant τ (Fig. 7(c)). Immediately after exposure, time constants were increasing. Peak values that were obtained 1 h after exposure to 32 pulses of 165 V were on average ∼2.7 times larger than pre-exposure values. For 2 pulses of 660 V and 8 pulses of 330 V were values for τ ∼1.5 times larger 1 h after exposure. From the peak values, time constants gradually decreased towards their initial values within 5 h after exposure. Altogether, average values for different time points for the comparison of these exposure protocols are afflicted by considerable errors. However, individual repetition of experiments unambiguously always showed the same general trend.

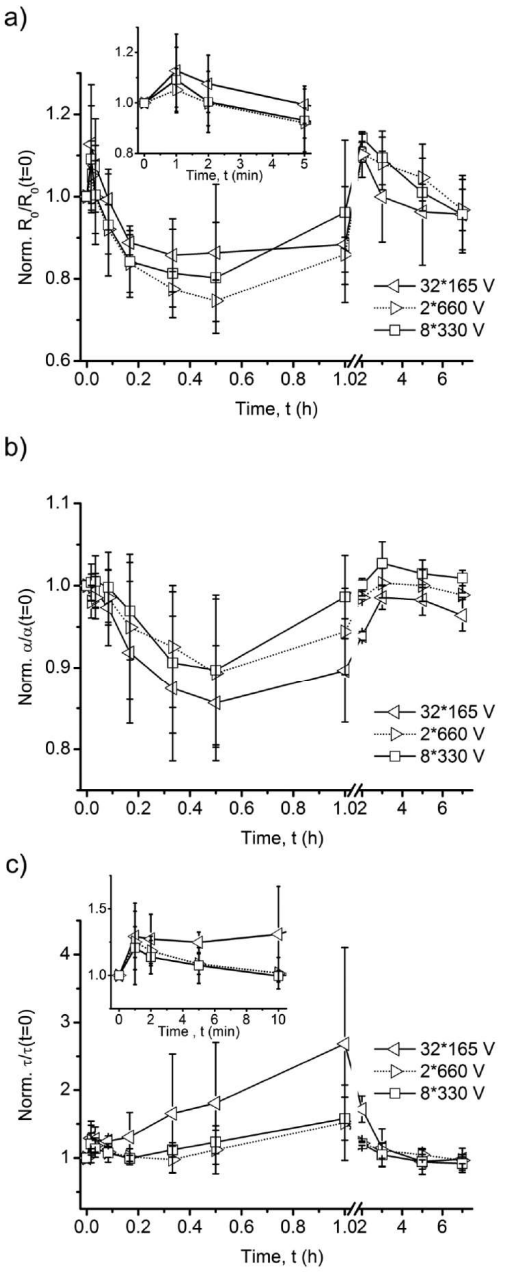

Fig. 7. Development of Cole parameters after exposure to different numbers of rectangular voltage pulses of 100-ns duration and with the same energy but different amplitudes (32 pulses of 165 V, 8 pulses of 330 V, 2 pulses of 660 V). Resistance at very low frequency, R_0 (a), Cole parameter, α, (b), and time constant, τ (c). The insets in panels (a) and (c) show the development of R_0 for the first five minutes and of τ for the first ten minutes, respectively.

IV. Discussion

Bioimpedance analysis is a powerful tool to obtain information about structural and functional changes of cell membranes

capacitance as well as intra- and extracellular conductivities. Values increased immediately after exposures, indicating pathways between and through cell membranes and water incorporated into membranes, e.g., in pores (Fig. 5), hence changing membrane capacitance [64]. However, the interpretation of Cole parameters should be more carefully evaluated for a high level of permeabilization [37], in particular for the highly heterogeneous permeabilization as a consequence of the underlying inhomogeneous electric field distribution for impedance measurements (Fig. 2(c)).

The large increase of τ observed for the intense exposure in Fig. 3(c) is presumably only in part related to changes of membrane capacitances and probably more significantly to a more extensive overall permeabilization across the monolayer. Water that is incorporated in the gaps in the monolayer is probably contributing accordingly. Nevertheless, mild exposures resulted in a lower permeabilization and no cell death. In this case, the increase of τ is much smaller and reflects cell membrane conductivities and capacitance more directly.

However, cell membrane related effects cannot completely explain the large increase of τ several tens of minutes after exposures. At this time, cell membranes have generally already resealed. Extending the discussion on changes of R_0, we hypothesize that τ is not only related to cell membrane capacitance but also the cohesion of cells in the monolayer which is foremost sustained by tight junctions [62]. The disruption of tight junctions might have increased the membrane capacitance and consequently the value of τ.

C. Changes of the Dispersion Width, α

Cole parameter α shows noticeable differences between before and after exposures and differences were markedly increased according to the pulse number. Genesca *et al.* argued that α reflects the morphology of the extracellular spaces [61]. In their study, they found that the detachment between tubule cells was accompanied by a decrease of α. In another investigation, a drug of Swinholide, which acts mainly on the cytoskeleton, was used to decrease α without significantly affecting other Cole parameters [39]. The evolution of α was found related to changes of cell morphology as a secondary effect of the disassembly of the cytoskeleton. Associated constrictions or imperfections of the extracellular spaces will then result in a decrease of α.

A reason for the decrease of α could be the disruption of TJs, introducing defects in the morphology of the extracellular spaces. This assumption is in agreement with changes of TJs observed by ZO-1 staining, together with the decrease of R_0 and the increase of the paracellular permeability, P_{app}. In Fig. 5(b), the largest change of the apparent permeability occurred 1.5 h after intense exposure, consistent with timelines observed for TJ-staining. Afterward, P_{app} decreased gradually, suggesting that the barrier for the diffusion resealed, in other words, TJs recovered simultaneously. The minimum of α was attained at 1 h after moderate and intense exposure, which was also the time when the most significant disruption of TJs (Fig. 4) and the largest value of P_{app} were recorded. ZO-1 lost continuity within 1 h after and partly recovered within 3 h after exposure as shown in Fig. 4.

Another mechanism constricting extracellular spaces and decreasing α is the change of cell morphology, such as cell swelling, which was not observed in the plane of the monolayer, but could have changed cell heights. Cell morphology is furthermore greatly dependent on the stabilization by the actin cytoskeleton and membrane elasticity [65]. Therefore, changes of the cellular membrane elasticity and cytoskeleton after exposure to 100-ns PEFs, which have been observed in WB-F344 by Steuer *et al.* [66], could also contribute to the changes of the extracellular spaces, which is then reflected by the decrease of α.

D. Analysis of Dose Dependency of nsPEF Effects

To investigate dose–dependent effects of nsPEFs on cell-cell interactions, different electric field strengths were administered with pulse numbers that in total deliver the same energy. Exposures with 32 pulses of 165 V and 2 pulses of 660 V were administered, resulting in electric field strengths of about 10 kV/cm and 40 kV/cm along the electrode-edges (Fig. 2(c)), respectively, and compared with exposures to 8 pulses of 330 V, corresponding to 20 kV/cm. For all conditions did the resistance at very low frequency more or less and transiently increase within the first 5 min after exposures (inset Fig. 7(a)) and the monolayer integrity was subsequently reduced within 30 min after exposures (Fig. 7(a)). R_0 started to recover 1 h after exposures, suggesting the recovery of monolayer integrity. Dispersion width, α, as well as the time constant, τ, recovered within 3 h after exposures, demonstrating the recovery of the extracellular spaces. In particular, τ derived for 32 pulses of 165 V showed much larger changes in magnitude than for the other 2 exposure conditions. In all cases was the overall trend the same. However, taking the high heterogeneity of the electric field distribution of the electrode configuration into account, an actual dose-dependency could not be confirmed.

V. Conclusion and Outlook

Impedance analysis combined with a Cole model is an effective real-time and essentially non-invasive method for the investigation of pulsed electric field effects on monolayers and accordingly potentially also for the evaluation of *in vivo* treatments. Cole parameters can be related to morphological and functional changes and provide a more refined understanding of underlying mechanisms. Based on the analysis, we can conclude that nsPEF-exposures lead to changes of paracellular pathways and subsequently the decrease of R_0. In particular, intense exposures reduce cell viability and hence promote the transmonolayer pathway.

Changes of the monolayer integrity are not only reflected in the decrease of low frequency resistance, R_0. Dispersion width, α, and relaxation time constant, τ, relate to associated changes of the morphology of the extracellular spaces and cell membrane permeabilization. Especially α correlates with changes of cell-cell interactions. Furthermore, Cole parameters offer the possibility to differentiate between different phenomena and to evaluate quantitatively changes of electrical properties of

cells after exposure to nsPEFs. Improvements of the experimental design, e.g., a more homogeneous exposure system, would increase the accuracy of results. Moreover, inducing known biological effects, e.g., by chemical treatments instead with electrical stimuli could assist the interpretation and validation of bioimpedance data. Eventually, a dedicated further development of the method might provide a monitoring system for clinical therapies with a real-time feedback not only for pulsed electric field applications but for other therapies as well.

ACKNOWLEDGMENT

Fukun Shi would especially like to thank Yining Xu from the Université Catholique de Louvain for useful discussions.

REFERENCES

[1] M. Marty *et al.*, "Electrochemotherapy—An easy, highly effective and safe treatment of cutaneous and subcutaneous metastases: Results of ESOPE (European Standard Operating Procedures of Electrochemotherapy) study," *Eur. J. Cancer Suppl.*, vol. 4, no. 11, pp. 3–13, 2006.

[2] L. M. Mir *et al.*, "Standard operating procedures of the electrochemotherapy: Instructions for the use of bleomycin or cisplatin administered either systemically or locally and electric pulses delivered by the Cliniporator (TM) by means of invasive or non-invasive electrodes," *Eur. J. Cancer Suppl.*, vol. 4, no. 11, pp. 14–25, 2006.

[3] J. Kulbacka *et al.*, "The effect of millisecond pulsed electric fields (msPEF) on intracellular drug transport with negatively charged large nanocarriers made of solid lipid nanoparticles (SLN): In vitro study," *J. Membrane Biol.*, vol. 249, no. 5, pp. 645–661, 2016.

[4] C. Y. Calvet and L. M. Mir, "The promising alliance of anti-cancer electrochemotherapy with immunotherapy," *Cancer Metastasis Rev.*, vol. 35, no. 2, pp. 165–177, 2016.

[5] C. Cabula *et al.*, "Electrochemotherapy in the treatment of cutaneous metastases from breast cancer: A multicenter cohort analysis," *Ann. Surg. Oncol.*, vol. 22, pp. S442–S450, 2015.

[6] T. Dolinsek *et al.*, "Electrochemotherapy with bleomycin is effective in BRAF mutated melanoma cells and interacts with BRAF inhibitors," *Radiol. Oncol.*, vol. 50, no. 3, pp. 274–279, 2016.

[7] G. Bianchi *et al.*, "Electrochemotherapy in the treatment of bone metastases: A Phase II trial," *World J. Surg.*, vol. 40, no. 12, pp. 3088–3094, 2016.

[8] G. Sersa *et al.*, "Electrochemotherapy of tumors as in situ vaccination boosted by immunogene electrotransfer," *Cancer Immunol. Immunotherapy*, vol. 64, no. 10, pp. 1315–1327, 2015.

[9] N. Goda *et al.*, "Evaluation of micromotion of vascular endothelial cells in electrical cell-substrate impedance sensing (ECIS) method using a mathematical model," *J. Mech. Med. Biol.*, vol. 5, no. 02, pp. 357–368, 2005.

[10] E. Cabuy, "Pulsed electric fields in cancer treatment," *Reliable Cancer Therapies, Energy-Based Therapies*, vol. 5, no. 2, pp. 1–30, 2012.

[11] R. V. Davalos *et al.*, "Tissue ablation with irreversible electroporation," *Ann. Biomed. Eng.*, vol. 33, no. 2, pp. 223–231, 2005.

[12] J. F. Edd *et al.*, "In vivo results of a new focal tissue ablation technique: Irreversible electroporation," *IEEE Trans. Biomed. Eng.*, vol. 53, no. 7, pp. 1409–1415, Jul. 2006.

[13] N. Goda *et al.*, "Quantitative evaluation of micromotion of cultured cells using electrical cell-substrate impedance sensing (ECIS) method-cell-to-cell distance and cell-to-substrate distance," 岡山大学医学部保健学科紀要, vol. 17, no. 1, pp. 9–15, 2007.

[14] R. Nuccitelli *et al.*, "Nanosecond pulsed electric fields cause melanomas to self-destruct," *Biochem. Biophys. Res. Commun.*, vol. 343, no. 2, pp. 351–360, 2006.

[15] K. H. Schoenbach *et al.*, "Intracellular effect of ultrashort electrical pulses," *Bioelectromagnetics*, vol. 22, no. 6, pp. 440–448, 2001.

[16] M. S. Markov and R. Nuccitelli, "Nanoelectroporation for nonthermal ablation," in *Electromagnetic Fields in Biology and Medicine*. Boca Raton, FL, USA: CRC Press, 2015, pp. 383–394.

[17] R. Nuccitelli, "Tissue ablation using nanosecond electric pulses," in *Handbook of Electroporation*, D. Miklavcic, Ed. Cham: Springer International Publishing, 2016, pp. 1–11.

[18] O. M. Nesin *et al.*, "Manipulation of cell volume and membrane pore comparison following single cell permeabilization with 60- and 600-ns electric pulses," *Biochimica et Biophysica Acta (BBA)—Biomembranes*, vol. 1808, no. 3, pp. 792–801, 2011.

[19] A. G. Pakhomov, B. L. Ibey, A. M. Bowman, F. M. Andre, and O. N. Pakhomova, "Nanosecond-duration electric pulses open nanometer-size pores in cell plasma membrane," *World Congress on Medical Physics and Biomedical Engineering, September 7-12, 2009, Munich, Germany* (IFBME Proceedings 2010, 25/13), Berlin, Germany: Springer, 2010, pp. 17–20, 10.1007/978-3-642-03895-2.

[20] M. Stacey *et al.*, "Nanosecond pulsed electric field induced cytoskeleton, nuclear membrane and telomere damage adversely impact cell survival," *Bioelectrochemistry*, vol. 82, no. 2, pp. 131–134, 2011.

[21] R. P. Joshi *et al.*, "Modeling studies of cell response to ultrashort, high-intensity electric fields-implications for intracellular manipulation," *IEEE Trans. Plasma Sci.*, vol. 32, no. 4, pp. 1677–1686, Aug. 2004.

[22] X. Chen *et al.*, "Histopathology of normal skin and melanomas after nanosecond pulsed electric field treatment," *Melanoma Res.*, vol. 19, no. 6, 2009, Art. no. 361.

[23] T. Taghian *et al.*, "Modulation of cell function by electric field: a high-resolution analysis," *J. Royal Soc. Interface*, vol. 12, no. 107, 2015, Art. no. 20150153.

[24] Y. Magori *et al.*, "In vivo experiment of applying nanosecond pulsed electric fields on solid tumor," in *Proc. IEEE Pulsed Power Conf.*, 2011, pp. 1253–1257.

[25] S. J. Beebe *et al.*, "Diverse effects of nanosecond pulsed electric fields on cells and tissues," *DNA Cell Biol.*, vol. 22, no. 12, pp. 785–796, 2003.

[26] A. Steuer *et al.*, "Transient suppression of gap junctional intercellular communication after exposure to 100-nanosecond pulsed electric fields," *Bioelectrochemistry*, vol. 112, pp. 33–46, 2016.

[27] K. Matter and M. S. Balda, "Functional analysis of tight junctions," *Methods*, vol. 30, no. 3, pp. 228–234, 2003.

[28] M. Tracey A *et al.*, "Cancer invasion and metastasis: Molecular and cellular perspective," in *Metastatic Cancer Clinical and Biological Perspectives,* A. T. L. Bioscience, Ed., Austin, TX, USA: Landes Bioscience, 2013.

[29] T. A. Martin and W. G. Jiang, *Tight Junctions in Cancer Metastasis*. New York, NY, USA: Springer-Verlag, 2013.

[30] T. A. Martin and W. G. Jiang, "Loss of tight junction barrier function and its role in cancer metastasis," *Biochimica et Biophysica Acta (BBA)—Biomembranes*, vol. 1788, no. 4, pp. 872–891, 2009.

[31] M. Strengert and U. G. Knaus, "Analysis of epithelial barrier integrity in polarized lung epithelial cells," in *Permeability Barrier: Methods and Protocols*, K. Turksen, Ed. Totowa, NJ, USA: Humana Press, 2011, pp. 195–206.

[32] I. Giaever and C. R. Keese, "Use of electric fields to monitor the dynamical aspect of cell behavior in tissue culture," *IEEE Trans. Biomed. Eng.*, vol. BME-33, no. 2, pp. 242–247, Feb. 1986.

[33] B. H. Brown *et al.*, "Cardiac and respiratory related electrical impedance changes in the human thorax," *IEEE Trans. Biomed. Eng.*, vol. 41, no. 8, pp. 729–734, Aug. 1994.

[34] E. B. Ghartey-Tagoe, "Electroporation-mediated delivery of macromolecules to intestinal epithelial models," Ph.D. dissertation, Georgia Inst. Technol., Atlanta, GA, USA, Georgia Tech Theses and Dissertations, 2004. [Online]. Available: http://hdl.handle.net/1853/5130.

[35] R. Szulcek, H. J. Bogaard, and G. P. van Nieuw Amerongen, "Electric cell-substrate impedance sensing for the quantification of endothelial proliferation, barrier function, and motility," *J. Visualized Exp.*, vol. 85, 2014, Art. no. e51300, doi: 10.3791/51300.

[36] C. Tiruppathi *et al.*, "Electrical method for detection of endothelial cell shape change in real time: Assessment of endothelial barrier function," *Proc. Nat. Acad. Sci.*, vol. 89, no. 17, pp. 7919–7923, 1992.

[37] C. Trainito *et al.*, "Analysis of pulsed electric field effects on cellular tissue with Cole–Cole model: Monitoring permeabilization under inhomogeneous electrical field with bioimpedance parameter variations," *Innov. Food Sci. Emerg. Technol.*, vol. 29, pp. 193–200, 2015.

[38] H. Kalvøy *et al.*, "New method for separation of electrode polarization impedance from measured tissue impedance," *Open Biomed. Eng. J.*, vol. 5, pp. 8–13, 2011.

[39] A. Ivorra *et al.*, "Bioimpedance dispersion width as a parameter to monitor living tissues," *Physiol. Meas.*, vol. 26, no. 2, pp. S165–S173, 2005.

[40] A. Ivorra and B. Rubinsky, "In vivo electrical impedance measurements during and after electroporation of rat liver," *Bioelectrochemistry*, vol. 70, no. 2, pp. 287–295, 2007.

[41] M.-S. Tsao *et al.*, "A diploid epithelial cell line from normal adult rat liver with phenotypic properties of 'oval' cells," *Exp. Cell Res.*, vol. 154, no. 1, pp. 38–52, 1984.
[42] K. Benson *et al.*, "Impedance-based cell monitoring: Barrier properties and beyond," *Fluids Barriers CNS*, vol. 10, no. 1, 2013, Art. no. 5.
[43] K. H. Schoenbach *et al.*, "A scaling law for membrane permeabilization with nanopulses," *IEEE Trans. Dielect. Elect. Insul.*, vol. 16, no. 5, pp. 1224–1235, Oct. 2009.
[44] J. Aman *et al.*, "Effective treatment of edema and endothelial barrier dysfunction with imatinib," *Circulation*, vol. 126, no. 23, pp. 2728–2738, 2012.
[45] D. Tasev *et al.*, "CD34 expression modulates tube-forming capacity and barrier properties of peripheral blood-derived endothelial colony-forming cells (ECFCs)," *Angiogenesis*, vol. 19, pp. 325–338, 2016.
[46] R. Wiltshire *et al.*, "Regulation of human cerebro-microvascular endothelial baso-lateral adhesion and barrier function by S1P through dual involvement of S1P1 and S1P2 receptors," *Sci. Rep.*, vol. 6, 2016, Art no. 19814.
[47] A. R. A. Rahman *et al.*, "A detailed model for high-frequency impedance characterization of ovarian cancer epithelial cell layer using ECIS electrodes," *IEEE Trans. Biomed. Eng.*, vol. 56, no. 2, pp. 485–492, Feb. 2009.
[48] R. Pradhan *et al.*, "Characterization of electrode/electrolyte interface of ECIS devices," *Electroanalysis*, vol. 24, no. 12, pp. 2405–2414, 2012.
[49] S. Grimnes and Ø. G. Martinsen, "Chapter 9—data and models," in *Bioimpedance and Bioelectricity Basics*, 3rd ed. Oxford, U.K.: Academic Press, 2015, pp. 329–404.
[50] P. Mirtaheri *et al.*, "Electrode polarization impedance in weak NaCl aqueous solutions," *IEEE Trans. Biomed. Eng.*, vol. 52, no. 12, pp. 2093–2099, Dec. 2005.
[51] C. Merla *et al.*, "A 3-D microdosimetric study on blood cells: A permittivity model of cell membrane and stochastic electromagnetic analysis," *IEEE Trans. Microw. Theory Techn.*, vol. 58, no. 3, pp. 691–698, Mar. 2010.
[52] A. Denzi *et al.*, "Assessment of cytoplasm conductivity by nanosecond pulsed electric fields," *IEEE Trans. Biomed. Eng.*, vol. 62, no. 6, pp. 1595–1603, Jun. 2015.
[53] J. Chen *et al.*, "A comparison between Gauss–Newton and Markov-chain Monte Carlo-based methods for inverting spectral induced-polarization data for Cole–Cole parameters," *Geophysics*, vol. 73, no. 6, pp. F247–F259, 2008.
[54] A. Ghorbani *et al.*, "Bayesian inference of the Cole–Cole parameters from time-and frequency-domain induced polarization," *Geophys. Prospecting*, vol. 55, no. 4, pp. 589–605, 2007.
[55] J. Cure, "Cancer an electrical phenomenon," *Resonant*, 1991. [Online]. Available: http://refhub.elsevier.com/S0304-3835(15)00770-3/sr0155
[56] M. Al Ahmad *et al.*, "Electrical characterization of normal and cancer cells," *IEEE Access*, vol. 6, pp. 25979–25986, 2018.
[57] D. G. Phinney, *Adult Stem Cells: Biology and Methods of Analysis*. Berlin, Germany: Springer Science & Business Media, 2011.
[58] A. S. Fanning *et al.*, "The tight junction protein ZO-1 establishes a link between the transmembrane protein occludin and the actin cytoskeleton," *J. Biol. Chem.*, vol. 273, no. 45, pp. 29745–29753, 1998.
[59] E. B. Ghartey-Tagoe *et al.*, "Increased permeability of intestinal epithelial monolayers mediated by electroporation," *J. Controlled Release*, vol. 103, no. 1, pp. 177–190, 2005.
[60] G. L. Amidon *et al.*, *Transport Processes in Pharmaceutical Systems*. Boca Raton, FL, USA: CRC Press, 1999.
[61] M. Genesca *et al.*, "Electrical bioimpedance measurement during hypothermic rat kidney preservation for assessing ischemic injury," *Biosensors Bioelectron.*, vol. 20, no. 9, pp. 1866–1871, 2005.
[62] T. Gowrishankar and J. C. Weaver, "Electrical behavior and pore accumulation in a multicellular model for conventional and supra-electroporation," *Biochem. Biophys. Res. Commun.*, vol. 349, no. 2, pp. 643–653, 2006.
[63] T. Garcia-Sanchez *et al.*, "Interpulse multifrequency electrical impedance measurements during electroporation of adherent differentiated myotubes," *Bioelectrochemistry*, vol. 105, pp. 123–135, 2015.
[64] V. Sridhara and R. P. Joshi, "Numerical study of lipid translocation driven by nanoporation due to multiple high-intensity, ultrashort electrical pulses," *Biochimica et Biophysica Acta (BBA)-Biomembranes*, vol. 1838, no. 3, pp. 902–909, 2014.
[65] D. Dutta *et al.*, "Effects of nanosecond pulse electric fields on cellular elasticity," *Micron*, vol. 72, pp. 15–20, 2015.
[66] A. Steuer *et al.*, "Elasticity and tumorigenic characteristics of cells in a monolayer after nanosecond pulsed electric field exposure," *Eur. Biophys. J.*, vol. 46, pp. 1–14, 2017.

2.2 Discrimination of different cell monolayers before and after exposure to nanosecond pulsed electric fields based on Cole-Cole and multivariate analysis

Journal of Physics D: Applied Physics, 2019, 52: 495401

DOI: http://dx.doi.org/10.1088/1361-6463/ab40d7

Author contributions

Term	Definition	Author name
Conceptualization	Ideas; formulation or evolution of overarching research goals and aims	F. Shi
Methodology	Development or design of methodology; creation of models	F. Shi
Software	Programming, software development; designing computer programs; implementation of the computer code and supporting algorithms; testing of existing code components	F. Shi, J. Zhuang
Validation	Verification, whether as a part of the activity or separate, of the overall replication/ reproducibility of results/experiments and other research outputs	F. Shi
Formal Analysis	Application of statistical, mathematical, computational, or other formal techniques to analyze or synthesize study data	F. Shi
Investigation	Conducting a research and investigation process, specifically performing the experiments, or data/evidence collection	F. Shi

Resources	Provision of study materials, reagents, materials, patients, laboratory samples, animals, instrumentation, computing resources, or other analysis tools	F. Shi
Data Curation	Management activities to annotate (produce metadata), scrub data and maintain research data (including software code, where it is necessary for interpreting the data itself) for initial use and later reuse	F. Shi
Writing – Original Draft	Preparation, creation and/or presentation of the published work, specifically writing the initial draft (including substantive translation)	F. Shi
Writing – Review & Editing	Preparation, creation and/or presentation of the published work by those from the original research group, specifically critical review, commentary or revision – including pre-or postpublication stages	F. Shi, A. Steuer, J. Kolb
Visualization	Preparation, creation and/or presentation of the published work, specifically visualization/ data presentation	F. Shi
Supervision	Oversight and leadership responsibility for the research activity planning and execution, including mentorship external to the core team	J. Kolb
Project Administration	Management and coordination responsibility for the research activity planning and execution	J. Kolb
Funding Acquisition	Acquisition of the financial support for the project leading to this publication	J. Kolb

OPEN ACCESS
IOP Publishing
Journal of Physics D: Applied Physics
J. Phys. D: Appl. Phys. 52 (2019) 495401 (12pp)
https://doi.org/10.1088/1361-6463/ab40d7

Discrimination of different cell monolayers before and after exposure to nanosecond pulsed electric fields based on Cole–Cole and multivariate analysis

Fukun Shi[1,2], Jie Zhuang[3] and Juergen F Kolb[1,2]

[1] Leibniz Institute for Plasma Science and Technology (INP), 17489 Greifswald, Germany
[2] Institute of Physics, University of Rostock, 18059 Rostock, Germany
[3] Suzhou Institute of Biomedical Engineering and Technology (SIBET), Chinese Academy of Sciences, 215163 Suzhou, People's Republic of China

E-mail: juergen.kolb@inp-greifswald.de

Received 18 April 2019, revised 10 July 2019
Accepted for publication 3 September 2019
Published 23 September 2019

Abstract

Normal and cancer cells, which were grown in monolayers, were investigated and discriminated by electrical bioimpedance spectroscopy (EBIS) before and after exposures to nanosecond pulsed electric fields (nsPEFs). Bioimpedance data were analysed with a Cole–Cole model and the principal component analysis (PCA). Normal and cancer cells could be clearly distinguished from each other either from Cole parameters (R_0, α, τ) or from two dominant principal components. The trend of changes for Cole parameters indicated distinctively different post-nsPEF-effects between normal and cancer cells. PCA was also able to distinguish characteristic impedance spectra 30 min after exposures. The first principal component suggested that post-nsPEF-effects for normal cells were revealed especially at lower frequencies. The results indicated further that the extracellular resistance, which is dominated by cell–cell connections, might be an important factor with respect to selective nsPEF-effects on cancer cells that are organized in a monolayer or a tissue, respectively. Accordingly, the results support the application of EBIS as an early, non-invasive, label-free, and time-saving approach for the classification of cells to provide in particular predictive information on the success of cancer treatments with nsPEFs.

Keywords: electrical bioimpedance spectroscopy, cancer, nanosecond pulsed electric fields, principal component analysis

Supplementary material for this article is available online

(Some figures may appear in colour only in the online journal)

1. Introduction

The investigation of effects on cancer and normal cells is of crucial importance for the development of novel anti-cancer strategies. Cancer and normal cells can be discriminated by their different electrical properties [1], which can be determined by electrical bioimpedance spectroscopy (EBIS) [2, 3]. EBIS measures the impedance by sending a series of very low voltage sinusoidal signals (typically of 10 mV) to the analyte and deriving the ratio of the output voltage and corresponding electrical currents [4]. Consequently, this constitutes an inherently non-invasive, real-time, sensitive and label-free

diagnosis of cell behavior, including cell–substrate interactions, cell–cell interactions and cell adhesion [5]. The method is already established for the diagnostic of cells that are grown and investigated under controlled conditions, such as monolayers on commercial EBIS-electrode arrays. Conversely, the challenge remains to further develop the approach into a viable method also for tissues *in vivo*. Therefore, reliable experimental and analytical methods and meaningful interpretations still need to be developed, which is one of the goals of this study.

The electrical properties of biological samples, including cells and tissues, determine also the primary effects of an applied stimulus, which is prone to change these characteristics as it is in particular relevant for currently pursuit treatment of skin tumors by pulsed electric fields [6]. Especially the application of nanosecond pulsed electric fields (nsPEFs) is an attractive alternative for the treatment of solid tumors [7, 8]. Conversely, electric field-induced changes of the electrical properties can be reflected in bioimpedance spectra, which can then be used for the evaluation of the respective treatments. Accordingly, impedance spectroscopy could offer a way to predict a patient-specific treatment success before any biological effects become obvious [9, 10].

With our previously reported work, we have established a method and procedures to use EBIS for the investigation of effects of pulsed electric fields with a duration of 100 ns on rat liver epithelial cells (WB-F344) that were grown in monolayers [11]. The information of a bioimpedance spectrum for the cell monolayer could be summarized by four descriptive parameters that were obtained by fitting spectra with a Cole model. The resistance-value at zero frequency, R_0, is commonly related to extracellular resistance and membrane integrity of individual cells. The dispersion width, α, has been correlated with the morphology of the extracellular space and to some degree with the distribution of cell size [12]. A significant decrease of R_0 and α suggested the disruption of cell–cell junctions, in particular tight junctions. This effect was confirmed by the increase of another parameter, the characteristic time constant, τ, which is, together with R_0, descriptive for the contribution of the capacity C_m of the cell membranes to the overall capacitance of the monolayer. Moreover, a transient increase of R_0 within 1 min after exposures suggested cell swelling, probably due to electroporation. Altogether, the study proved the possibility to use EBIS to monitor nsPEF-treatments.

Compared to treatments with longer pulses of microseconds to milliseconds, exposures with nanosecond pulses are essentially non-thermal and are known to induce intracellular effects, especially apoptosis, without the need for chemotherapeutics [13, 14]. Interestingly, there has been some theoretical and experimental evidence for different sensitivities of cancer cells and normal cells towards nsPEF-exposures [15–17].

Regardless of the extensive research on the differences of nsPEF-effects on cancer and normal cells, underlying mechanisms and criteria that are responsible for the differences are not well described. Sensitivities are presumably determined by morphologies [18], mechanical properties [19] and also electrical properties [15]. The latter dominate electrical field distributions as well as current distributions and densities and will therefore directly determine electroporation mechanisms or any other mechanism of electrical manipulation [20–23].

A cell monolayer expresses an extracellular matrix and cell–cell connections similar to tissues while it reduces the overall complexity. Two normal epithelial cell lines, WB-F344 and human keratinocytes (HaCat) were cultivated, which express more compact cell–cell connections compared with cancer cells. A possible reason (or consequence) for the degradation of cell–cell connections of cancer cells is the facilitation of invasion and metastasis [24, 25]. The liver epithelial cells were compared to a syngenic counterpart, WB-ras, which was derived from WB-F344 cells by transfection with the oncogene ras. Since such a direct comparison was not possible for HaCat-cells, these were compared to a human melanoma cell line (Sk-Mel-28).

Since the primary goal of the study was the investigation of differences with respect to electrical characteristics and exposures, preferably non-fatal conditions were chosen for exposures. Cell death and extensive electroporation would dominate the bioimpedance spectra regardless of the cell line. Such unselective nsPEF-effects were observed in our previous work and were likewise reported for example for the response of normal skin and melanoma after exposure to 100 pulses of 300 ns PEFs with 40 kV cm^{-1} [6].

Due to its simplicity, popularity and explanatory power, the first choice for the interpretation of bioimpedance spectra is the analysis by a Cole model and a corresponding equivalent circuit. However, there are limitations to such a parameterized approach [26]. Fitting errors are inevitable and Cole parameters extracted from repetitive measurements for the same specimen are prone to large errors [27, 28]. Typical errors are due to the implementation of different algorithms for the analysis together with statistical variations of measurements. Even errors of only a few percents might prevent discrimination of cell types and assessment of therapeutic results.

Therefore, in addition, a multivariate model, i.e. principal component analysis (PCA), was applied as a non-parametric representation. PCA is commonly implemented to reduce the dimensionality of a raw spectrum without *ab initio* assumptions on the physiological or physical meaning of the parameters (principal components) that are extracted for a description. PCA has been widely applied for the classification of phenomena and for process monitoring [29–31]. Linearly uncorrelated eigenvectors are derived from an observed dataset by an orthogonal transformation. The eigenvector with the highest eigenvalue is chosen as the first principal component (PC) of the dataset, representing the most salient information. The inherent error of the approach is determined by the number of principal components that are included in the analysis in addition to the variation of results for individual measurements.

2. Methodology

2.1. Cell culture

The electrical properties of normal and cancer cells with either the same origin, i.e. syngeneic liver cells, or cells that can be

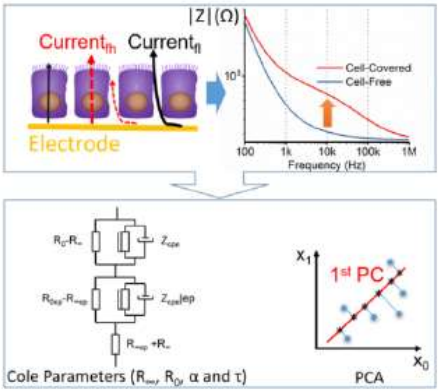

Figure 1. Schematic for the principle of the conducted bioimpedance analysis. The impedance spectra of monolayers, grown on interdigitated electrode arrays, were analysed using a Cole–Cole model or PCA.

found together in the same organ, i.e. skin, were investigated. The WB-F344 cell line was derived from a normal adult male Fischer 344 rat liver by Grisham *et al* [32]. The cancerous cell line WB-ras was derived by transfecting WB-F344 cells with the HRAS oncogene. As a result, these cells are characterized by the absence of contact inhibition, a spindle shape, and tumorigenicity *in vivo* [33]. Both cell lines were obtained from Prof J E Trosko, Michigan State University, East Lansing, MI, USA. In addition, cells that are typically found in skin tissue, i.e. Sk-Mel-28 melanoma cells and non-tumorogenic HaCat cells (both from ATCC, LGC Standards GmbH, Germany) were compared. The pairing is typical also for other studies on the comparison of melanoma cells with normal cells [34, 35].

All cell lines were cultivated in DMEM with 1 g l^{-1} glucose supplemented with 2 mM L-glutamine, 5% fetal calf serum (FCS) and 1% penicillin/streptomycin (all purchased from PAN-Biotech GmbH, Aidenbach, Germany). The osmolality of the medium was determined to be 300 mOsmol kg^{-1} based on the freezing point depression (OSMOMAT 3000, Gnotec GmbH, Berlin, Germany).

2.2. Bioimpedance analysis

A detailed description of setup and procedures for the conducted bioimpedance measurements has been presented previously [9]. Basic steps and approaches are summarized in figure 1.

In brief, ECIS-8W20idf-plates (Applied Biophysics, Inc., NY, USA) with an integrated interdigitated electrode array were pre-treated with 10 mM L-cysteine 15 min before seeding cells to obtain a stable impedance [36]. Each well was filled with 300 μl cell culture medium and a cell seeding density of 50 000 cells/well. The monolayer was considered confluent when the impedance at 20 kHz became stable for two consecutive days. The impedance at 20 kHz is close to the largest increment of the impedance module when the cell is grown on electrodes and avoids ambiguous contributions from electrode polarization. Impedance measurements as well as nsPEF-exposures were conducted with the electrode arrays embedded in the wells. The impedance was measured from 100 Hz to 10 MHz using an impedance analyser (Agilent 4294A, Keysight Technologies, Inc., USA) together with the appropriate test fixture (Agilent 16047E, Keysight Technologies, Inc., USA). Recorded data were analysed on the one hand by two individual Cole-models for the respective electrical components, i.e. describing electrode processes or monolayers, connected in series and on the other hand by a PCA. The information of impedance spectra was summarized by four Cole parameters (R_∞, R_0, α, and τ) and score and loading plots for the PCA, respectively.

The impedance for the Cole-models in series can be expressed by:

$$Z = Z_{\mathrm{ep}} + Z_{\mathrm{cells}} = \left[R_{\infty \mathrm{ep}} + \frac{R_{0\mathrm{ep}} - R_{\infty \mathrm{ep}}}{1+(i\omega\tau_{\mathrm{ep}})^{\alpha_{\mathrm{ep}}}}\right] + \left[R_\infty + \frac{R_0 - R_\infty}{1+(i\omega\tau)^\alpha}\right]. \quad (1)$$

The first term in brackets represents electrode polarization; the term in the second bracket describes the contribution of the cell monolayer. Parameters R_∞ and R_0 are describing the respective resistance at infinite frequency and at very low frequency. The expression $(i\omega\tau)^\alpha$ is known as constant phase element (CPE) to describe non-ideal capacitance, Z_{cpe}, with α a dimensionless dispersion factor ($0 < \alpha < 1$) and τ the characteristic time constant. The latter is commonly related to the average cell capacitance, for example, according to Trainito *et al* [37]:

$$C_m = \frac{\tau^\alpha}{R_0 - R_\infty}. \quad (2)$$

Parameters with a subscript 'ep' represent parameters associated with electrode polarization. The parameter $R_{\infty \mathrm{ep}}$ was omitted in the fitting process since it should be much smaller than $R_{0\mathrm{ep}}$ and R_∞.

2.3. Pulsed electric field exposures

A series of rectangular 100 ns pulses were produced by an in-house built Blumlein transmission line square wave pulse generator [38]. The high voltage pulses were delivered to the ECIS-chip with a pair of copper clamps. A high voltage probe (P5100A, Tektronix, Beaverton, OR) was connected to a fast oscilloscope (TDS3054, Tektronix, Beaverton, OR) to monitor the amplitude and the shape of pulses. The advantage of providing nsPEFs by the interdigitated electrode array is that only cells close to the electrodes are affected. Consequently, these cells determine changes of the impedance spectra. A lethal stimulation would kill cells and let dead cells float away, resulting in gaps with similar changes to the spectrum that are determined by the medium regardless of the particular cell line. Therefore especially interesting for comparison are non-fatal exposures to pulses with a voltage of 330 V and pulse numbers of 8, 16 and 24 that were applied with a repetition rate of 1 Hz. Corresponding to the voltage is an average

Table 1. Mean values for Cole parameters together with their standard deviations, δ, of untreated WB-F344 and WB-ras cell monolayers ($^{*}p < 0.05$, $^{**}p < 0.01$).

Cole parameter	WB-F344	δ	WB-ras	δ	p-value
R_∞ (Ω·cm^2)	255.21	38.81	234.82	24.84	
$R_0 * 1 \times 10^3$ ($\Omega \cdot$ cm^2)	1.81	0.32	1.07	0.20	**
α	0.71	0.02	0.73	0.01	
$\tau * 1 \times 10^{-6}$ (μs)	7.42	2.03	7.91	1.71	
C_m (μF cm^{-2})	0.15	0.05	0.24	0.04	**

Table 2. Mean values for Cole parameters together with their standard deviations, δ, of HaCat and Sk-Mel-28 cell monolayers ($^{*}p < 0.05$, $^{**}p < 0.01$).

Cole parameter	HaCat	δ	Sk-Mel-28	δ	p-value
R_∞ ($\Omega \cdot$ cm^2)	224.70	31.94	212.41	31.46	*
$R_0 * 1 \times 10^3$ ($\Omega \cdot$ cm^2)	0.82	0.04	0.62	0.06	**
α	0.72	0.01	0.49	0.04	**
$\tau * 1 \times 10^{-6}$ (μs)	3.54	0.14	13.196	3.71	**
C_m (μF cm^{-2})	0.19	0.01	11.929	7.32	**

electric field strength close to the edge of the electrodes of about 20 kV cm^{-1} [9].

2.4. Principal component analysis

The magnitude |Z| and phase angle θ as a function of frequency of nine samples for each untreated cell line and three samples for each treated cell line were computed for PCA with Origin 2017 (OriginLab, Northampton, MA) and PCA score plots and loading spectra were derived accordingly.

2.5. Statistical analysis

Impedance measurements for all exposure conditions were conducted at least in triplicates and mean values and standard deviations, δ, for each Cole parameter were calculated correspondingly. For monolayers exposed to pulsed electric fields, three independent monolayers were analysed. Nine samples were investigated for each cell line for the comparison between different untreated cell lines. For this case, the statistical significance (p-value) of each Cole parameter was evaluated by a paired-sample t-test with MATLAB (MathWorks, Natick, MA, USA).

3. Results

Cole parameters were extracted for cell monolayers before and after exposures from the equivalent circuit model that is shown in figure 1. Mean values and standard deviations for untreated cell lines, as well as the associated statistical significance, are presented in tables 1 and 2. Data for normal and cancer cell monolayers were considered significantly different for $p < 0.05$ (*) or $p < 0.01$ (**), respectively.

The PCA score plot is presented in the subsequent section. Values, in general, were normalized against values obtained for untreated monolayers for the analysis of the temporal evolution of each Cole parameter.

3.1. Cole parameters for untreated normal and cancer cell monolayers

Cole parameters of WB-F344 and WB-ras cell monolayers are summarized in table 1. The value of R_∞ for a WB-F344 cell monolayer was $255.21 \pm 39.81\ \Omega \cdot \text{cm}^2$. Hence, the mean value was about 8.7% higher than for corresponding tumorigenic WB-ras cell monolayers ($234.82 \pm 24.84\ \Omega \cdot \text{cm}^2$). Overall the difference was not statistically significant ($p > 0.05$). Likewise, no significant differences were revealed for the dispersion width, α, between WB-F344-monolayers (0.71 ± 0.02) and WB-ras cell monolayers (0.73 ± 0.01) or for the time constant, τ, of WB-F344 cells ($7.42 \pm 2.03\ \mu$s) in comparison to WB-ras cells ($7.91 \pm 1.71\ \mu$s).

However, a significant difference was found for R_0 and the cell membrane capacitance, C_m. The value of R_0 for WB-F344 monolayers was $1806 \pm 317\ \Omega \cdot \text{cm}^2$, and therefore almost twice that of R_0 for WB-ras cell monolayers, i.e. $1065 \pm 200\ \Omega \cdot \text{cm}^2$. The cell membrane capacitance, C_m, of WB-F344 cells and WB-ras cells was also significantly different, with $0.15 \pm 0.05\ \mu\text{F m}^{-2}$ and $0.24 \pm 0.04\ \mu\text{F m}^{-2}$, respectively. Hence, C_m for WB-ras cells was 1.6 times larger than for WB-F344 cells. It should be noted that C_m is not a completely independently determined parameter, unlike R_0, α, and τ, and hence respective changes are in particular associated with R_0 and together with R_0 also with τ.

Table 2 shows the mean values and standard deviations of the Cole parameters R_∞, R_0, α, and τ for monolayers of HaCat cells and Sk-Mel-28 cells. The values for R_∞ were again similar for cancer cells and normal cells but still significantly different. For HaCat cells, R_∞ is with $224.69 \pm 31.94\ \Omega \cdot \text{cm}^2$ about 6% larger than for Sk-Mel-28 cells ($212.41 \pm 31.46\ \Omega \cdot \text{cm}^2$). Values for R_∞ were not much different from WB-F344 cells and WB-ras cells.

Differences were more pronounced for other Cole parameters. Values of R_0 for HaCat cell monolayers ($816 \pm 37\ \Omega \cdot \text{cm}^2$) were about 32% higher than R_0 for Sk-Mel-28 cell monolayers ($620 \pm 60\ \Omega \cdot \text{cm}^2$). The dispersion width α, of a

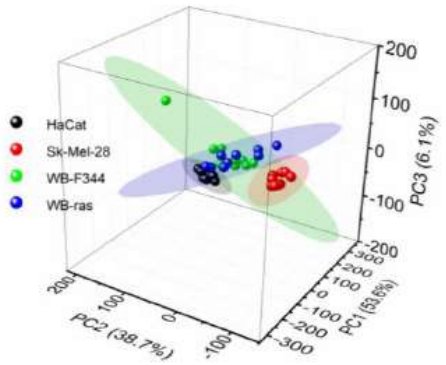

Figure 2. The largest three principal components (PCs) for phase spectra for untreated cell monolayers. Every sphere represents an EBIS-measurement and the ellipsoidal envelopes define the 95% confidence regions for individual cell lines.

HaCat cell monolayer is 0.72 ± 0.01, which is about 1.5 times larger than for a Sk-Mel-28 cell monolayer (0.49 ± 0.04). On the contrary, τ for HaCat cells is almost 4.7 times smaller than τ obtained for Sk-Mel-28 cells, i.e. 3.54 ± 0.14 μs versus 13.20 ± 3.71 μs. Values of C_m for HaCat cells and Sk-Mel-28 cells were again significantly different, with 0.19 ± 0.01 μF m^{-2} and 11.93 ± 7.32 μF m^{-2}, respectively.

Cole parameters for electrode polarization showed no significant differences regardless of the cell line, as shown in tables S1 and S2 of the supplementary information (SI) (stacks.iop.org/JPhysD/52/495401/mmedia).

3.2. PCA for untreated normal and cancer cell monolayers

Figure 2 displays the PCA score plot of phase spectra for untreated cell monolayers for the four investigated cell lines. A score plot describes the transformation of original variables into new coordinates (principal components) with the goal to give an alternative representation of a data set. The approach offers a better visual differentiation of the measurements. The first three principal components contributed with a variance of 98.45% to the phase spectra. In the 3D-space, which is defined by the principal components (PC1, PC2, PC3), every sphere represents an individual EBIS-measurement for a sample. In addition, the ellipsoidal envelopes describe the 95% confidence regions for each cell line. The distinct separation of each ellipsoid indicates a clear and significant differentiation between cell lines. (Additional views, showing the separation with respect to pairs of PCs, are provided with the supplementary information for this manuscript in figure S1.)

The PCA score plot for the magnitude |Z| can be found in figure S2 of the supplementary information (SI). In this case, PC1 and PC2 contribute with more than 99.97% variance

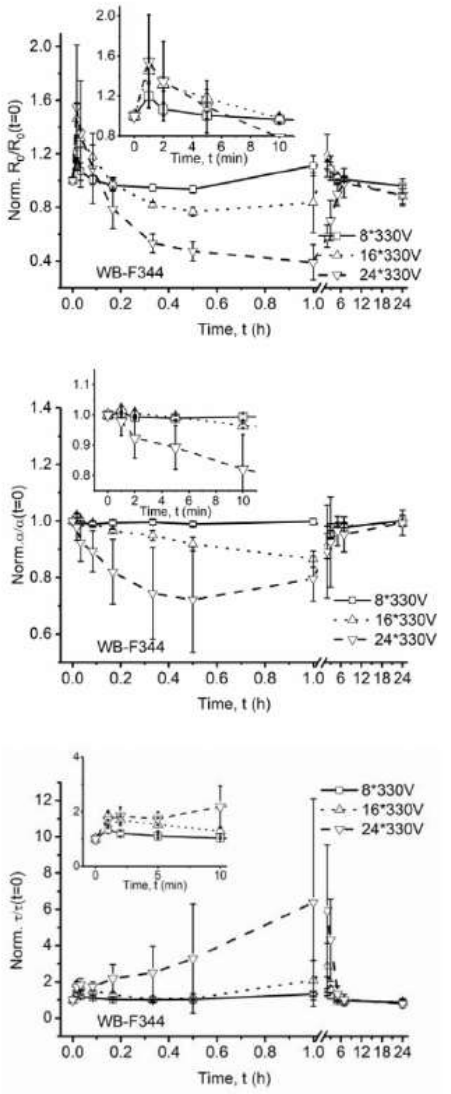

Figure 3. Temporal evolution of normalized Cole parameters for WB-F344 cell monolayer before and after exposure to 100 ns PEFs: (a) low frequency resistance R_0, (b) dispersion width α and (c) time constant τ.

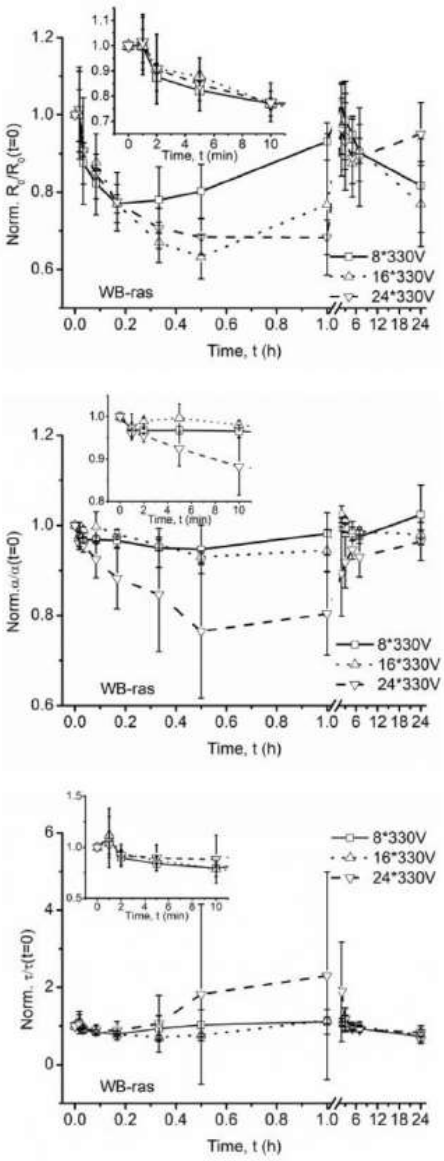

Figure 4. Temporal evolution of normalized Cole parameters for WB-ras cell monolayers before and after exposure to 100 ns pulsed electric fields: (a) low frequency resistance R_0, (b) dispersion width α and (c) time constant τ.

and the ellipsoidal envelopes for different cell lines are not well-differentiated.

3.3. *Temporal evolution of cole parameters for WB-F344 and WB-ras cell monolayers after nsPEF-exposures*

The change with time of normalized Cole parameters (R_∞, R_0, α, τ) was pulse number-dependent for both normal and cancer cell monolayers. The results are shown in figure 3.

The temporal evolution of R_0 for WB-F344 cell monolayers is shown in figure 3(a). A transient increase was observed within 1 min after exposure to either 8, 16, or 24 pulses with values that were 20%, 40%, and 28% higher than the initial values, respectively (see inset of figure 3(a)). The data confirm a transient increase that was also observed in our previous study for the same exposure conditions [9], although values were actually lower. A medium with lower glucose concentration was used in the present investigation which is presumably responsible for the difference. After the brief increase, R_0 gradually decreased before it recovered again. The decrease was more pronounced for higher pulse numbers and also took longer. For eight pulses, R_0 went down to 76.5% of the initial value and recovery started at about 30 min after exposure. The same temporal development was observed for 16 pulses although with slightly larger changes. A larger decrease of R_0 of 67.2%, compared to the initial value, was observed 1 h after exposure to 24 pulses. Values for R_0 even increased above the initial values 2 h after exposure with 11.6% and 18.7%, respectively, during the recovery after the application of 8 and 16 pulses.

Figure 3(b) shows the changes of Cole parameter α with time. There was scarcely any change for exposures to eight pulses and only a moderate decrease for 16 and 24 pulses. Within 1 h after the respective exposures, α was still reduced at most by about 12% before the values had recovered again after 2 h.

Another Cole parameter, τ, which generally exhibited a tentative increase, is depicted in figure 3(c). The largest increases for τ were observed 1 h after exposure to either 8, 16 and 24 pulses, with values about 1.3, 2.8, and 6 times larger than observed for untreated cell monolayers. Eventually, values for τ had recovered for both cell types 3 h after exposures.

In contrast, R_0 decreased for WB-ras cell monolayers already within 1 min after exposures as shown in figure 4(a). Within 10 min after exposures to eight pulses, R_0 was reduced to the lowest value, which was about 23% lower than the value obtained for untreated controls. During recovery, R_0 returned to the initial value that was measured for untreated cells within 1 h. Large reductions of R_0 can be observed also within 1 h after exposure to 16 and 24 pulses. Values for the decrease were close, i.e. a decrease by 37% and 32%, respectively. Afterward, R_0 recovered but did reach the values comparable with untreated cells again only after 24 h.

Figure 4(b) describes the time course of changes of α for WB-ras cell monolayers, with the biggest decrease observed within 30 min after exposures to 8, 16 and 24

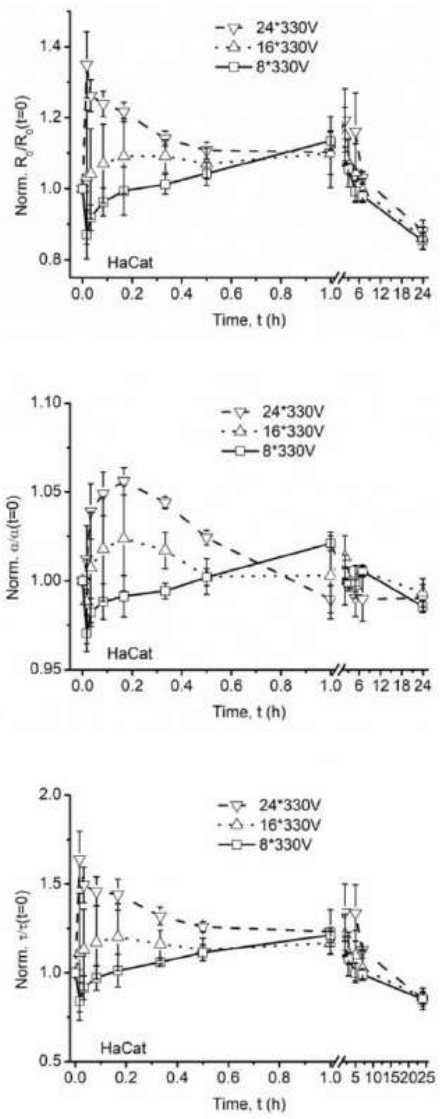

Figure 5. Temporal evolution of normalized Cole parameters for HaCat cell monolayer before and after exposure to 100 ns pulsed electric fields: (a) low frequency resistance R_0, (b) dispersion width α and (c) time constant τ.

pulses, with 5%, 7% and 27% in comparison to untreated cells, respectively.

The characteristic time constant, τ, that is shown in figure 4(c) increased slightly within 1 min after exposures followed by a decrease. Values for τ went down to 80%, 71% or 88% in comparison to untreated cells within 10 min after exposures to 8, 16 or 24 pulses. Overall, the changes are not distinct, in particular taking error bars into account.

3.4. Temporal evolution of Cole parameters for HaCat and Sk-Mel-28 cell monolayers after nsPEF-exposures

Changes of normalized Cole parameters with time are displayed in figure 5 for HaCat cell monolayers and for Sk-Mel-28 cell monolayers in figure 6. Figure 5(a) describes a fast drop of R_0 for HaCat cell monolayers within 1 min after exposure to eight pulses followed by a recovery eventually even exceeding initial values at 1 h. Conversely, for 24 pulses, R_0 jumped to values 35% above values obtained for untreated cells in 1 min before values decreased again for the next hour. The response for the application of 16 pulses followed development between the results for exposures to more or fewer pulses. After a slight ascent for about 20 min, values were not changing by much anymore. After 1 h, values about 15% higher in comparison to untreated cell monolayers, were observed for all exposure regimens.

The dispersion width, α, as shown in figure 5(b) changed only slightly after exposures. For eight pulses, α decreased by about 3% after 1 min and recovered again towards values similar to initial values within 30 min. An opposite trend, i.e. a small increase at the beginning with the highest values that are 2.5% and 6% above the initial values after 10 min, was observed for 16 or 24 pulses.

The development of the characteristic time constant, τ, which is presented in figure 5(c), was very similar to the changes that were recorded for R_0. For the smallest number of pulses, i.e. eight, values dropped by 16% by 1 min before increasing again. In contrast, τ increased to values about 1.6 times larger than for untreated cells right after exposure to 24 pulses before values declined afterward. For 16 pulses, a slow initial increase within 10 min could be observed to values 20% higher in comparison to untreated cells. Similar to the development of R_0, values for τ were eventually very similar again for all exposure conditions and about 15% lower than the values that were determined for the untreated monolayers.

For Sk-Mel-28 cell monolayers, R_0 increased by 18%, in comparison to untreated controls, within 1 h after exposure to eight pulses, which is followed by a gradual decrease towards initial values during the next couple of hours (figure 6(a)). Values fluctuated for about 5 min after the application of 16 and 24 pulses before a maximum increase was observed for R_0 half an hour later with values that were 22% and 30% above control values. For later times, values did not quite drop back again to values that were determined for unexposed cell monolayers.

Comparable characteristics were also observed for α and τ as shown in figures 6(b) and (c). After a hardly noticeable increase, α slightly decreased within 1 min after exposures. Values for α reached maxima of about 5%, 12% and 20% above values obtained for untreated cell monolayers 1 h after exposures to 8, 16 and 24 pulses, respectively. The dispersion width, α, was similar again to untreated monolayers 24 h after exposures. The time constant τ did hardly change for the application of eight pulses. A fast increase, of about 50% was recorded for exposures to 16 and 24 pulses, which was succeeded by a decrease towards initial values that was almost as fast as the increase until 4 min later. Notably, values then increased again to maxima of about 29% and 43% above values obtained for untreated cell monolayers 30 min after exposure to 16 and 24 pulses.

4. Discussion

4.1. Discrimination between normal and cancer cells from Cole parameter R_0

The electrical properties of the cell monolayers can be described according to an equivalent circuit model by the Cole parameters R_0, α, and τ [9] and in addition by the derived quantity C_m. The results that are presented in tables 1 and 2 demonstrate significant differences at least for one and often for several of these parameters for all of the cell lines that were investigated. Notable in particular are the differences that were observed for similar cell lines or respectively normal and cancer cells that can be found together in the same tissue, such as HaCat cells and Sk-Mel-28 cells or WB-F344 cells and WB-ras cells. The comparison of the latter is in particular of interest since it allows to distinguish normal from cancer cells of the same 'type'.

The low frequency resistance R_0 can describe in particular the organization of cells in monolayers and hence presumably also in tissues. With our previous investigation, we could already show that R_0 represents the extracellular resistance, which is dominated by cell–cell junctions, and especially adhesion junctions and tight junctions [9]. The largest value for R_0 was recorded for WB-F344 cells, followed by WB-ras, HaCat and eventually Sk-Mel-28 cells. Hence values for untreated normal cells were indeed consistently larger than for their respective tumorigenic counterpart, indicating tighter cell–cell connections for normal cells. The results further show that such a comparison cannot be arbitrary but has to take into account the 'primary' tissue where cancer cells develop from similar normal cells, which is, in this case, either liver tissue or skin. The characteristic differences for R_0 are in agreement with other reports that cancer cells suppress the expression of tight junctions as well as of adherens junctions which is a prerequisite for the ability to metastasize [24, 25]. The smallest R_0 for Sk-Mel-28 cells corresponds to the loss of the connection between each cell in the monolayer, where a lot of gaps between cells could be found visually (data not shown).

After exposure to nsPEFs, changes of R_0 can be ascribed to the disruption of cell–cell connections. Cell monolayers of normal cells with more or/and stronger cell–cell connections (figures 3(a) and 5(a)) were accordingly more significantly affected compared to cancer cell monolayers with less or weaker connections, resulting in bigger changes of R_0 (figures 4(a) and 6(a)). This effect on cell–cell junctions was further confirmed by values for R_0 that were 30 min after exposures similar to the value determined for untreated Sk-Mel-28 cells. The cell line is generally known to rarely exhibit cell–cell connections [39]. The associated higher extracellular permeability of cell monolayers with lacking dysfunctional or degraded junctions resulted in R_0 to decrease to values equal to a value that is not determined by cell–cell connections.

For shorter times after exposures, i.e. within the first 10 min, two other phenomena are likely also affecting R_0 in addition to the disruption of cell–cell connections. During this time, some reversible electroporation of cell membranes might still provide another pathway for ions to pass through the monolayer and consequently reduce values for R_0. Due to the limitations of the present experimental procedures and limitations of the Cole model, respective changes of R_0 cannot be distinguished in the impedance spectra from the effect on cell–cell junctions. To separate electroporation-effects, an EBIS measurement system with a higher temporal resolution and an improved equivalent circuit model need to be developed.

A second phenomenon affecting R_0 after exposures may result from changes in the overall cell morphology, such as in particular cell swelling or other changes of cell shape or size. Cell swelling narrows the extracellular space and reduces the pathway for ionic transport, hence leading to an increase of R_0. An obvious increase of R_0 within 1 min after exposures was indeed observed for normal cell monolayers. For WB-F344 cells, R_0 experienced a transient increase within 1 min after exposures (figure 3(a)). Also, R_0 for HaCat cell monolayers (figure 5(a)) increased within 1 min after exposure to 16 and 24 pulses of nsPEFs. This increase was sustained much longer than for WB-F344 cells. A small transient increase of R_0 for Sk-Mel-28 cell monolayers within 1 min after exposure to 16 and 24 pulses (figure 6(a)) was also found. However, for this very small change, still measurement errors could be responsible. The presumed changes of cell morphologies and corresponding changes of R_0 are again superimposed in the impedance spectra. Similar mechanisms might also account for the second increase of R_0 that was observed for WB-F344 cells around 2 h after exposures.

4.2. Evaluation of morphologies of cells and extracellular space from Cole parameter α

Information on morphologies of cells in the monolayers, in general, was reflected by another Cole parameter. The dispersion width, α, is commonly believed to be associated with the heterogeneity of cell shapes and sizes and has accordingly been argued to be also related to the morphology of the extracellular space and in particular to be a measure of its tortuosity. A decrease of α hence indicates an increase of tortuosity of the extracellular space [12, 40]. The values of α for untreated WB-F344, WB-ras, and HaCat cell monolayers were similar and in the range from 0.71 to 0.72. The reason

is presumably their similar epithelial-like cell morphology. In contrast, Sk-Mel-28 cell monolayers had the smallest value of α with 0.49, which reflects the extremely irregular polygonal morphology of the cells

Changes of α with time after nsPEF-exposures likewise exhibited clear differences for different cell monolayers (figures 3(b), 4(b), 5(b) and 6(b)). Notable is the second increase of α that was observed for Sk-Mel-28 cells starting 5 min after exposures, indicating a significant change of the morphology of the extracellular spaces. This was probably due to the high mobility of Sk-Mel-28 cells during culture.

4.3. Derivation of membrane capacitance from Cole parameter τ

The characteristic time constant, τ, is related to the membrane capacitance C_m as described by equation (2). A distinction between normal and cancer cells was also prominently observed for this parameter (tables 1 and 2). The capacitances were consistently higher for the cancer cell lines in comparison to their normal counterparts. The differences were small for WB-F344 and WB-ras cells, which is ostensibly explained by their very close relationship, considering that in principle differences are only due to a particular artificially selected genetic mutation. Conversely, the difference between the normal HaCat skin cells and the genuine Sk-Mel-28 melanoma cells was with a difference of two orders of magnitude much more pronounced.

Distinctively higher membrane capacitance for cancer cells was also reported by Mulhall *et al* [41], who compared the effective cell membrane capacitance C_{eff} for oral cancer cells, pre-cancer cells, and normal keratinocytes. However, it should be remembered, that in our study, cell membrane capacities were not determined directly and that the parameter C_m was derived from impedance spectra for the entire monolayer. Large gaps in the extracellular space of Sk-Mel-28 cell monolayers, that are filled with medium with higher dielectric constant, are expected to be contributing accordingly. Conversely, a highly irregular organization of cells is known as a specific characteristic for tumor tissues and therefore will likely be presented in the parameter C_m in a similar fashion.

An analogous contribution to the overall capacitance might also arise for a high degree of permeabilization by pulsed electric field exposures, which causes medium to be incorporated in conductive membrane channels at least temporarily and correspondingly change membrane permeabilities [37]. Consequently, a distinction of normal from cancer cells based on values for the capacitances should be considered very carefully at least for monolayers (or tissues) treated by pulsed electric fields. Altogether the temporal evolution of τ appears to be a better and more direct accessible parameter for the evaluation of nsPEF-effects (figures 3(c), 4(c), 5(c) and 6(c)).

4.4. Discrimination between untreated normal and cancer cells by PCA

PCA provides a different way for the organization and analysis of the data that were obtained from impedance spectra.

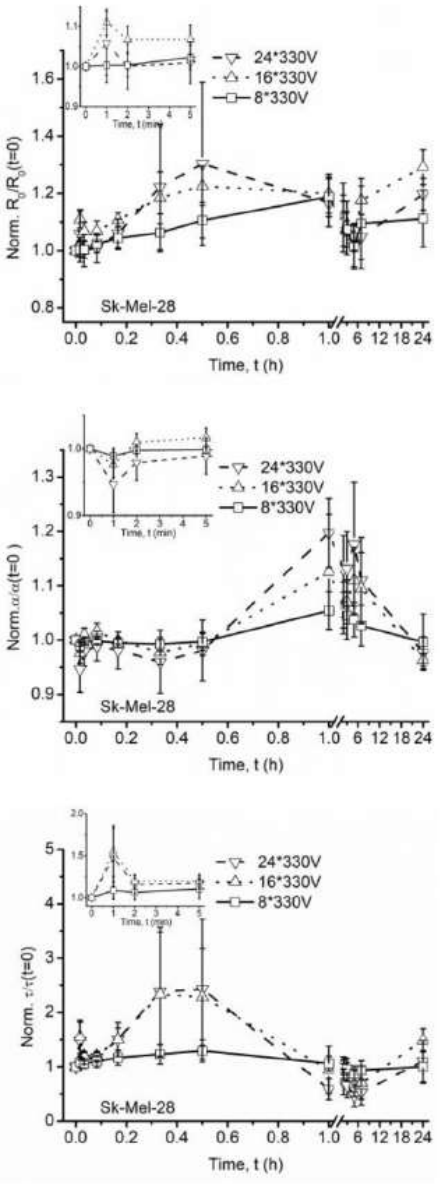

Figure 6. Temporal evolution of normalized Cole parameters for Sk-Mel-28 cell monolayer before and after exposure to 100 ns pulsed electric fields: (a) low frequency resistance R_0, (b) dispersion width α and (c) time constant τ.

The strength of the method is to exclude redundant information that is contained for different frequencies by deriving linearly independent variables (principal components) that might allow an alternative view to distinguish the most important criteria that are responsible for a particular result from less relevant contributions.

The PCA score plot for the phase spectra of untreated cell monolayers for different cell lines showed well-differentiated ellipsoidal envelopes indicating that each cell line can be discriminated. The separation between spheres inside of an ellipsoid illustrates the dispersion of the measurements for an individual cell line (figure 2).

A principal component can be expressed by a linear combination of variables with respective coefficients that are called loadings. The magnitudes of the loadings represent the weight of each variable. Consequently, contributions for frequencies with larger loadings are more important. The loadings as a function of frequency for the first three PCs are shown in figure S3 (SI). PC1 has larger loadings for middle frequencies from 1.4 kHz to 562.3 kHz with a peak at 6 kHz. In contrast, peaks that were found for PC2 and PC3 at 3 kHz and 150 kHz were subsequently ignored due to their small contribution to the overall variance.

In general, PCA is difficult to link with physiological properties of the cells or physical characteristics. However, often an instructive interpretation can still be found for the principal components. For the most important principal component, PC1, the impedance spectrum for the respective frequency range was determined by properties of the cell monolayer. In particular, the extracellular resistance R_{ex}, which is dominated by cell–cell connections, was the determining salient feature when comparing cell lines. Moreover, the influence of electrode polarization has been inherently avoided since its impact on phase is generally decreasing as the frequency is increasing. Consequently, it can be omitted for frequencies higher than 1 kHz.

In contrast, the PCA score plot for the magnitude |Z| for untreated cell lines did not discriminate variances between normal and cancer cell monolayers (figure S2 (SI)). This may be explained by the loading spectra shown in figure S4 (SI), i.e. the PCA loadings of the main two PCs as a function of frequency for the magnitude |Z|. Obviously, PC1 accounted for the lower frequencies (<1 kHz), where electrode polarization dominated the impedance spectra. As shown in tables S1 and S2 (SI), no significant differences could be found for the contributions due to electrode polarization for untreated cells. Consequently, electrode polarization may be the reason why the PCA score plot for |Z| could not discriminate variances between normal and cancer cell monolayers.

4.5. Discrimination between nsPEF-treated normal and cancer cells by PCA

PCA score plots and loading spectra for the phase of impedance spectra for each cell line are presented in figure S5 (SI). The variances were calculated from the impedance spectra of cell monolayers for untreated, and for exposed monolayers, 1 min and 30 min after treatment with 24 pulses. (A number of 24 pulses had led to the most obvious changes of Cole parameters for these two time points.)

Similar to the results for changes of Cole parameters, the scores for WB-F344, WB-ras, and Sk-Mel-28 cells were distinctively different 30 min after treatments in comparison to results at 1 min after treatment and compared to untreated cells. For later times were the distributions too similar to be discriminated by PCA. A likewise more indistinguishable distribution was also observed for HaCat cells, however, scores for untreated cells and for cells 1 min after exposure are further apart than for the other cell lines. This confirms the findings for changes of Cole parameters for HaCat cells as shown in figure 5, with Cole parameters changing more obviously 1 min after exposures than for other cell lines.

The corresponding loading spectra for PC1, according to figure S4 (SI), suggests an important frequency range for the monolayer development after exposures from several kHz to hundreds of kHz for WB-F344, WB-ras and Sk-Mel-28 cell monolayers. The frequencies for the peaks are found at 2 kHz, 6 kHz, and 14 kHz, respectively. Conversely, peaks were found at 1 kHz and 60 kHz for HaCat cell monolayers. The peaks at lower frequency for normal cells suggest that PEF-effects are rather reflected by the response at lower frequencies in comparison to cancer cells.

In conclusion, the PCA confirms trends and observations that were already derived from changes of Cole parameters. In general, PCA requires large data sets and in this case the analysis of Cole parameters might be more convenient for an assessment of effects. However, PCA, in addition, offers the possibility to identify in particular outliers, which is helpful for any experimental design.

5. Conclusion

The investigation of cells in a monolayer is another step towards the conceivable application of impedance analysis on tissues *in vivo*. Normal cells could be clearly distinguished from cancer cells in laboratory experiments but more studies and developments are necessary before the method can be successful in clinical settings the effects of pulsed electric field treatments could already be evaluated from impedance spectra through Cole parameters and PCA. Different values and respective changes with time for electrical characteristics were not just found between inherently different cells from different organs but also for very similar normal and cancer cells from the same primary tissue, e.g. liver or skin. However, the overall analysis remains challenging, especially for exposures to pulsed electric fields, since different phenomena contribute simultaneously to the underlying impedance spectra and as a consequence are superimposed in the derived Cole parameters. To separate electroporation-effects, an EBIS measurement system with a higher temporal resolution and an improved equivalent circuit model need to be developed.

A PCA that is conducted in addition can, therefore, provide important additional information and decision criteria for therapies. Nevertheless, the study, in particular, suggests

that the extracellular resistance of cell monolayers does play a vital role for the discrimination of cell lines and monitoring of nsPEF-effects. In the future, this might present a way to predict the success of such treatments already within the first hours after exposures.

Acknowledgments

This work was supported in part by the Collaborative Research Center CRC 1270 funded by the German Research Foundation (DFG). Fukun Shi is the recipient of a grant from the China Scholarship Council (CSC) (File No. 20150670010).

ORCID iDs

Fukun Shi https://orcid.org/0000-0003-0347-217X
Juergen F Kolb https://orcid.org/0000-0002-0434-5001

References

[1] Huclova S, Erni D and Fröhlich J 2010 Modelling effective dielectric properties of materials containing diverse types of biological cells *J. Phys. D: Appl. Phys.* **43** 365405
[2] Zhang F, Jin T, Hu Q and He P 2018 Distinguishing skin cancer cells and normal cells using electrical impedance spectroscopy *J. Electroanal. Chem.* **823** 531–6
[3] Polevaya Y, Ermolina I, Schlesinger M, Ginzburg B-Z and Feldman Y 1999 Time domain dielectric spectroscopy study of human cells: II. Normal and malignant white blood cells *Biochim. Biophys. Acta* **1419** 257–71
[4] Barsoukov E and Macdonald J R 2018 *Impedance Spectroscopy: Theory, Experiment, and Applications* (New York: Wiley)
[5] Chang F-Y, Chen M-K, Wang M-H and Jang L-S 2016 Highly sensitive three-dimensional interdigitated microelectrode for microparticle detection using electrical impedance spectroscopy *J. Phys. D: Appl. Phys.* **49** 075403
[6] Chen X, James Swanson R, Kolb J F, Nuccitelli R and Schoenbach K H 2009 Histopathology of normal skin and melanomas after nanosecond pulsed electric field treatment *Melanoma Res.* **19** 361–71
[7] Stolwijk J A, Hartmann C, Balani P, Albermann S, Keese C R, Giaever I and Wegener J 2011 Impedance analysis of adherent cells after *in situ* electroporation: non-invasive monitoring during intracellular manipulations *Biosens. Bioelectron.* **26** 4720–7
[8] Ivorra A and Rubinsky B 2007 *In vivo* electrical impedance measurements during and after electroporation of rat liver *Bioelectrochemistry* **70** 287–95
[9] Shi F, Steuer A, Zhuang J and Kolb J F 2019 Bioimpedance analysis of epithelial monolayers after exposure to nanosecond pulsed electric fields *IEEE Trans. Biomed. Eng.* **66** 2010–21
[10] Nuccitelli R, Berridge J C, Mallon Z, Kreis M, Athos B and Nuccitelli P 2015 Nanoelectroablation of murine tumors triggers a CD8-dependent inhibition of secondary tumor growth *PLoS One* **10** e0134364
[11] Beebe S J, White J, Blackmore P F, Deng Y, Somers K and Schoenbach K H 2003 Diverse effects of nanosecond pulsed electric fields on cells and tissues *DNA Cell Biol.* **22** 785–96
[12] Genescà M, Ivorra A, Sola A, Palacios L, Goujon J-M, Hauet T, Villa R, Aguiló J and Hotter G 2005 Electrical bioimpedance measurement during hypothermic rat kidney preservation for assessing ischemic injury *Biosens. Bioelectron.* **20** 1866–71
[13] Schoenbach K H, Beebe S J and Buescher E S 2001 Intracellular effect of ultrashort electrical pulses *Bioelectromagnetics* **22** 440–8
[14] Guo J, Dang J, Wang K, Zhang J and Fang J 2018 Effects of nanosecond pulsed electric fields (nsPEFs) on the human fungal pathogen *Candida albicans*: an *in vitro* study *J. Phys. D: Appl. Phys.* **51** 185402
[15] Joshi R P, Qin H and Schoenbach K H 2004 Modeling studies of cell response to ultrashort, high-intensity electric fields-implications for intracellular manipulation *IEEE Trans. Plasma Sci.* **32** 1677–86
[16] Yang W, Wu Y, Yin D, Koeffler H, Sawcer D, Vernier P and Gundersen M 2011 Differential sensitivities of malignant and normal skin cells to nanosecond pulsed electric fields *Technol. Cancer Res. Treat.* **10** 281–6
[17] Awasthi K, Nakabayashi T, Li L and Ohta N 2017 Effects of nanosecond pulsed electric field on intracellular NADH autofluorescence: a comparison between normal and cancer cells *ACS Omega* **2** 2916–24
[18] Kulbacka J 2015 Nanosecond pulsed electric fields (nsPEFs) impact and enhanced Photofrin II® delivery in photodynamic reaction in cancer and normal cells *Photodiagn. Photodyn. Ther.* **12** 621–9
[19] Steuer A, Wende K, Babica P and Kolb J 2017 Elasticity and tumorigenic characteristics of cells in a monolayer after nanosecond pulsed electric field exposure *Eur. Biophys. J.* **46** 567–80
[20] Schoenbach K H *et al* 2007 Bioelectric effects of intense nanosecond pulses *IEEE Trans. Dielectr. Electr. Insul.* **14** 1088–109
[21] Wei K, Li W, Gao S, Ji B, Zang Y, Su B, Wang K, Yao M, Zhang J and Wang J 2016 Inactivation of ricin toxin by nanosecond pulsed electric fields including evidences from cell and animal toxicity *Sci. Rep.* **6** 18781
[22] Ben-David E, Ahmed M, Faroja M, Moussa M, Wandel A, Sosna J, Appelbaum L, Nissenbaum I and Goldberg S N 2013 Irreversible electroporation: treatment effect is susceptible to local environment and tissue properties *Radiology* **269** 738–47
[23] Zhang K, Guo J, Ge Z and Zhang J 2014 Nanosecond pulsed electric fields (nsPEFs) regulate phenotypes of chondrocytes through Wnt/β-catenin signaling pathway *Sci. Rep.* **4** 5836
[24] Matter K and Balda M S 2003 Functional analysis of tight junctions *Methods* **30** 228–34
[25] Martin T A and Jiang W G 2009 Loss of tight junction barrier function and its role in cancer metastasis *Biochim. Biophys. Acta* **1788** 872–91
[26] McAdams E T and Jossinet J 1996 Problems in equivalent circuit modelling of the electrical properties of biological tissues *Bioelectrochem. Bioenerg.* **40** 147–52
[27] Atefi S, Seoane F, Thorlin T and Lindecrantz K 2013 Stroke damage detection using classification trees on electrical bioimpedance cerebral spectroscopy measurements *Sensors* **13** 10074–86
[28] Nejadgholi I, Caytak H, Bolic M, Batkin I and Shirmohammadi S 2015 Preprocessing and parameterizing bioimpedance spectroscopy measurements by singular value decomposition *Physiol. Meas.* **36** 983
[29] Párta L, Zalai D, Borbély S and Putics Á 2014 Application of dielectric spectroscopy for monitoring high cell density in monoclonal antibody producing CHO cell cultivations *Bioprocess. Biosyst. Eng.* **37** 311–23
[30] Nejadgholi I and Bolic M 2015 A comparative study of PCA, SIMCA and Cole model for classification of bioimpedance spectroscopy measurements *Comput. Biol. Med.* **63** 42–51

[31] Sierpowska J, Hakulinen M, Töyräs J, Day J, Weinans H, Kiviranta I, Jurvelin J and Lappalainen R 2006 Interrelationships between electrical properties and microstructure of human trabecular bone *Phys. Med. Biol.* **51** 5289

[32] Tsao M-S, Smith J D, Nelson K G and Grisham J W 1984 A diploid epithelial cell line from normal adult rat liver with phenotypic properties of 'oval' cells *Exp. Cell Res.* **154** 38–52

[33] Ruch R J, Madhukar B V, Trosko J E and Klaunig J E 1993 Reversal of ras-induced inhibition of gap-junctional intercellular communication, transformation, and tumorigenesis by lovastatin *Mol. Carcinog.* **7** 50–9

[34] Tulley S and Chen W-T 2014 Transcriptional regulation of seprase in invasive melanoma cells by transforming growth factor-β signaling *J. Biol. Chem.* **289** 15280–96

[35] Haridas P, McGovern J A, Kashyap A S, McElwain D L S and Simpson M J 2016 Standard melanoma-associated markers do not identify the MM127 metastatic melanoma cell line *Sci. Rep.* **6** 24569

[36] Szulcek R, Bogaard H J and van Nieuw Amerongen G P 2014 Electric cell–substrate impedance sensing for the quantification of endothelial proliferation, barrier function, and motility *J. Vis. Exp.* **85** 51300

[37] Trainito C I, Français O and Le Pioufle B 2015 Analysis of pulsed electric field effects on cellular tissue with Cole–Cole model: monitoring permeabilization under inhomogeneous electrical field with bioimpedance parameter variations *Innovative Food Sci. Emerg. Technol.* **29** 193–200

[38] Steuer A, Schmidt A, Labohá P, Babica P and Kolb J F 2016 Transient suppression of gap junctional intercellular communication after exposure to 100-nanosecond pulsed electric fields *Bioelectrochemistry* **112** 33–46

[39] Lee J *et al* 2016 Interleukin-32α induces migration of human melanoma cells through downregulation of E-cadherin *Oncotarget* **7** 65825–36

[40] Ivorra A, Genescà M, Sola A, Palacios L, Villa R, Hotter G and Aguiló J 2005 Bioimpedance dispersion width as a parameter to monitor living tissues *Physiol. Meas.* **26** S165

[41] Mulhall H, Labeed F, Kazmi B, Costea D, Hughes M and Lewis M 2011 Cancer, pre-cancer and normal oral cells distinguished by dielectrophoresis *Anal. Bioanal. Chem.* **401** 2455–63

2.3 Ultrasensitive Impedimetric Analysis of Cell Responses from the Distribution of Relaxation Times

Biosensors and Bioelectronics, under review

Author contributions

Term	Definition	Author name
Conceptualization	Ideas; formulation or evolution of overarching research goals and aims	F. Shi
Methodology	Development or design of methodology; creation of models	F. Shi
Software	Programming, software development; designing computer programs; implementation of the computer code and supporting algorithms; testing of existing code components	F. Shi
Validation	Verification, whether as a part of the activity or separate, of the overall replication/ reproducibility of results/experiments and other research outputs	F. Shi
Formal Analysis	Application of statistical, mathematical, computational, or other formal techniques to analyze or synthesize study data	F. Shi
Investigation	Conducting a research and investigation process, specifically performing the experiments, or data/evidence collection	F. Shi

Resources	Provision of study materials, reagents, materials, patients, laboratory samples, animals, instrumentation, computing resources, or other analysis tools	F. Shi
Data Curation	Management activities to annotate (produce metadata), scrub data and maintain research data (including software code, where it is necessary for interpreting the data itself) for initial use and later reuse	F. Shi
Writing – Original Draft	Preparation, creation and/or presentation of the published work, specifically writing the initial draft (including substantive translation)	F. Shi
Writing – Review & Editing	Preparation, creation and/or presentation of the published work by those from the original research group, specifically critical review, commentary or revision – including pre-or postpublication stages	F. Shi, J. Kolb
Visualization	Preparation, creation and/or presentation of the published work, specifically visualization/ data presentation	F. Shi
Supervision	Oversight and leadership responsibility for the research activity planning and execution, including mentorship external to the core team	J. Kolb
Project Administration	Management and coordination responsibility for the research activity planning and execution	J. Kolb
Funding Acquisition	Acquisition of the financial support for the project leading to this publication	J. Kolb

Ultrasensitive Impedimetric Analysis of Cell Responses from the Distribution of Relaxation Times

Fukun Shi[1,2], Juergen F. Kolb[1,2*]

[1]Leibniz Institute for Plasma Science and Technology (INP Greifswald), Greifswald 17489, Germany

[2]Institute of Physics, University of Rostock, Rostock 18059, Germany

juergen.kolb@inp-greifswald.de (J. Kolb)

[*]Corresponding author at: Leibniz Institute for Plasma Science and Technology (INP), Greifswald 17489, Germany

Abstract

A universal strategy for the sensitive investigation of cell responses to external stimuli, in particular nanosecond pulsed electric fields (nsPEFs), was developed based on electrical impedance spectroscopy (EIS) in combination with a multi-peak analysis for the distribution of relaxation times (DRT). The DRT method provides high resolution for the identification of different polarization processes without a priori assumptions, as they are needed by more conventional approaches, such as an evaluation by equivalent circuit models. Accordingly, the physical properties of cells and their changes due to external stimuli can be uncovered and visualized. Relaxation processes at about 100 kHz are associated with cell membrane characteristics and dominate respective changes of the distribution function for epithelial cell monolayers after exposure. A relatively moderate evolution at about 10 kHz may represent the polarization of extracellular matrices. Relaxation processes at around 1 MHz are suggested to be associated with intracellular changes. Conversely, the distribution of relaxation times can aid the optimization of the experimental design with respect to intended responses by an external stimulus.

Keywords: Electrical impedance spectroscopy, nanosecond pulsed electric fields, distribution of relaxation times, multi-peak analysis, Gaussian functions

1 Introduction

Electrical impedance spectroscopy (EIS) has been widely used to investigate the interactions of electric fields with biological materials due to advantages including non-invasiveness, sensitivity, being label-free and providing a real-time analysis (García-Sánchez et al. 2018). The information on cells is contained in the complex impedance $Z = Z' + iZ''$ as a function of applied AC signals of different frequencies. A conventional impedance analysis is mostly based on graphical representations of the complex impedance in conjunction with equivalent circuit models, in which each circuit element represents a physical characteristic (Huang et al. 2016; Lvovich 2012). However, both approaches perform poorly in distinguishing close relaxation processes (McAdams and Jossinet 1996). In particular, equivalent circuit models are circumspect since they depend on a priori knowledge of physical or chemical systems. Moreover, different equivalent circuit models can be suitable to describe an impedance spectrum, resulting in ambiguities with respect to their physical meaning (Effat and Ciucci 2017).

Approach and description for the assessment of distinct and possibly different responses on cellular constituents by external stimuli have also to include stimulation methods and systems. Only exposure conditions, which result in reproducible observations, can unmistakably be associated with respective effects and mechanisms. Accordingly, we have used EIS in our previous work to study cell responses after exposure to nanosecond pulsed electric fields (nsPEFs) by means of a Cole model (Shi et al. 2019a). The original interest in the study of nsPEF-exposures is motivated by their potential for tumor

ablation (Dalmay et al. 2011; Nuccitelli et al. 2015). Cole parameters together with immunofluorescence staining successfully exhibited an increase in cell membrane permeabilities and the disruption of cell-cell connections. However, drawbacks of the Cole model included rather large errors for individual Cole parameters that were derived from repetitive measurements on the same specimen. Moreover and as already mentioned, the physical interpretation of the results strongly depends on the underlying model. Therefore, we evaluated the data in addition by a multivariate analysis, i.e. principal component analysis (PCA), to differentiate normal and cancer cells and the responses of normal and cancer cells after exposures (Shi et al. 2019b). However, PCA is primarily a method based on statistics, that ideally relies on a large number of samples and measurements and also lacks direct biophysical meaning (Czolkos et al. 2016). Although efforts have been made to guide the physical interpretation of the analysis (Zagar and Krizaj 2008), frequency dependent relaxation mechanisms of cell and tissue constituents can so far not be well extracted.

Conversely, relaxation times and amplitudes represent the dynamics of an electrophysiological system directly. Unfortunately, different relaxation processes are often superimposed in the impedance spectrum for a given frequency and the derivation of respective relaxation times and amplitudes is not possible or at least not straightforward. However, especially in the last decade progress has been made on the derivation of relaxation distributions from the deconvolution of electrical impedance spectra. This distribution of relaxation times (DRT) has since gained increasing attention (Ramírez-Chavarría et al. 2018; Schichlein et al. 2002) and proven its strength in electrochemical studies to distinguish relaxation processes directly from the experimental impedance spectrum without a priori assumptions (Ivers-Tiffee and Weber 2017). Underlying polarization processes can be differentiated from the individual peaks in the plot of the distribution function. Hence, DRT is a model-free and universal approach for a sensitive, visual and detailed analysis of EIS. However, to the best of our knowledge, this approach has not been applied towards the analysis of the exposure of cells, in particular for the evaluation of electrical stimuli.

Another unavoidable problem in EIS is electrode polarization, which restricts the deconvolution of impedance spectra. In our study, we accounted for electrode polarization by subtracting an impedance spectrum for only the medium from impedance spectra with cells and then derived the DRT for cells by means of an algorithm based on the Tikhonov regularization (Effat and Ciucci 2017; Wan et al. 2015). Individual polarization processes were quantified by a multi-peak analysis using a series of Gaussian functions. A comparison of the method with our previously published assessment of pulsed electric field effects on cells by either a Cole model or multivariate analysis, eventually points out the additional information that can be obtained by this approach.

2 Material and Methods

2.1 The Workflow

The different steps for the developed analysis are shown in Fig.1. First, the impedance spectrum for the cell monolayer was corrected to exclude electrode polarization. This was done by subtracting impedance spectra that were obtained only for media, i.e. without cells, from impedances spectra for the actual measurements with cells. A Kramers-Kronig relation test of the real part and the imaginary part of the impedance spectrum was constructed before the data was considered valid for the calculation of the distribution of relaxation times. Subsequently, the DRT was verified by comparing the reconstructed impedance spectra with the measured impedance spectra. Eventually, individual relaxation mechanisms were distinguished by means of a multi-peak analysis. A detailed description of the pertinent procedures is presented in the following sections.

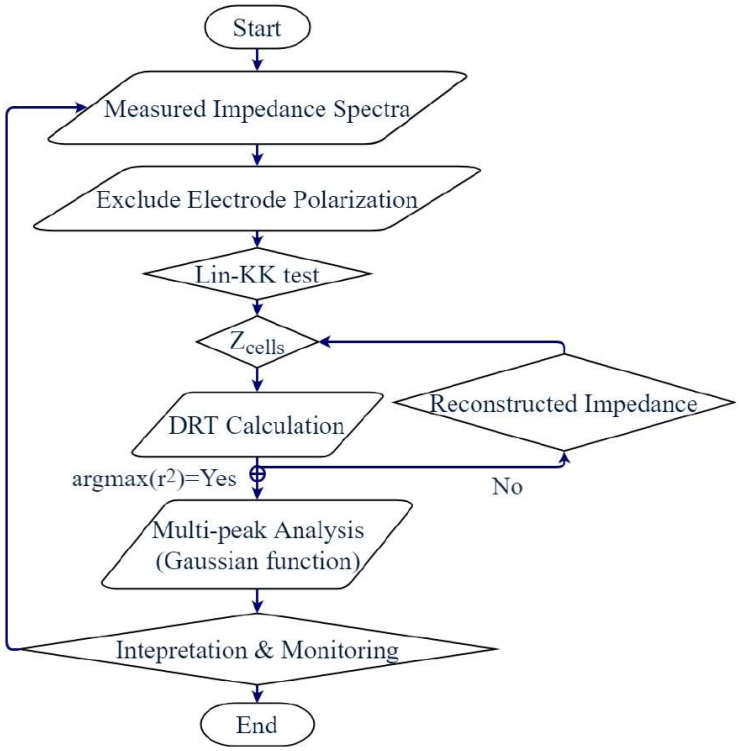

Fig. 1. Flowchart of DRT and multi-peak analysis for processing of measured impedance spectra. After the contribution of electrode polarization was accounted for, impedance spectra were analyzed and validated by a Kramers-Kroning relation test (Lin-KK) before the DRT was derived. From the distribution, the measured impedance spectra could be reconstructed. A multi-peak analysis with Gaussian function was the basis for the interpretation of the relaxation processes that were identified in the DRT.

2.2 Distribution of Relaxation Times (DRT)

The development of the DRT method relies on the basic principle that an impedance spectrum can be represented by an infinite sum of different time constants. This approach is intuitive since most electrochemical processes are in fact relaxation processes (Effat and Ciucci 2017). When frequency data is collected on a logarithmic scale, the equivalent impedance for specific frequencies, f, i.e. $Z_{DRT}(f)$, can then be expressed as a function of their distribution:

$$Z_{DRT}(f) = R_{\infty} + \int_0^{\infty} \frac{\gamma(ln\tau)}{1 + i2\pi f\tau} d(\ln \tau) \qquad \text{(eq. 1)}$$

where R_{∞} describes the resistance at infinite frequency. For the analysis, the actual distribution function, $\gamma(\ln\tau)$ needs to be derived to describe the multiple relaxation times ($\tau = f^{-1}$) that are underlying the impedance spectrum that was determined. However, fitting eq.1 is an intrinsically ill-posed problem. Therefore, an approximation of $\gamma(\ln\tau)$ is commonly obtained by a Tikhonov regularization approach (Wan et al. 2015). The distribution function $\gamma(\ln\tau)$ is hereby discretized by a series of radial basis functions (RBFs), $\Psi(\tau)$:

$$\gamma(\ln\tau) = \sum_{n=1}^{N} \kappa_n \Psi(x) \qquad \text{(eq. 2)}$$

where κ_n describes the amplitude of the associated RBF with the argument $x = |\ln\tau - \ln\tau_n|$. The parameter τ_n indicates the center of the RBF. There are various options for the choice of RBFs to

approximate a DRT. Here we decided on Gaussian functions, *G(x)*, as suggested by Ramírez-Chavarría et al., due to the modifiable broad of the kernel, which gave a better resolution for the fitting of experimentally determined impedance data in comparison to Dirac distributions (Ramírez-Chavarría et al. 2018):

$$G(x) = \exp(-\mu(x)^2) \quad \text{(eq. 3)}$$

with the parameter μ as specific shape factor, determined by the full width at half maximum (FWHM) of the RBF. Accordingly, the impedance, $Z_{DRT}(f)$, as described by eq. 1, can be rewritten by combing eq. 2 and eq. 3, resulting in eq. 4:

$$Z_{DRT}(f) = R_\infty + \sum_{n=1}^{N} \kappa_n \int_0^\infty \frac{G_n(x)}{1 + i2\pi f\tau} dx = R_\infty + Z'_{DRT}(f) + iZ''_{DRT}(f) \quad \text{(eq. 4)}$$

Z'_{DRT} and Z''_{DRT} describe the real and imaginary part of the reconstructed impedance, respectively. Eq.4 can also be expressed in matrix notation by $\mathbf{Z_{DRT}} = R_\infty \mathbf{1} + \mathbf{Z'_{DRT}} + \mathbf{Z''_{DRT}}$, with the unit vector $\mathbf{1}$. Accordingly, a cost function $\mathbf{\Lambda(\kappa)}$ for regularized least squares for the fit of calculated values of $Z_{DRT}(f)$ with experimental values $Z_{exp}(f)$ can be obtained:

$$\mathbf{\Lambda(\kappa)} = \left\| R_\infty \mathbf{1} + \mathbf{Z'_{DRT}} - \mathbf{Z'_{exp}} \right\|^2 + \left\| \mathbf{Z''_{DRT}} - \mathbf{Z''_{exp}} \right\|^2 + \lambda \|\boldsymbol{LX}\|^2 \quad \text{(eq. 5)}$$

with the column vector $\boldsymbol{\kappa}$ which needs to be determined by minimizing $\mathbf{\Lambda(\kappa)}$. The penalty to prevent overfitting is given by $\lambda\|\boldsymbol{LX}\|^2$ with the regularization factor λ and $\|\boldsymbol{LX}\|^2$ being proportional to the norm of the second derivative of γ(τ), i.e., $\left\| \frac{d^2\gamma(\tau)}{d^2 \ln \tau} \right\|^2$.

Eventually, a reconstructed impedance spectrum is obtained from the derived DRT (Schichlein et al. 2002):

$$Z_{DRT}(f) = R_\infty + \sum_{n=1}^{N} \frac{\kappa_n}{1 + i2\pi f\tau_n} \quad \text{(eq. 6)}$$

The difference between the reconstructed impedance and measured impedance was evaluated by the normalized root mean square error (NRMSE, r^2) to return optimal values of the shape factor μ and regularization factor λ when r^2 is at a maximum. The initial range of each factor was decided according

Algorithm 1 Derivation of the Distribution of Relaxation Times.

Input:
1. Experimental impedance $Z_{cells} = [f_n, Z'_{cells}, Z''_{cells}]$, n = 1, 2…N;

Output: find the optimal values of shape factor and regularization factor.
2. Discretize γ(lnτ) with Gaussian functions;
3. Minimize the cost function $\mathbf{\Lambda(\kappa)}$
4. Reconstruct impedance Z_{DRT}
5. Calculate the goodness of fit, r^2, between Z_{cells} and Z_{DRT} by NRMSE
6. **for** μ ∈ [0,3] and λ ∈ $[10^{-7}, 10^{-1}]$ **do**:
   steps 1 to 3
   γ(lnτ) ⇔ argmax(r^2)
7. **end**
8. **return** γ(lnτ)

to experience and references. The complete process is summarized in Algorithm 1.

2.3 Electrical Impedance Spectroscopy of Biological Cell Monolayers

For this study, the evaluation of impedance information for and about biological cells by DRT-analysis

was developed and verified for the reliable induction of defined changes by nanosecond pulsed electric fields. Therefore, electrical impedance spectra of rat liver epithelial WB-F344 cell monolayers were recorded before and after exposure to 100-ns pulsed electric fields with a mean electric field strength of 20 kV/cm. Details on experimental setup and procedures can be found in elsewhere (Shi et al. 2019a). In brief, impedance spectra were obtained with an impedance analyzer (Agilent 4294A, Keysight Technologies, Inc., USA) from 100 Hz to 10 MHz for confluent cell monolayers that were grown on ECIS-8W20idf electrode arrays (Applied Biophysics, Inc., NY, USA). In addition to the impedance measurements, pulsed electric fields of 100-ns duration were applied to the same electrode array by a custom-made transmission line pulse generator. Applied voltage pulses were monitored on a fast oscilloscope (TDS3054, Tektronix, Beaverton, OR), connected with a high voltage probe (P5100A, Tektronix, Beaverton, OR). Previously, changes in dielectric characteristics were derived from impedance spectra for 8, 20 or 60 consecutive voltage pulses that were applied with a repetition rate of 1 Hz. In the present work, the DRT-analysis is in particular applied towards the analysis of treatments with 60 pulses, which were difficult to interpret by the conventional approach of an equivalent circuit model due to different biological effects, such as reversible and irreversible electroporation and cell death.

Impedance measurements on biological cells are generally conducted with a two-electrode system (such as aforementioned ECIS-8W20idf electrode arrays) which, however, suffer from electrode polarization. Electrode polarization has to be described by a non-ideal capacitance resulting in a very large impedance. This relative strong polarization will dominate the distribution of relaxation times, causing poor DRT estimates for cells. Therefore, the impedance, Z_{medium}, was recorded for electrode systems that were only covered with cell culture medium, which was then subtracted from any measurements with cells, $Z_{measured}$, to account for the influence of electrode polarization on the results for the impedances of the actual cells, Z_{cells}, according to eq. 7.

$$Z_{cells} = Z_{measured} - Z_{medium} \quad \text{(eq. 7)}$$

The analysis was ultimately conducted for values of Z_{cells} obtained for frequencies above 3.3 kHz, since measurements at lower frequencies were prone to strongly fluctuating results.

The Kramers-Kronig relation between the real and imaginary parts of the impedance, Z_{cells}, was tested by the approach and algorithm (i.e. Lin-KK) developed by the group of E. Ivers-Tiffée (Schönleber et al. 2014). A measured spectrum is considered to be valid, as long as the relative discrepancy between the measured spectrum and the impedance spectrum reconstructed from Kramers-Kronig test is less than 1%. The respective residuals are presented in Fig. A1 (Appendix) and smaller than 1%, in particular the discrepancy below 3 MHz is smaller than 0.5%, suggesting the system fulfills the fundamental demands of EIS, i.e. linearity, causality and time invariance. Mean values for Z_{cells}, as input for algorithm 1, i.e. the derivation of DRT, were calculated from at least three independent experiments.

2.4 Multi-peak Analysis

In order to separate polarization processes, a multi-peak analysis was performed by fitting the distribution function, $\gamma(\ln\tau)$, by a series of Gaussian functions, G_i $(i = 0,1,\dots,M)$, according to eq. 8:

$$G_i(\tau) = \frac{A_i}{\sigma_i\sqrt{2\pi}} e^{\left[-(\tau-\eta_i)^2/2\sigma_i^2\right]}, i = 0,1 \dots M \quad \text{(eq. 8)}$$

A_i describes the amplitude of $G_i(\tau)$with respect to the peak, i.e. height, of the function according to $h_i = \frac{A_i}{\sigma_i\sqrt{2\pi}}$. The characteristic time η_i determines the center relaxation time of the peak and the parameter σ_i is related to the full-width-half-maximum (FWHM) of the profile of $G_i(\tau)$ according to $2\sigma_i\sqrt{2\ln 2}$. A Gaussian distribution is considered a good default choice in the absence of prior knowledge about the system (Goodfellow et al. 2016). The number of the peaks of the DRT was found by a function provided by a python library, i.e. *scipy* (*find_peaks_cwt*). The fitting is conducted with non-linear least-squares, i.e. *minimize*, that are included in a python package *lmfit*. The success of the fitting was confirmed by maximizing the goodness of fit (r^2) between the reconstructed impedance

spectrum and measured impedance, Z_{cells}.

3 Results and Discussion

3.1 Distribution of Relaxation Times of WB-F344 Cell Monolayers

The distribution function was constructed with the optimal values $\mu = 1.78$ and $\lambda = 10^{-2}$ for impedance spectra from 3.3 kHz to 10 MHz. We also conducted a real and imaginary cross-validation test as suggested by Saccoccio and Ciucci (Saccoccio et al. 2014), which is computationally heavy, and got the same values for μ and λ. Fig. 2 shows the discrepancies between the respective real and imaginary parts of Z_{DRT} and Z_{cells}, exhibiting a good agreement between measured and reconstructed spectra (r^2>0.98 by NRMSE). Discrepancies for both imaginary and real parts differed by less than 5%, except for the impedance spectrum at a frequency above 3 MHz. The fast-increasing residual with higher frequencies presumably resulted from increasingly more significant inductive contributions. This assumption is consistent with the abovementioned relatively large residuals according to the Lin-KK test for the high frequency tail (>0.5% above 3 MHz). The same behavior was also found by Hahn et al. (Hahn et al. 2019) in support of the suggestion that an inductive component leads to serious problems for the correct calculation of the DRT (Ivers-Tiffee and Weber 2017). Therefore, the upper frequency limit was set at 3 MHz for the analysis. The corresponding relaxation times lie within a range from 0.33 μs to 100 μs.

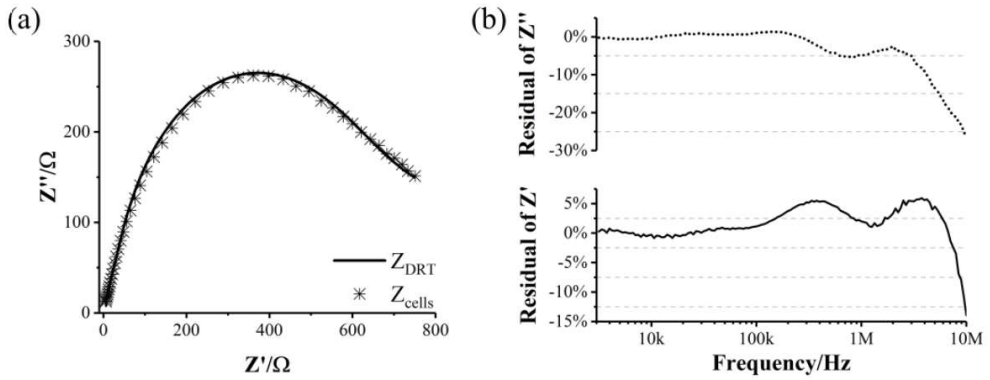

Fig. 2. Comparison of the reconstructed impedance Z_{DRT} and the originally measured cell impedance Z_{cells}, shown as a Nyquist plot (a), and discrepancies between the real and imaginary parts of Z_{DRT} and Z_{cells}, as described by the respective residuals (b).

The DRT for cells before nsPEF-exposure are shown in Fig. 3(a) and exhibited several peaks with the most prominent peak found for a relaxation time of 2.86 μs and a second peak for 84.37 μs. The different profiles displayed in Fig. 3(b) describe the temporal evolution of DRTs after exposure. The individual DRT curves reveal obvious time-dependent changes. A significant shift of the highest peak towards longer relaxation times emerged 1 min after exposure. The magnitude of the highest peak kept decreasing until 1 h after exposure before values started to increase again. Concurrently, the highest peak moved gradually back to shorter relaxation times. Profiles, including peak position and magnitude, were eventually similar to pre-treatment results again after 24 h, indicating a healing process of the cell monolayer, i.e., adjacent living cells have presumably slowly migrated into the gaps left by cells that did not survive the exposure.

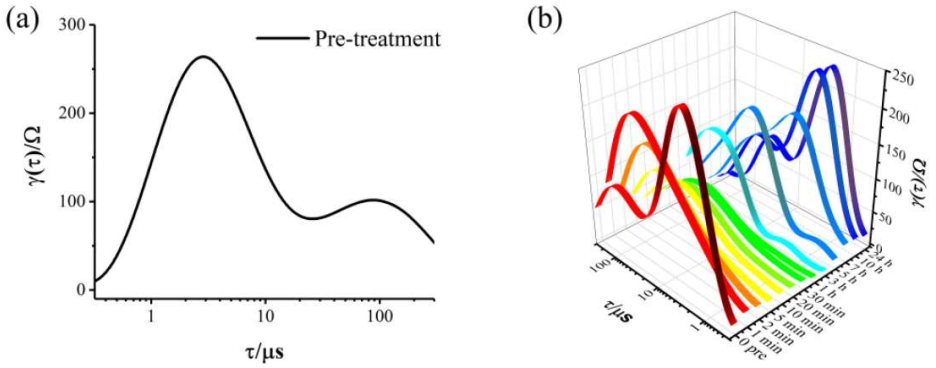

Fig. 3. Distribution of relaxation times (DRT) as described by the distribution function γ(τ) for a not exposed (pre-treated) cell monolayer (a) and for the temporal evolution before and after exposure to 60 electric field pulses of 100 ns and 20 kV/cm (b).

3.2 Multi Peak Analysis of the Distribution of Relaxation Times

In order to analyze the changes of the distribution function γ(τ) after exposure, generally two and sometimes three Gaussian functions $G_i(\tau)$ $(i = 0,1,2)$ were needed to fit the distribution function. The vicinal polarization processes described in the distribution function could be clearly distinguished by the Gaussian functions as shown in Fig. 4. The presented results for cells before treatment (pre-treated) as well as for cells 1 min, 1 h, 3 h, 7 h, and 24 h after exposure were chosen based on the respective profiles for these times according to Fig. 3(b) and based on the observation that these distribution functions provided the most significant distinction. An intuitive conclusion is that $G_1(\tau)$ dominated the changes in the temporal evolution of γ(τ).

A drastic change of the shape of the distribution function that was observed within 1 min after exposure (cf. Fig. 4(a) and Fig. 4(b)), in particular, for the peak of $G_1(\tau)$ shifting from 2.89 μs to a longer relaxation time of 15.07 μs, associated with half of the height of the foregoing peak. In contrast, the peak of $G_0(\tau)$ showed almost no changes, i.e. only a minor shift of relaxation time from 82.4 μs to 85.2 μs. The height of the peak for $G_1(\tau)$ for treatments 1 h after exposure was even lower and only one-fortieth of the pre-treatment value before it increased again during the subsequent recovery of the monolayer within 24 hours.

Only for 1 h, 3 h, 5 h, and 7 h after exposure, a small additional dispersion was notable, corresponding to a very short relaxation time (on the order of 1 μs). Accordingly, a third Gaussian function, $(G_2(\tau))$, was required for a correct fit of the respective DRTs. The dispersion first appeared for the lower boundary (0.33 μs) of relaxation times at 1 h after exposure and then moved to a longer relaxation time (2.03 μs) within 3 hours after exposure. Afterwards, it moved back to a shorter relaxation time again and eventually outside the defined lower frequency limit for the analysis till 7 h after exposure.

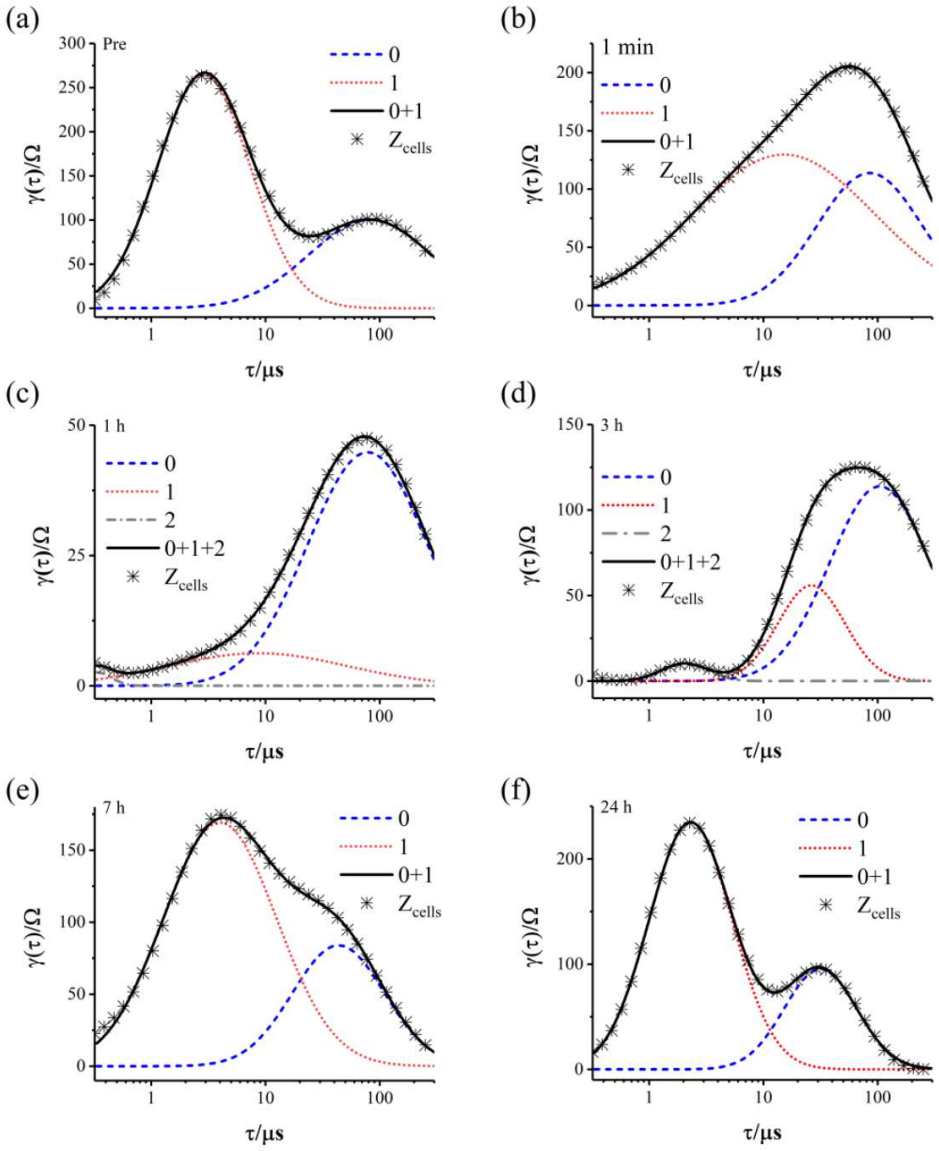

Fig. 4. Multi-peaks analysis for cells before treatment and 1 min, 1 h, 3 h and 7 h after exposure to 60 electric field pulses of 100 ns and 20 kV/cm. Two Gaussian functions, $G_0(\tau), G_1(\tau)$, were used to fit the DRT for pre-treated cells (a) and cell monolayers 1 min after exposure (b). For cell monolayers analyzed 1 h (c) and 3 h (d) and 7 h (e) after exposure an additional Gaussian function, $G_2(\tau)$, needed be included to describe the DRT. However, for 7 h the third Gaussian function is not presented in the figure since its peak is found just outside the lower relaxation time limit, defined for the analysis, and therefore a significant deviation between the DRT for the experimental impedance, Z_{cells}, and the fitted DRT could be observed during relaxation times of less than 1 μs. The DRT for cell monolayers, 24 h after exposure, recovered to be similar to the DRT for pre-treated cells (f).

The important information on each polarization process in the cell monolayer is comprised of center relaxation times, η_i, (or respective frequencies), characteristic amplitudes, A_i, and the shape of the dispersion, in particular the width, i.e. $FWHM_i$, of the descriptive functions (Hahn et al. 2019; Schichlein et al. 2002; Teyssedre et al. 1996). For the chosen analysis, these parameters and their temporal evolution determined the specific Gaussian functions ($G_0(\tau), G_1(\tau), G_2(\tau)$) and the

respective values for the different parameters are displayed in Fig. 5.

Center relaxation times (cf. Fig. 5(a)) were determined for η_0 of about 100 µs, for η_1 of about 10 µs and for η_2 of about 1 µs (or corresponding frequencies of 10 kHz, 100 kHz and 1 MHz). The center relaxation time, η_0, of $G_0(\tau)$ experienced a relatively slow decrease from 82.43 µs to 50.04 µs within 10 min after exposure followed by an increase up to 104.43 µs until 3 h after exposure and another subsequent decrease down to 35.21 µs for 7 h after exposure; a value which did not change for later times any more.

In contrast, the center relaxation time of $G_1(\tau)$ increased drastically from 2.89 µs to 15.07 µs within 1 min after exposure. During the following 20 minutes, η_1 decreased further to 2.33 µs. Afterwards, the development of η_1 followed the same trend as was observed for η_0 but with more pronounced relative changes. Values increased up to 26.34 µs for cells 3 h after exposure. As mentioned above, a third Gaussian function, $G_2(\tau)$, was only necessary to describe the DRT for cells within 1 h to 7 h after exposure. The respective changes and trends resembled the development for $G_1(\tau)$.

Fig. 5(b) exhibits the temporal evolution of the amplitudes A_i. The amplitude A_0 decreased gently from values of 134.81 Ω to 58.85 Ω within 1 h after exposure, followed by an increase up to 125.48 Ω within 3 h after exposure. Afterwards, A_0 decreased again and went eventually down to 75.85 Ω within 24 h after exposure. In contrast, A_1 fell drastically from 270.14 Ω to 12.25 Ω within 1 h after exposure. Moreover, within 2 min after exposure the value of the amplitude was only half of that derived for pre-treated cells. Afterwards, a monotonic increase of A_1 can be observed and a steady state was reached at 10 h after exposure. The values for A_2 were altogether much smaller than for the other amplitudes and increased from 0.82 Ω for 1 h after exposure to 15.24 Ω for 5 h after exposure, which was then followed by amplitudes that decreased to 9.05 Ω at 7 h after exposure.

The FWHMs for each Gaussian function showed changes that were similar to the development of the center relaxation times. $FWHM_0$ remained rather stable until 5 h after exposure and then decreased to one-fifth of the initial value within the next 19 hours. $FWHM_1$ immediately increased significantly from the initial value of 7.77 µs to 128.73 µs within 1 min after exposure. This was followed by a gradual decline with some fluctuations until values for $FWHM_1$ were comparable again to the initial values at about 10 h after exposure. $FWHM_2$ also showed some changes, however, an interpretation is presumably meaningless since the changes are related to a dispersion outside the bounds for the frequency range that was determined of the analysis (as described above) and furthermore only observed 1 h and 7 h after exposure.

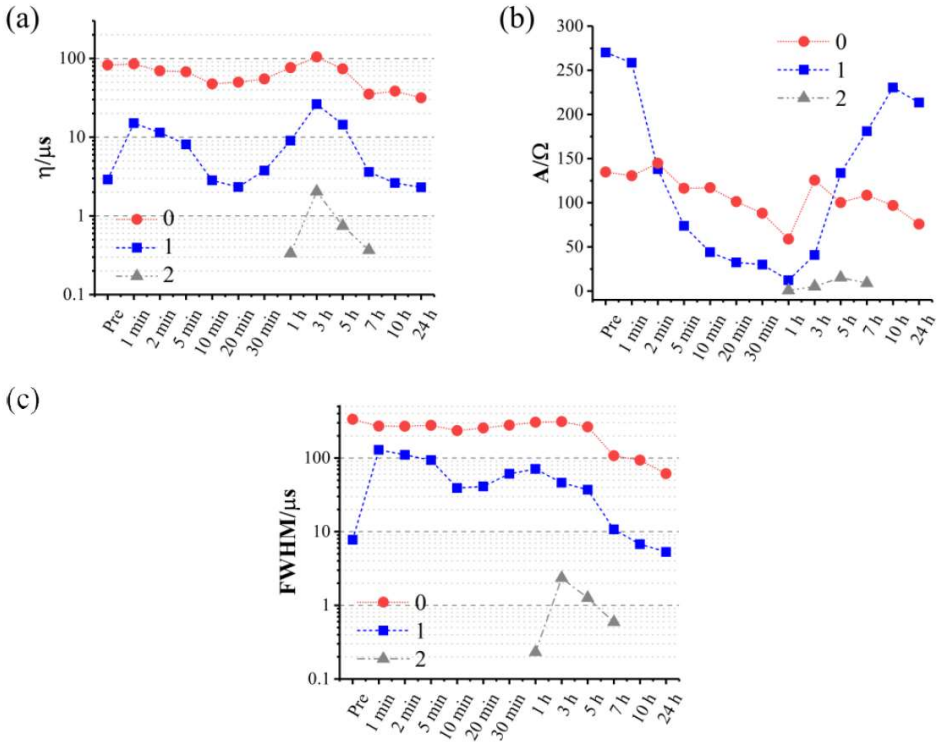

Fig. 5. Temporal evolution of the parameters that define the Gaussian functions, $G_i(\tau)$ *(i = 1, 2, 3)*, describing the DRT, i.e. center relaxation time η_i, (a), amplitude A_i (b) and FWHM_i (c). The values were determined for the peaks of each Gaussian function and evaluated by a multi-peak analysis.

3.3 Biological Interpretation of the DRT

Generally, a well-separated peak in the DRT corresponds to a specific polarization process. For the analysis so far, the calculated distribution functions had been differentiated by a multi-peak analysis into several domains. The complexity and lack of prior knowledge on many of the potential mechanisms that are associated with complex biological systems poses the risk of mistakes in the interpretation of the descriptive Gaussian functions. However, valuable conclusions on dispersion mechanisms can be drawn based on previous findings, especially by Kuang and Nelson as well as Schwan (Kuang and Nelson 1998; Schwan 1994).

Schwan found that the dielectric dispersion of biological matter can be divided into three distinct regimes, i.e. α-, β- and γ-dispersion, that are based on different prominent relaxation processes. The first one, α-dispersion, is usually dominant for frequencies below a few kHz and is associated with the polarization of a counterion layer (electrical double layer) at charged surfaces. In the β-dispersion regime, cellular and intercellular membranes are dominating the response in the range from tens of kHz to tens of MHz due to a membrane charging effect, i.e. Maxwell-Wagner effect. For the highest frequencies above 100 MHz, γ-dispersion results from the polarization of small molecules, including water.

The Gaussian function $\mathrm{G}_1(\tau)$is presumably directly related to membrane relaxation processes. Changes of the amplitude A_1 agree with the equivalent evaluation of a simplified two-layer model with a single-time dispersion as described by Kuang and Nelson (Kuang and Nelson 1998). This model (eq. A1 and A2 in Appendix A) indicates that the magnitude of this dispersion is inverse proportional to the relative area of ions passing through the membrane. Therefore, an increase of this relative area due to membrane permeabilization, e.g. after exposure to nsPEFs, may correspond to the decrease of A_1.

However, the large continuous decline of A_1 observed even 1 h after exposure (Fig. 5(b)) resulted more likely from disrupted cells, associated with a complete loss of membrane integrity of dead cells also in addition to irreversibly electroporated cells.

Respective relaxation times have been revealed to be also a function of cell microstructures and changes superimposed in the impedance spectra by differences in membrane thicknesses and contributions from the bulk electrolyte (eq. A2). The complicated interrelationship may be responsible for the observed fluctuations of the center relaxation time η_1 (Fig. 5(a)). Furthermore, the initial rapid increase of $FWHM_1$ suggests a corresponding increase in the heterogeneity of the investigated cell monolayer. Given the time scales for membrane permeabilization and the disruption of cell-cell connections that was previously observed for the chosen exposure parameters (Shi et al. 2018), this seems a reasonable and significant contribution.

Unfortunately, the interpretation of the contribution of the other two Gaussian functions is not as evident or could be easily related to underlying biological processes. The function $G_0(\tau)$, associated with lower relaxation frequencies (around 10 kHz), may conceivably be related to characteristics of the extracellular matrix. WB-F344 cells are tightly bound together in monolayers to form an epithelial cell sheet that is expressing a scanty extracellular matrix and is therefore prone to only a minor dispersion. Accordingly, no significant changes of the extracellular matrix and corresponding changes of $G_0(\tau)$ have been observed after exposure. Conversely, the function $G_2(\tau)$, which contributed to the DRT for the pre-treated cell monolayer at higher frequencies (around 3 MHz) may be related to the dispersion of intracellular membranes, such as of organelles or the nucleus. However, future measurement at higher frequencies with reduced inductive contributions are needed to investigate this assumption in more detail.

In comparison to the analysis of impedance spectra by a Cole model for cell monolayers that were exposed to nanosecond pulsed electric fields, the previously identified sole main dispersion mechanism (Shi et al. 2019a) could now be related to actually up to three different superimposed processes that were represented in the DRT by three distinct Gaussian functions. Accordingly, DRT provides a much more detailed evaluation, i.e. finer view.

The peak and FWHM of DRT for the Cole model could then be evaluated by an analytical solution (Wan et al. 2015), which resulted in center relaxation time of 3.3 µs and FWHM of 9.2 µs for the pre-treated cell monolayer. This peak is close to the center relaxation time $\eta_1 = 2.89$ µs of the Gaussian function $G_1(\tau)$. The FWHM of the DRT corresponding to the Cole model is a little larger than $FWHM_1 = 7.8$ µs, The larger value for the Cole model is a consequence of the actual representation of characteristic time constants, i.e. the calculation of a mean value from different relaxation time constants, which results in an actual superposition of different dispersions that could not be separated by this approach – unlike it is possible by the DRT-analysis. Accordingly, the amplitude of $G_1(\tau)$ from 5 min to 3 h after exposure, as shown in in Fig. 5(b), exhibited a large decrease, suggesting the contribution of the respective relaxation process to the overall relaxation characteristics becoming smaller and comparable to other contributing dispersions. This might explain the difficulty for fitting the impedance measurements with a Cole model. At least a more sophisticated equivalent circuit model with additional elements, including missing polarization processes, seems required for a more accurate physical description by a Cole model.

An alternative approach to describe the influence of different dispersion processes on impedance spectra is provided by a principal component analysis (PCA) (Shi et al. 2019b). Some important frequency ranges for the differentiation of different cell types and responses after exposure to nsPEFs could be discriminated by this method. However, the respective principle components are rather difficult to relate to actual physical mechanisms. The first principal component, P1, included mostly contributions from the low frequency range at around 6 kHz. This value is very close to the frequency corresponding to the center relaxation time, η_0, for $G_0(\tau)$. Given the interpretation of the equivalent process, this may confirm the assumed representation of the extracellular matrix in the DRT. The largest loading for the second principal component, P2, was found for a frequency close to the frequency that is associated with the peak of $G_1(\tau)$, suggesting P2 was rather related with relaxation processes of cell membranes. The reason why the value of P1 is larger than P2 cannot be determined

unambiguously due to the larger lower limit of 3.3 kHz of the frequency range defined for the DRT-analysis in comparison to the limit for the PCA-analysis of 100 Hz.

4 Summary and Conclusion

An ultrasensitive method for the identification of relaxation mechanisms of biological cells in a monolayer has been established by means of a deconvolution of electrical impedance spectra. The analysis, based on the distribution of relaxation times and a multi-peak fitting procedure, revealed details of different polarization mechanisms that could not be distinguished by a Cole analysis. However, deconvolution of the DRT is not a trivial task. A successful solution strongly depends on the reduction of noise and uncertainties in the data and a sufficient number of experimental data points. In addition, the abstraction of electrode polarization contributions to the impedance needs to be assured together with the absence of inductive contributions. Therefore, a workflow was established that included an indispensable test of the Kramers-Kronig relation and a comparison with experimental impedance data as shown in Fig. 1 and Algorithm 1. Furthermore, both the effect of electrode polarization on the data at low frequencies and the influence of stray capacities and parasitic inductances at higher frequencies should be minimized by a dedicated sensor design.

A particular strength of method and approach is to distinguish the effects of stimuli, in this case nanosecond pulsed electric fields, which have demonstrated reliable and reproducible effects previously (Shi et al. 2019a). Accordingly, three distinct and independent relaxation processes could be determined in response to the exposure. The temporal evolution of the impedance spectrum obtained for WB-F344 cell monolayers after exposure was dominated by the cell membrane interfacial polarizations, as it was observed for frequencies of hundreds of kilohertz. Relaxation processes distinguished for lower frequencies at around 10 kHz may be related to mechanisms affecting the extracellular matrix instead. For the other end of the investigated frequency range, i.e. the MHz-range, relaxation processes were more likely related to the response of subcellular organelles, including the nucleus.

In general, the DRT-analysis is a model-free approach which provides high resolution and sensitivity for the identification of different relaxation processes and requires neither a priori assumptions, such as an equivalent circuit model, nor other prior knowledge of the system. As such, the method can decidedly help to optimize the experimental design for bioimpedance measurements in general and the development of dedicated biosensors in particular.

5 Acknowledgment

This work was supported in part by the Collaborative Research Center CRC 1270 funded by the German Research Foundation (DFG.) Fukun Shi is the recipient of a grant from the China Scholarship Council (CSC) (File No.20150670010).

6 Appendix A

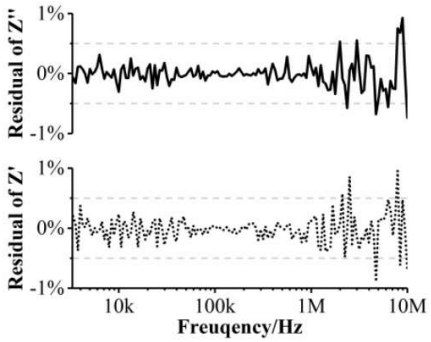

Fig. A1. The residual plots of the Lin-KK test of Z_{cells} for pre-treated cells.

Equations of the simplified two-layer model:

$$\tau = \varepsilon_0 \frac{[(1-s)\varepsilon_m + s\varepsilon_b]t_b + \varepsilon_b t_m}{\sigma_b(st_b + t_m)} \quad \text{(eq. A1)}$$

$$\Delta\varepsilon = \frac{\varepsilon_m^2(1-s)^2(t_b + t_m)t_b t_m}{\{[(1-k)\varepsilon_m + s\varepsilon_b]t_b + \varepsilon_b t_m\}(st_b + t_m)^2} \quad \text{(eq. A2)}$$

where s is the relative area for ion passages, ε_0 is the permittivity of vacuum, ε_m and ε_b are relative permittivity for the membrane and bulk electrolyte, t_m and t_b describe the thickness of the membrane and the bulk electrolyte, respectively. $\Delta\varepsilon$ and τ are the increment of permittivity and the single relaxation time.

References

Czolkos, I., Dock, E., Tønning, E., Christensen, J., Winther-Nielsen, M., Carlsson, C., Mojzikova, R., Skladal, P., Wollenberger, U., Nørgaard, L., 2016. Prediction of wastewater quality using amperometric bioelectronic tongues. Biosensors and Bioelectronics 75, 375-382.

Dalmay, C., Villemejane, J., Joubert, V., Silve, A., Arnaud-Cormos, D., Français, O., Mir, L.M., Lévêque, P., Le Pioufle, B., 2011. A microfluidic biochip for the nanoporation of living cells. Biosensors and Bioelectronics 26(12), 4649-4655.

Effat, M.B., Ciucci, F., 2017. Bayesian and Hierarchical Bayesian Based Regularization for Deconvolving the Distribution of Relaxation Times from Electrochemical Impedance Spectroscopy Data. Electrochimica Acta 247, 1117-1129.

García-Sánchez, T., Bragós, R., Mir, L.M., 2018. In vitro analysis of various cell lines responses to electroporative electric pulses by means of electrical impedance spectroscopy. Biosensors and Bioelectronics 117, 207-216.

Goodfellow, I., Bengio, Y., Courville, A., 2016. Deep learning. MIT press.

Hahn, M., Schindler, S., Triebs, L.-C., Danzer, A.M., 2019. Optimized Process Parameters for a Reproducible Distribution of Relaxation Times Analysis of Electrochemical Systems. Batteries 5(2).

Huang, J., Li, Z., Liaw, B.Y., Zhang, J., 2016. Graphical analysis of electrochemical impedance spectroscopy data in Bode and Nyquist representations. J. Power Sources 309, 82-98.

Ivers-Tiffee, E., Weber, A., 2017. Evaluation of electrochemical impedance spectra by the distribution of relaxation times. Journal of the Ceramic Society of Japan 125(4), 193-201.

Kuang, W., Nelson, S.O., 1998. Low-frequency dielectric properties of biological tissues: a review with some new insights. Transactions of the ASAE-American Society of Agricultural Engineers 41(1),

173-184.

Lvovich, V.F., 2012. Impedance spectroscopy: applications to electrochemical and dielectric phenomena. John Wiley & Sons.

McAdams, E.T., Jossinet, J., 1996. Problems in equivalent circuit modelling of the electrical properties of biological tissues. Bioelectrochem. Bioenerg. 40(2), 147-152.

Nuccitelli, R., Berridge, J.C., Mallon, Z., Kreis, M., Athos, B., Nuccitelli, P., 2015. Nanoelectroablation of murine tumors triggers a CD8-dependent inhibition of secondary tumor growth. PLoS One 10(7), e0134364.

Ramírez-Chavarría, R.G., Sanchez-Perez, C., Matatagui, D., Qureshi, N., Pérez-García, A., Hernandez-Ruiz, J., 2018. Ex-vivo biological tissue differentiation by the Distribution of Relaxation Times method applied to Electrical Impedance Spectroscopy. Electrochimica Acta 276, 214-222.

Saccoccio, M., Wan, T.H., Chen, C., Ciucci, F., 2014. Optimal Regularization in Distribution of Relaxation Times applied to Electrochemical Impedance Spectroscopy: Ridge and Lasso Regression Methods - A Theoretical and Experimental Study. Electrochimica Acta 147, 470-482.

Schichlein, H., Müller, A.C., Voigts, M., Krügel, A., Ivers-Tiffée, E., 2002. Deconvolution of electrochemical impedance spectra for the identification of electrode reaction mechanisms in solid oxide fuel cells. Journal of Applied Electrochemistry 32(8), 875-882.

Schönleber, M., Klotz, D., Ivers-Tiffée, E., 2014. A method for improving the robustness of linear Kramers-Kronig validity tests. Electrochimica Acta 131, 20-27.

Schwan, H.P., 1994. Electrical properties of tissues and cell suspensions: mechanisms and models. Proceedings of 16th Annual International Conference of the IEEE Engineering in Medicine and Biology Society, pp. A70-A71 vol. 71. IEEE.

Shi, F., Steuer, A., Zhuang, J., Kolb, J.F., 2019a. Bioimpedance Analysis of Epithelial Monolayers After Exposure to Nanosecond Pulsed Electric Fields. IEEE Trans. Biomed. Eng. 66(7), 2010-2021.

Shi, F., Zhuang, J., Kolb, J.F., 2019b. Discrimination of different cell monolayers before and after exposure to nanosecond pulsed electric fields based on Cole-Cole and multivariate analysis. J. Phys. D: Appl. Phys. DOI: 10.1088/1361-6463/ab40d7 in print.

Teyssedre, G., Demont, P., Lacabanne, C., 1996. Analysis of the experimental distribution of relaxation times around the liquid–glass transition of poly (vinylidene fluoride). Journal of applied physics 79(12), 9258-9267.

Wan, T.H., Saccoccio, M., Chen, C., Ciucci, F., 2015. Influence of the discretization methods on the distribution of relaxation times deconvolution: implementing radial basis functions with DRTtools. Electrochimica Acta 184, 483-499.

Zagar, T., Krizaj, D.J.P.m., 2008. Multivariate analysis of electrical impedance spectra for relaxed and contracted skeletal muscle. Physiol. Meas. 29(6), S365.

List of Contributions

Publications

1. **Fukun Shi**, Jie Zhuang, Juergen F. Kolb, 'Discrimination of different cell monolayers before and after exposure to nanosecond pulsed electric fields based on Cole-Cole and multivariate analysis', Journal of Physics D: Applied Physics 52 495401, 2019

2. **Fukun Shi**, Anna Steuer, Jie Zhuang, Juergen F. Kolb, 'Bioimpedance Analysis of Epithelial Monolayers after Exposure to Nanosecond Pulsed Electric Fields', IEEE Transactions on Biomedical Engineering 66 (7), 2010-2021, 2019

3. **Fukun Shi**, Juergen F. Kolb, 'Ultrasensitive Impedimetric Analysis of Cell Responses using the Distribution of Relaxation Times', Biosensors and Bioelectronics, Under Review (2019/10)

4. Hongmei Liu#, **Fukun Shi#**, Xiao Tang, Shuang Zheng, Yajun Zhao, Shoulong Dong, Juergen F. Kolb, Chenguo Yao, 'Applications of Bioimpedance Spectroscopy on Characterizing Chemo-resistant Tumor Cell Selectivity of Nano-pulse Stimulation', Bioelectrochemistry, Under Review (2019/11)

Conference Abstract

1. **F. Shi**, A. Steuer, C. Wolff, J. Kolb, 'Bioimpedance Spectroscopy to Distinguish Non-malignant and Malignant Cells before and after Exposure to Nanosecond Pulsed Electric Fields', Abstract Book, 11th International Workshop on Impedance Spectroscopy, ISBN:978-3-9817630-5-8

Conferences

2. **F. Shi**, J. Zhuang, A. Steuer, J. Kolb, 'Impedance Measurement of Epithelial Cells after

Exposure to Nanosecond Pulsed Electric Fields', Bioelectrics Symposium 2016, Rostock, Germany, 2016

3. **F. Shi**, J. Zhuang, A. Steuer, J. Kolb, 'Bioimpedance Analysis of Epithelial Monolayer after Exposure to Nanosecond Pulsed Electric Fields (nsPEFs)' at 2nd World Congress on Electroporation and Pulsed Electric Fields in Biology, Medicine and Food & Environmental Technologies, Norfolk (VA), USA, 2017

4. **F. Shi**, J. Rao, J. Kolb, 'Applications of Graphene on the Surface Modification of Implant Materials' at 29th GCCCD Annual Conference - 17th Parallel Forum of 2017 CIESC Annual Meeting, Hamburg, Germany, 2017

5. **F. Shi**, J. Kolb, 'Dielectric Characterization of Biological Materials with External Stimulus-Non-thermal Plasma and Pulsed Electric Fields' at 27th GCPD-2018-Munchen, Munich, Germany, 2018

6. **F. Shi**, A. Steuer, C. Wolf, J. Kolb, 'Bioimpedance Spectroscopy to Distinguish Non-malignant and Malignant Cells before and after Exposure to Nanosecond Pulsed Electric Fields', 11th International Workshop on Impedance Spectroscopy (IWIS 2018), Chemnitz, Germany, 2018

7. **F. Shi**, J. Zhuang, A. Steuer, J. Kolb, 'The Application of Nanosecond Pulsed Electric Fields on Cancer Therapy: A Study based on Dielectric Characteristics' at 19th Asian Conference on Electrical Discharge, Xi'an, China, 2018

8. W. Wei**, F. Shi**, J. Kolb, 'Dielectric and Electrical Properties of Porcine Femur fitted with CPE Element and Cole Model', 12th International Workshop on Impedance Spectroscopy (IWIS 2019), Chemnitz, Germany, 2019

Curriculum Vitae

Fukun Shi

Leibniz Institute for Plasma Science and Technology (INP Greifswald)

Felix-Hausdorff-Str. 2, 17489 Greifswald, Germany

Email: fukun.shi@uni-rostock.de

Personals:

Date of birth: 27. Sept. 1988

Place of birth: Fujian

Nationality: Chinese

Education:

- 09/2007-06/2011 Bachelor, School of Physics and Technology, Sichuan University, Sichuan, China
- 09/2012-06/2015 Master, School of Information and Optoelectronic Science and Engineering, South China Normal University, Guangzhou, China
- 10/2015-present Ph.D. candidate, Leibniz Institute for Plasma Science and Technology (INP Greifswald), Greifswald, Germany

Awards:

- Outstanding Oral Report Award of 19th Asian Conference on Electrical Discharge, 2018
- Scholarship from China Scholarship Council, 2015
- South China Normal University Advanced Individual, 2013
- South China Normal University Advanced Individual of Social Service, 2013
- South China Normal University Postgraduates' Creative Advanced Individual, 2013

Relevant Skills:

- Skilled in python, MATLAB; COMSOL and Origin for the data analysis and simulation
- Impedance spectroscopy, dielectric spectroscopy, immunofluorescence, cell experiments, plasma synthesis of materials, and biosensor design
- Machine learning, uncertainty quantification, experimental design optimization

Publications:

1. **F. Shi**, J. Zhuang, J. Kolb, 'Discrimination of different cell monolayers before and after exposure to nanosecond pulsed electric fields based on Cole-Cole and multivariate analysis', Journal of Physics D: Applied Physics 52 495401, 2019
2. **F. Shi**, A. Steuer, J. Zhuang, J. Kolb, 'Bioimpedance Analysis of Epithelial Monolayers after Exposure to Nanosecond Pulsed Electric Fields', IEEE Transactions on Biomedical Engineering 66 (7), 2010-2021, 2019
3. **F. Shi**, L. Peng and G. Zhou et al, "An Elliptical Core D-Shaped Photonic Crystal Fiber-Based Plasmonic Sensor at Upper Detection Limit", Plasmonics 10 (6), 1263-1268, 2015
4. **F. Shi**, G. Zhou, and D. Li et al, "Surface plasmon mode coupling in photonic crystal fiber symmetrically filled with Ag/Au alloy wires", Plasmonics 10 (2), 335-340, 2015
5. S. Ge, **F. Shi** et al, "U-Shaped Photonic Crystal Fiber Based Surface Plasmon Resonance Sensors", Plasmonics 11 (5), 1307-1312, 2016
6. L. Peng, **F. Shi** et al, "A Surface Plasmon Biosensor based on a D-shaped Microstructured Optical Fiber with Recstangular Lattice", IEEE Photonics Journal 7 (5), 1-9, 2015
7. Q. Chen, G. Zhou, and **F. Shi** et al, "Study of near-infrared dispersion wave generation for microstructure fiber" (IN CHINESE) , Acta Physica Sinica 64(3):034215, 2015

Selbstständigkeitserklärung

Doktorandinnen/Doktoranden-Erklärung gemäß § 4 Absatz 1 Buchstaben g und h der Promotionsordnung der Mathematisch-Naturwissenschaftlichen Fakultät der Universität Rostock

Name Shi, Fukun
(Name, Vorname)

Anschrift Erich-Schlesinger-Str. 19, #1.06.02.2, 18059, Rostock
(Straße, PLZ, Wohnort)

Ich habe eine Dissertation zum Thema

Impedimetric Analysis of Biological Cell Monolayers before and after Exposure to Nanosecond Pulsed Electric Fields

an der Mathematisch-Naturwissenschaftlichen Fakultät der Universität Rostock angefertigt. Dabei wurde ich von Frau/Herrn

Prof. Dr. Juergen Kolb betreut.

Ich gebe folgende Erklärung ab:

1. Die Gelegenheit zum vorliegenden Promotionsvorhaben ist mir nicht kommerziell vermittelt worden. Insbesondere habe ich keine Organisation eingeschaltet, die gegen Entgelt Betreuerinnen/Betreuer für die Anfertigung von Dissertationen sucht oder die mir obliegenden Pflichten hinsichtlich der Prüfungsleistungen für mich ganz oder teilweise erledigt.

2. Ich versichere hiermit an Eides statt, dass ich die vorliegende Arbeit selbstständig angefertigt und ohne fremde Hilfe verfasst habe. Dazu habe ich keine außer den von mir angegebenen Hilfsmitteln und Quellen verwendet und die den benutzten Werken inhaltlich und wörtlich entnommenen Stellen habe ich als solche kenntlich gemacht.

Rostock, den .....

.....
(Unterschrift)